A MOLECULAR ANALYSIS OF PROTEIN TRAFFICKING IN THE VERTEBRATE RETINA: IMPLICATIONS FOR INTRAFLAGELLAR TRANSPORT AND HUMAN DISEASE

A Dissertation

by

BRYAN L. KROCK

Submitted to the Office of Graduate Studies of
Texas A&M University
in partial fulfillment of the requirements for the degree of

DOCTOR OF PHILOSOPHY

May 2009

Major Subject: Biology

A MOLECULAR ANALYSIS OF PROTEIN TRAFFICKING IN THE VERTEBRATE RETINA: IMPLICATIONS FOR INTRAFLAGELLAR TRANSPORT AND HUMAN DISEASE

A Dissertation

by

BRYAN L. KROCK

Submitted to the Office of Graduate Studies of
Texas A&M University
in partial fulfillment of the requirements for the degree of

DOCTOR OF PHILOSOPHY

Approved by:

Chair of Committee,	Brian D. Perkins
Committee Members,	Bruce Riley
	Hongmin Qin
	Louise Abbott
Head of Department,	U.J. McMahon

May 2009

Major Subject: Biology

ABSTRACT

A Molecular Analysis of Protein Trafficking in the Vertebrate Retina: Implications for Intraflagellar Transport and Human Disease.

(May 2009)

Bryan L. Krock, B.S., The Pennsylvania State University

Chair of Advisory Committee: Dr. Brian D. Perkins

Vertebrate photoreceptors are highly specialized sensory neurons that utilize a modified cilium known as the outer segment to detect light. Proper trafficking of proteins to the outer segment is essential for photoreceptor function and survival and defects in this process lead to retinal disease. In this dissertation I focus on two aspects of protein trafficking, intracellular vesicular trafficking in photoreceptors and retinal pigmented epithelial (RPE) cells and how it relates to the human disease choroideremia (CHM), and the trafficking of proteins through the photoreceptor cilium. The human retinal degenerative disease choroideremia (CHM) is caused by mutation of the Rab escort protein-1 (REP1) gene, which is required for proper intracellular vesicular trafficking. However, it was unclear whether photoreceptor degeneration in this disease is cell-autonomous, due to defective opsin transport within the photoreceptor, or is noncell-autonomous and a secondary consequence of defective RPE. Utilizing the technique of blastomere transplantation and a zebrafish line with a mutation in the *rep1*

gene, I show that photoreceptor degeneration in CHM is noncell-autonomous and is caused by defective RPE.

The molecular machinery responsible for protein trafficking through the photoreceptor cilium remained unclear for a long time. Recent studies found Intraflagellar Transport (IFT) is the process that mediates cilia formation and transport of proteins through a cilium, and further analyses showed IFT is important for trafficking proteins to the outer segment. However, many details about how IFT works in photoreceptors remained unclear. By analyzing zebrafish harboring a null mutation in the *ift57* gene, I show that *Ift57* is only required for efficient IFT, and that the *Ift57* protein plays a role in the ATP-dependent dissociation of kinesin II from the IFT particle. Lastly, I investigate the role of retrograde IFT in photoreceptors, a process that had yet to be investigated. By utilizing antisense morpholino oligonucleotides to inhibit expression of cytoplasmic dynein-2 (the molecular motor that mediates retrograde IFT) , I show that retrograde IFT is required for outer segment extension and the recycling of IFT proteins.

DEDICATION

This dissertation is dedicated to my Nana and my parents, Keith and Carolyn, for all of their love and support through the years. The encouragement from my Nana was vital to my successful education and helped me through the difficult times. Completion of this research and Ph.D. would be impossible without the endless dedication and generosity of my parents, for which I am forever indebted to them.

ACKNOWLEDGEMENTS

I would like to thank my advisor, Dr. Brian Perkins, for his guidance and support throughout the course of my graduate studies. Brian gave me tremendous freedom in the lab to pursue new avenues and ask my own questions, for which I am very grateful. I feel well prepared to continue my career as a scientist, which I owe to Brian's instruction. I appreciate the many opportunities Brian gave me to attend meetings, where we certainly made the most of the opportunities to enjoy a few drinks during the off time. Our escapades during the down time at meetings are some of my best memories from graduate school.

I would also like to thank my committee members Bruce Riley, Hongmin Qin, and Louise Abbott for their helpful comments and advice throughout the course of my research. Additionally, I would like to thank Bruce Riley for use of his laser pointer.

E. Ann Ellis of the Microscopy and Imaging Center has been a tremendous help throughout my research, providing years of expertise in specimen preparation for electron microscopy. Every time I presented EM data at conferences and for my job interviews, I was complemented on the high quality of those data, which is due almost entirely to the work of Ann. It has been an honor to learn EM from one of the best, and I thank Ann for her patient instruction and assistance.

I would also like to thank all the past and present members of the Perkins laboratory for their assistance with experiments, maintenance of zebrafish. Specifically, I would like to thank Tony "Pedro" Kreipe, Mike Lindsey and Ethan Winkler for making

the lab a fun place to work. Many thanks to Sujita Sukumaran; she was always very generous with her time and willing to lend a hand. Thanks to Chace Craig for his camaraderie and for careful reading of this document, best of luck as the remaining student in the lab.

I thank the members of the Lekven and Riley labs for their help with experiments, reagents and pleasant conversations. Special thanks to Anand "The Hog" Narayanan for his endless optimism; nothing cheered me up on a tough day like chatting with "The Hog".

My deepest gratitude to Lindsay Bennett, I could not have done this without her friendship and support over the years. She is a truly good person whom I will deeply miss.

I thank Dr. Jacqueline McLaughlin for her continued mentorship and advice since my undergraduate days. She has been a great friend, and I owe much of my success to her guidance.

Finally, I would like to thank my family and especially my parents for their support, I could not have done this without you.

TABLE OF CONTENTS

CHAPTER Page

LIST OF FIGURES

Page

LIST OF TABLES

CHAPTER I

INTRODUCTION

BACKGROUND

The Retina

Vision, or the detection of environmental light stimuli, is mediated by a thin layer of cells lining the back of the eye known as the retina. The retina is part of the central nervous system and is composed of two synaptic layers intercalated between three cellular layers (Fig. 1). The most proximal cellular layer is the ganglion cell layer, which is composed of neurons that collect information from the cells of the middle layer and send it to the brain via their axonal processes that coalesce and leave the eye as the optic nerve. The middle layer of cells is known as the inner nuclear layer and is composed of four neuronal types, the horizontal, bipolar, amacrine and Müller cells. The basic function of these cells is to collect sensory impulses generated by the photoreceptors of the distal most retinal layer, perform rudimentary neuronal processing of this information, and transmit this information to the ganglion cells.

Photoreceptors occupy the most distal layer of the retina, meaning light must pass through the proximal ganglion cell layer and inner nuclear layer before striking these light sensing cells. Photoreceptors are classified into two subtypes: rods and cones, which mediate vision during dim light and normal light conditions, respectively. Rods cannot distinguish color, but are exquisitely sensitive, as they are able to detect as

---

This dissertation follows the style of *Journal of Cell Science*.

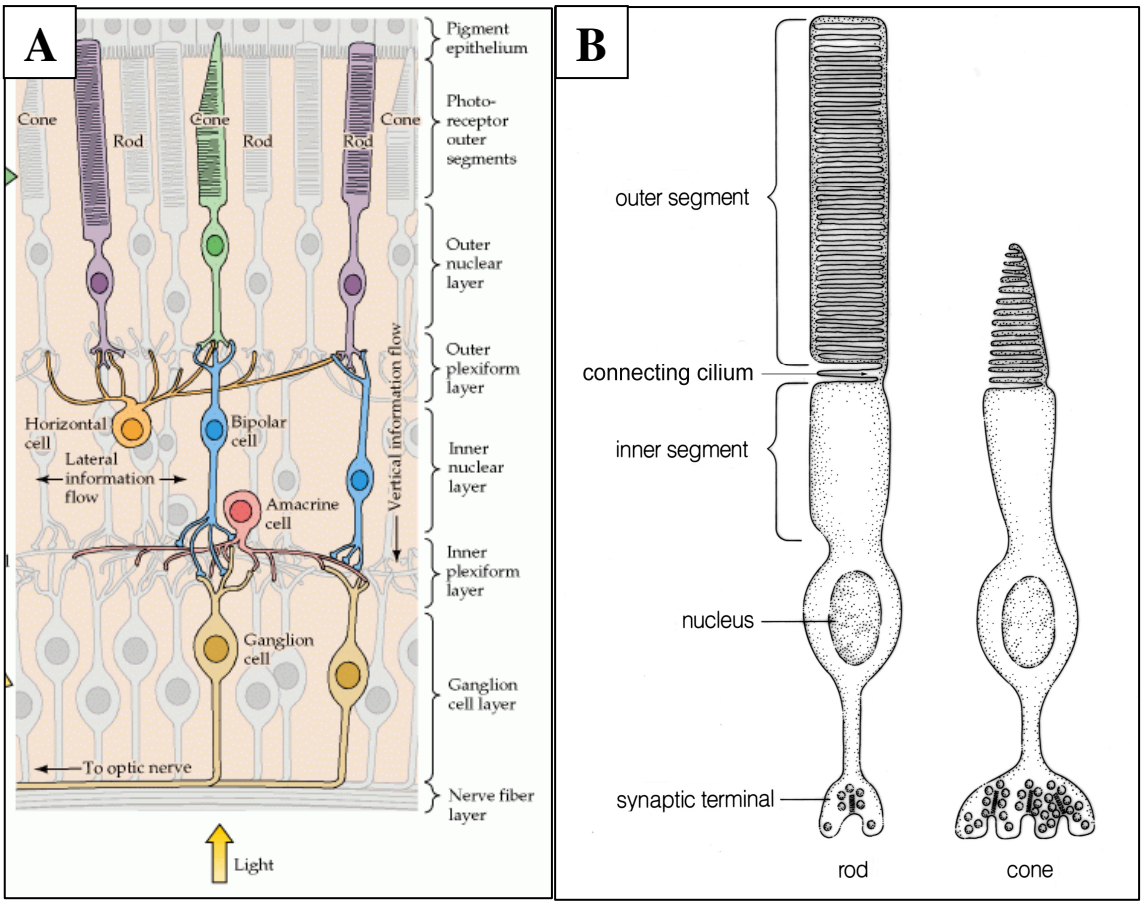

Fig.1. Cell types of the retina. (A) Diagrammatic representation of the vertebrate retina, illustrating the major retinal cell types and the basic circuitry of the retina. (B) Structure of rod and cone photoreceptors. (A) Modified from (Purves and Williams, 2001). (B) Modified from (Dowling, 2001).

little as one photon of light (Baylor et al., 1979). Cones, however, are less sensitive but are able to distinguish color based on the subtype of opsin (the protein component of the visual photopigment) that is expressed within a particular cell. Photoreceptors are highly polarized neurons that consist of an outer segment, inner segment, nucleus and a synaptic region at the basal side of the cell (Fig. 1). The outer segment is a modified sensory cilium and is the compartment of the cell that contains the proteins responsible for detection of light, and is the site where electrical signals are first generated in response to light stimuli. The inner segment is the site of protein synthesis within the photoreceptor, while the synapse is where the photoreceptor communicates with the second order neurons of the inner nuclear layer.

The molecular basis for light detection involves a signaling cascade called phototransduction. The molecule responsible for directly detecting light is rhodopsin (in rods), which is a prototypical G-protein coupled receptor that is bound to the chromophore, 11-cis-retinal. Phototransduction in cones is highly similar to rods but utilizes cone-specific versions of the rod phototransduction proteins, such as cone opsins, which are tuned to detect certain wavelengths of light. Absorption of light causes 11-cis-retinal to undergo isomerization to all-trans retinal, which induces several conformational changes in rhodopsin, generating an active form, R*. R*, in turn, activates the heterotrimeric G-protein transducin (Kwok-Keung Fung and Stryer, 1980). This is achieved through rhodopsin catalyzed exchange of GDP for GTP on the transducin α-subunit. GTP binding induces the dissociation of transducin-α from the α-β-γ transducin heterotrimer (Lerea et al., 1986). Liberated transducin-α then binds to

and activates a cGMP phosphodiesterase, which degrades intracellular cGMP, resulting in a decrease in intracellular cGMP levels. cGMP gated cation channels in the plasma membrane of the photoreceptor outer segment close as a result of lower cGMP levels, lowering the net influx of cations (primarily Na+) which causes hyperpolarization of the membrane (Tomita, 1970; Yau and Nakatani, 1985). Hyperpolarization of the membrane at the synaptic terminals slows the tonic release of neurotransmitter and thereby communicates the detection of a light stimulus to the second-order neurons of the inner nuclear layer.

Deactivation of the phototranduction machinery involves several steps. R* activity is first inhibited by phosphorylation at its C-terminus by rhodopsin kinase, though phosphorylated rhodopsin retains some activity (Palczewski et al., 1991). Phosphorylated rhodopsin is subsequently bound by arrestin, causing further deactivation (Hargrave and McDowell, 1992). The intrinsic GTPase activity of transducin-α hydolyzes bound GTP to return transducin-α to the inactive state. However, the intrinsic GTPase activity of transducin-α is slow, so this process is accelerated by the GTPase accelerating protein RGS9 (He et al., 1998). This complex biochemical pathway occurs in a sensory cilium, and the nature of the outer segment as a cilium has very specific implications for the manner by which the components of phototransduction reach the outer segment.

Cilia

Cilia and flagella are microtubule based organelles that protrude from nearly all eukaryotic cells (Fig. 2) that require the process of intraflagellar transport for their

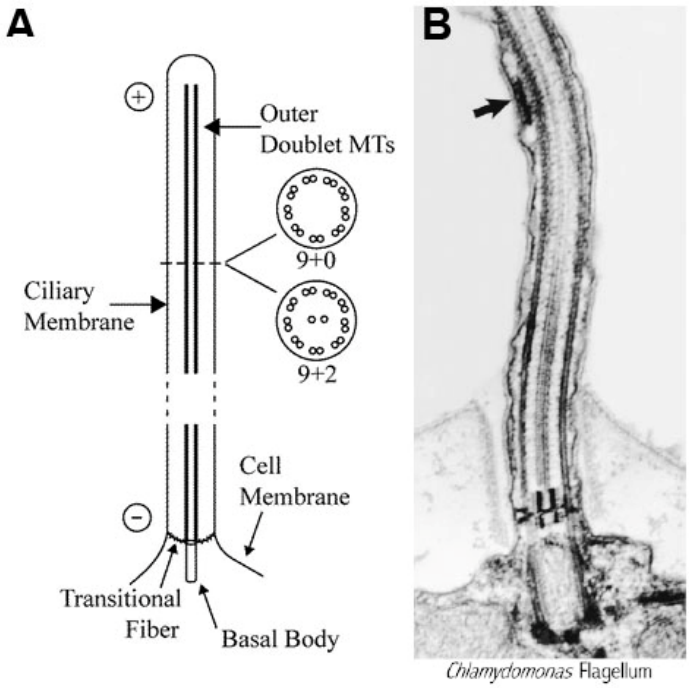

Fig. 2. The structure of cilia and flagella. (A) Diagrammatic representation of a cilium that also illustrates the organization of the microtubules of the axoneme. (B) Electron micrograph of a *Chlamydomonas* flagellum. (A) Modified from (Scholey, 2003) (B) Modified from (Rosenbaum et al., 1999).

formation and maintenance (Kozminski et al., 1995; Kozminski et al., 1993). The term flagella originally referred to long motile appendages used for locomotion (e.g. sperm flagellum), while cilia referred to shorter structures that could be motile or nonmotile. It is now clear that cilia and flagella are functionally and structurally indistinct, and these terms are used interchangeably as a result. The microtubule cytoskeleton of the cilium, known as the axoneme, is composed of an array of 9 outer doublet microtubules surrounding either central pair of microtubules (a 9 + 2 cilium) or no central pair of microtubules (a 9 + 0 cilium). Classically, 9 + 2 cilia have been known as motile cilia, while 9 + 0 cilia were called nonmotile, or primary cilia, though exceptions to these classifications exist. The axoneme extends from a microtubule based organelle called the basal body, which is derived from the maternal centriole. The basal body is composed of an array of 9 triplet microtubules termed the a, b and c subfibers, of which the a and b subfibers extend to form the ciliary axoneme. At the intersection between the basal body and axoneme is a region of the cilium called the transition zone, where filamentous fibers stretch between the ciliary membrane and distal microtubules of the basal body. The transition zone is likely a regulatory region, determining what proteins enter the cilium, and serving as an assembly site for flagellar precursor proteins. In addition to the microtubules of the axoneme, there are proteins that function to generate motility and maintain the structural integrity of the axoneme, which include the inner and outer dynein arms, radial spoke proteins and nexin. It should be noted that recent proteomic studies have identified more than 3,000 different ciliary proteins, illustrating

the tremendous structural complexity of this organelle (Liu et al., 2007; Ostrowski et al., 2002; Pazour et al., 2005; Smith et al., 2005).

Early ultrastructural studies identified cilia on many vertebrate cells where they performed functions including locomotion (sperm), fluid and mucous flow (respiratory epithelia), and sensation (photoreceptors). The various roles of cilia in these cells were obvious at the time, though perplexingly, cilia were eventually identified on nearly all eukaryotic cells where the functions of these primary cilia were not clear. In fact, the identification of cilia on fibroblasts, kidney tubule cells, neurons, Schwann cells, smooth muscle cells, and many other cells led some to initially consider these primary cilia vestigial organelles. It has only been recently with the discovery of the molecular processes that mediate cilia formation and maintenance that we have begun to understand the various and complex functions of this cryptic organelle.

Intraflagellar Transport: Discovery

IFT was first discovered in the unicellular biflagellate alga *Chlamydomonas reinhardtii* through video enhanced differential interference contrast (DIC) microscopy on paralyzed flagella mutants (Kozminski et al., 1993). Imaging of these cells revealed a bidirectional movement of granular particles within the flagellum at rates of 2-3.5μm/sec. Initial electron microscopic analyses of *Chlamydomonas* flagella found electron-dense rafts of protein between the outer doublet microtubules of the ciliary axoneme and plasma membrane. Indeed, correlative microscopy techniques later demonstrated these rafts to be the particles observed to undergo IFT (Kozminski et al., 1995).

Studies utilizing a temperature-sensitive flagella mutant, *fla10*, which encodes the *Kif3A* subunit of kinesin II, demonstrated flagellar IFT movements ceased when these mutants were moved to the restrictive temperature, implicating kinesin II as a molecular motor involved in IFT. The *fla10* mutant has been an invaluable resource in the study of IFT, as it was later used to generate flagellar protein extracts lacking IFT particles (Piperno and Mead, 1997). Comparison of these extracts to flagellar extracts with IFT particles on sucrose density gradients revealed that the IFT proteins form a 17s complex, and was the basis for identification of nearly all IFT proteins (Cole et al., 1998; Piperno and Mead, 1997), the number of which is currently 17 (Table 1).

The Mechanism of IFT

The process of IFT is currently defined as the movement of a multisubunit protein complex (the IFT particle) and its associated cargoes along a ciliary axoneme (Fig. 3). Studies in organisms as diverse as *Chlamydomonas, Tetrahymena, C. elegans, Drosophila,* trypanosomes, mice and zebrafish have shown that the process of IFT is conserved among nearly all eukaryotes (Avidor-Reiss et al., 2004; Han et al., 2003; Kozminski et al., 1995; Pazour et al., 2000; Qin et al., 2001). The IFT particle itself is composed of two subcomplexes, complex A and complex B, based on differential sedimentation on sucrose density gradients (Cole et al., 1998; Ou et al., 2005; Piperno and Mead, 1997). In general, complex A is thought to mediate retrograde IFT as mutations in complex A genes yield short cilia that accumulate IFT particles at the distal tip (Cortellino et al., 2009; Iomini et al., 2001; Lee et al., 2008). In contrast, complex B mediates anterograde IFT, as null mutations in *ift88*, *ift172*, and *ift52* all lack flagella

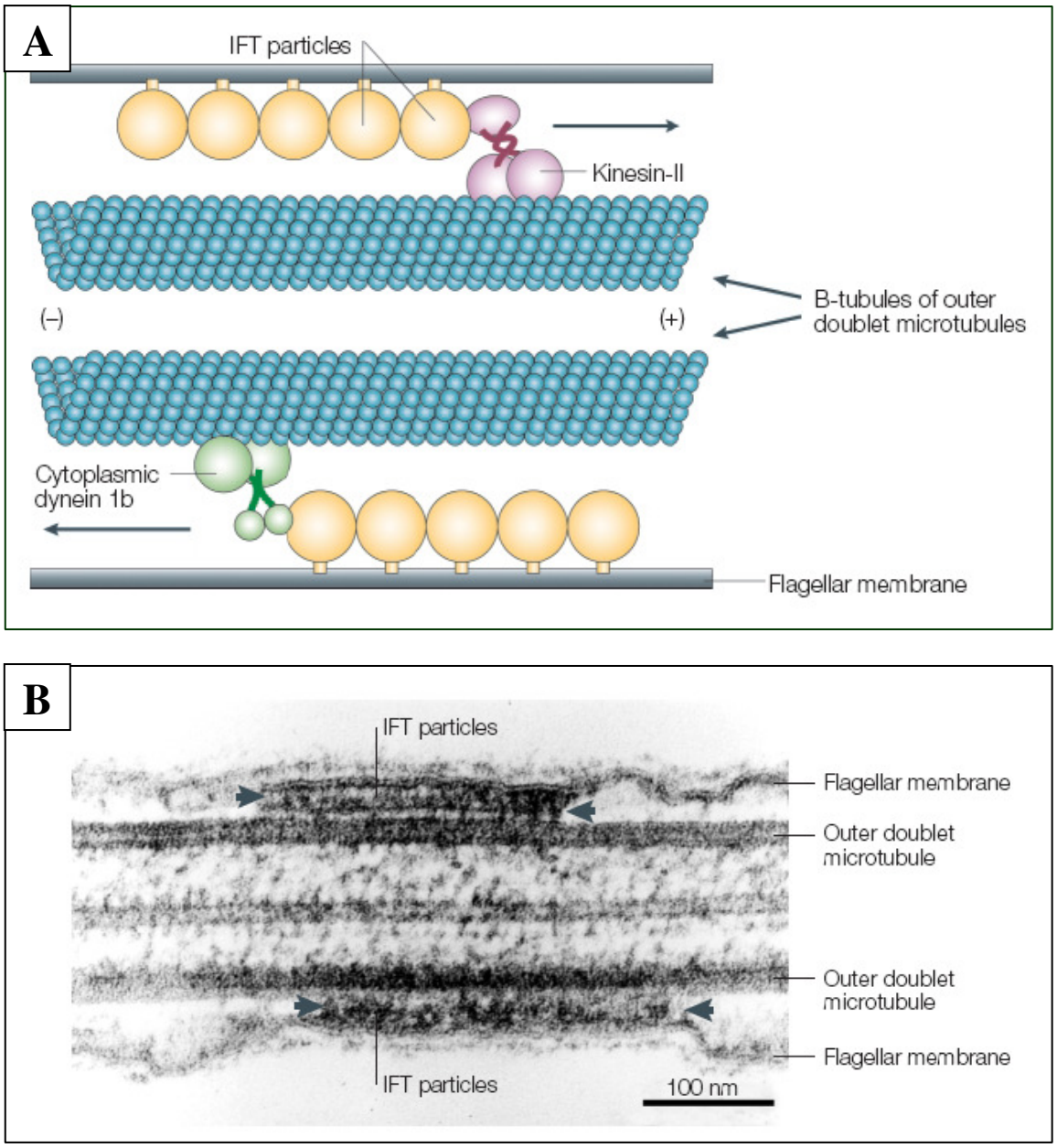

Fig. 3. Intraflagellar transport. (A) A diagrammatic representation of IFT illustrates the IFT particles associate with both molecular motors and cargoes and move along the outer doublet microtubules of the ciliary axoneme. (B) An electron micrograph of IFT particles in a *Chlamydomonas* flagellum, arrows indicate IFT particle oligomers. (A) and (B) Modified from (Rosenbaum and Witman, 2002).

(Rosenbaum and Witman, 2002). The anterograde movement of the IFT complex is mediated by two molecular motors, kinesin II and OSM-3 (Cole et al., 1998; Snow et al., 2004). Kinesin II is a heterotrimeric microtubule plus-end motor consisting of two motor domains, *Kif3A* and *Kif3B*, and an accessory subunit, *KAP*. OSM-3 is a homodimeric kinesin first identified in *C. elegans*, and is homologous to mammalian KIF17. In *C. elegans*, these two motors function in a cooperative manner, where kinesin II drives anterograde movement along the proximal cilium composed of doublet microtubules, while OSM-3 drives anterograde movement along the distal singlet microtubules (Snow et al., 2004). Once the IFT particle reaches the tip of the cilium, through a poorly understood mechanism, the IFT particle undergoes structural rearrangements and switches from the anterograde motors to the retrograde IFT motor, cytoplasmic dynein-2. Recent data suggest *ift172* may play a role in this process (Pedersen et al., 2005; Tsao and Gorovsky, 2008).

The retrograde IFT motor, cytoplasmic dynein-2, is composed of a homodimeric heavy chain, *dync2-h1* (Pazour et al., 1999; Porter et al., 1999; Signor et al., 1999), and the accessory subunits cytoplasmic dynein-2 light intermediate chain, *dync2-li1* (Hou et al., 2004; Mikami et al., 2002; Perrone et al., 2003), intermediate chain, *dync2-i1* (Rompolas et al., 2007), and light chain known as LC8 (Pazour et al., 1998; Rompolas et al., 2007). *Dync2-h1* is a force-generating adenosine triphosphatase (ATPase) that forms the core of a macromolecular complex though its associate with the accessory subunits, which are thought to mediate physical interactions between cytoplasmic dynein-2 and

Table 1. Components of the IFT machinery. Table shows the IFT genes identified for *Chlamydomonas, C. elegans*, and humans. Modified from (Pedersen and Rosenbaum, 2008).

IFT polypeptide	Chlamydomonas	C. elegans	H. sapiens
Kinesin-2			
Heterotrimeric	FLA10	KRP85/ KLP-20	KIF3A
	FLA8	KRP95/ KLP-11	KIF3B
	FLA3	KAP/KAP-1	KAP
Homodimeric	?	OSM-3	KIF17
Cytoplasmic dynein 2			
	DHC1b	CHE-3	DYNC2H1/ DHC2
	D1bLIC	D2LIC/ XBX-1	DYNC2LI1/ D2LIC
	FAP133	?	WD34
	LC8/FLA14	?	?
Complex A			
IFT144	FAP66	DYF-2	WDR19
IFT140	IFT140	CHE-11	IFT140
IFT139	FAP60	ZK328.7	THM-1
IFT122A	XP_001700201.1	DAF-10	IFT122/ WDR10
IFT122B	IFT122B	IFTA-1	WDR35
IFT43	FAP118	?	?
Complex B			
IFT172	IFT172	OSM-1	IFT172
IFT88	IFT88	OSM-5	IFT88/Polaris
IFT81	IFT81	F32A6.2	IFT81
IFT80	IFT80	CHE-2	IFT80
IFT74/72	IFT74/72	C18H9.8	IFT74/72
IFT57	IFT57	CHE-13	IFT57/Hippi
IFT52	IFT52	OSM-6	IFT52/NGD5
IFT46	IFT46	DYF-6	C11orf60
IFT27	IFT27	?	RABL4
IFT20	IFT20	Y110A7A.20	IFT20
New putative IFT proteins			
	FAP259	DYF-1	TPR30A
	FAP22	DYF-3	CLUAP1
	XM_001698717.1	DYF-13	TTC26
	FAP116	DYF-11	MIP-T3

cargoes (Gibbons et al., 1994; Zhang et al., 1993). Mutations in *dync2-h1*, *dync2-li1* and LC8 all result in defective retrograde IFT and exhibit similar ciliary phenotypes, characterized by stunted cilia with swollen ciliary tips that contain disorganized microtubules, IFT proteins and cellular debris. *dync2-i1*, however, was only shown biochemically to be part of the cytoplasmic dynein 2 macromolecular complex (Rompolas et al., 2007), but the ciliary phenotype resulting from *dync2-i1* dysfunction remains unknown. Consistent with a role in IFT, knockdown of the *Trypanosome dync2-i1* homologue resulted in flagellar dysfunction (Baron et al., 2007).

Structure of the IFT Complex and Roles of Individual IFT Particle Proteins

Recent biochemical studies, predominantly in *Chlamydomonas*, have started to reveal the structural composition of the IFT particle and specific interactions between individual IFT proteins, particularly within complex B. Complex B is composed of at least 11 proteins in *Chlamydomonas*, and a subset of these form a core consisting of an *Ift72/74-Ift80* tetramer along with *Ift88*, *Ift81*, *Ift52* and *Ift46* (Lucker et al., 2005). The outer surface of complex B is composed of *Ift20*, *Ift57* and *Ift172*. Data from yeast two-hybrid experiments indicate direct interactions between *Ift72/74* and *Ift81* and between *Ift57* and *Ift20*. Similar approaches indicated interactions between *Ift20* and the *Kif3B* subunit of kinesin II (Baker et al., 2003; Lucker et al., 2005). While the *Ift72/74-IFT80* interaction likely forms the structural core of complex B, the functional nature of the interactions described for the outer surface IFT proteins remains unclear.

Evaluating the function of individual IFT proteins within the IFT particle has been difficult, as mutation of most IFT genes results in failed ciliogenesis. This has been

compounded by the fact that little functional data can be gleaned from analyses of IFT protein structures, as they are composed principally of domains associated with transient protein-protein interactions, with the notable exception of *Ift27*, which has a predicted enzymatic function as a small GTPase (Cole, 2003). However, mutational and biochemical analyses have elucidated the functional importance of several IFT proteins. First, *Ift27* has been shown to be a small G-protein (Qin et al., 2007) that plays a role in cell-cycle control, as partial knockdown yields defective cytokinesis and abnormal progression of the cell cycle in *Chlamydomonas*. *Ift46* appears to play a role in transport of outer dynein arms, a component of the axoneme (Hou et al., 2007) through its interaction with the outer dynein arm-16 gene product (Ahmed et al., 2008), suggesting that some IFT proteins may be specialized for transport of specific cargoes. *Ift20* plays a role in transport of membrane bound cargoes from the Golgi to the ciliary base (Follit et al., 2006a; Omori et al., 2008). Finally, *Ift172* mediates the exchange of molecular motors at the ciliary tip, an integral step in the transition from anterograde to retrograde IFT (Pedersen et al., 2005; Tsao and Gorovsky, 2008). Though these studies have provided valuable insights into the mechanism of IFT, much of the mechanistic details behind IFT are unknown. For example, the IFT complex associates with three molecular motors, however, it is unknown which IFT proteins directly mediate these interactions or how the IFT complex dissociates from these motors, an important step in switching motors at the ciliary tip and at the base of the cilium. It is known that IFT complexes dissociate once they return to the base of the cilium, presumably to liberate IFT proteins for assimilation into new IFT particles (Cole et al., 1998; Iomini et al., 2001), however,

the mechanisms behind IFT particle assembly and disassembly are completely unknown. Though progress has been made in the study of IFT, much of the fine mechanistic details behind IFT and its regulation remain to be elucidated.

IFT Cargoes

As early studies found that IFT was required for cilia formation and maintenance, it is not surprising that the first identified cargoes of IFT were structural components of the axoneme, such as tubulin, radial spoke proteins and outer dynein arms (Hou et al., 2007; Qin et al., 2004). Though these cargoes are soluble, it is apparent that many of the putative cargoes of IFT are membrane bound, such as the TRPV channel, polycystin 1 and 2, cyclic-nucleotide gated channel -1, the G-protein coupled receptors rhodopsin, and possibly somatostatin receptor type 3 and melanin-concentrating hormone receptor-1 (Bae et al., 2006; Berbari et al., 2008b; Follit et al., 2006a; Pazour et al., 2002b; Qin et al., 2005; Tsujikawa and Malicki, 2004). Several of these potential cargoes, however, were identified based on mislocalization data. The fact that IFT dysfunction compromises cilium integrity necessitates rigorous validation of these cargoes, which has been done with only a few cargoes, including the TRPV channel and rhodopsin. For example, co-immunoprecipitation studies found that rhodopsin interacts with the IFT particle (Insinna and Besharse, 2008). It is striking that direct interactions between IFT proteins and cargoes have not been shown. This may be due to the presence of adaptor proteins, as has been shown for the transport of outer dynein arms (Ahmed et al., 2008), or the transport of cargoes in large pre-assembled complexes, as is the case for radial spoke proteins (Qin et al., 2004). Another possibility is that IFT is a general mechanism

for protein transport and that specificity of cargoes transported is defined by the composition of the vesicle in which a cargo is packaged. Consistent with this, a recent study found that the outer segment is the default destination for membrane bound cargoes in a photoreceptor, raising the possibility that many cargoes 'hitch a ride' with others targeted for the cilim (Baker et al., 2008)

IFT and Photoreceptors

As described earlier, photoreceptors are highly polarized neurons that have a modified sensory cilium known as the outer segment. Though the study of IFT has only been around for 16 years, important details about how this process works in photoreceptors can be learned from much earlier studies of the retinal photoreceptors. The nature of the outer segment as a cilium was one of the earliest ultrastructural observation of photoreceptors, described by Eduardo De Robertis in 1956 (De Robertis, 1956). Indeed, a following study on the developing retina of rats and mice revealed that the early stages of outer segment morphogenesis resembled that of ciliogenesis (Fig. 4), and could be defined in three stages. The initial budding of a primary cilium (then called a primitive cilium) was followed by an accumulation of membrane and protein at the distal tip of the cilium. In the third stage, the disorganized membrane and protein became organized into arrays of membrane arranged in parallel with a periodicity of approximately 210Å. Though it could be inferred from these early studies that the connecting cilium was the route by which proteins moved to the outer segment, it was not formally addressed until a series of illuminating experiments were performed by

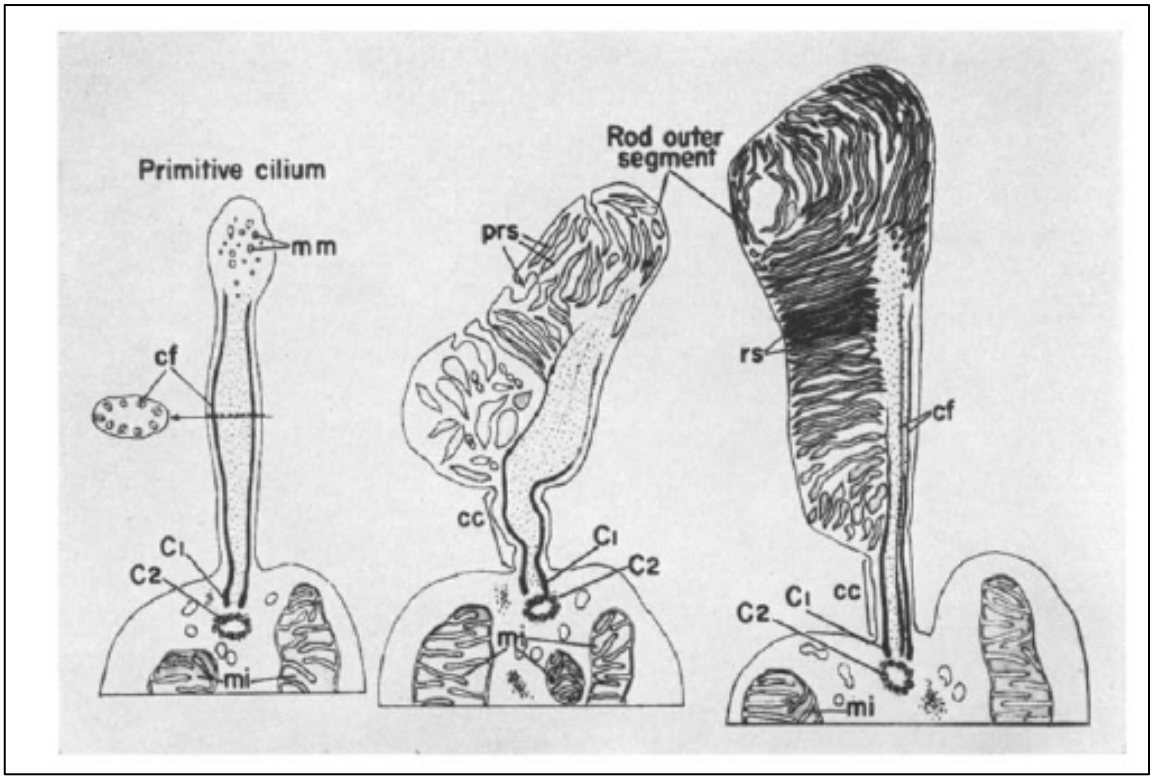

Fig. 4. The initial stages of outer segment formation resemble ciliogenesis. Morphogenic material (mm) accumulates at the distal tip of a primary cilium, which aggregates to form photoreceptor sacs (prs), that later become organized rod sacs. (cc) connecting cilium, (cf) ciliary fibers, (C1 and C2) basal body. Modified from (De Robertis, 1960).

Richard Young in the 1960s. Utilizing a procedure whereby radioactive amino acids were administered to rats, mice and frogs, they could monitor where in the photoreceptor these newly synthesized proteins were integrated. Their striking results showed that in rods, newly synthesized proteins are first observed in the Golgi, then migrate through the connecting cilium to the outer segment. Within the outer segment, newly synthesized proteins were integrated at the base of the outer segment (as seen by a band of radioactivity on micrographs). This band of radioactivity progressively migrated apically along the outer segment until it was eventually integrated into adjacent retinal pigmented epithelial (RPE) cells. These studies revealed three important things about the biology of the photoreceptor. First, it provided important data to suggest that proteins move to the outer segment through the connecting cilium. Second, it showed that the outer segment is replaced periodically, approximately every two weeks, and that the RPE phagocytosed the shed tips of outer segments. Lastly, when the process of IFT is considered, it indicates that the IFT complex releases some of its cargoes at the base of the outer segment. In contrast, it was determined that in the frog cones, that newly synthesized proteins were integrated diffusely throughout the outer segment, raising the possibility that the mechanism of IFT differs slightly between rods and cones (Young, 1967; Young, 1969). These data indicate that in photoreceptors, there are at least two sites of cargo release by IFT, the base of the outer segment, and the tip of the outer segment where the structural components of the axoneme are delivered. This suggests that photoreceptor regulation of cargo dissociation may occur differently than in other cilia.

The observations by Richard Young that the outer segment is periodically replaced raised an important problem in the field of photoreceptor cell biology. It had been shown in *Xenopus* that approximately 64 new outer segment discs were formed within an eight hour period, which corresponds to ~3,600 μm^2 of membrane (Besharse et al., 1977a; Besharse et al., 1977b; Besharse and Pfenninger, 1980). The mechanism by which a photoreceptor managed to traffic such a tremendous amount of membrane to the outer segment was unclear. A series of ultrastructural studies of light adapting *Xenopus* photoreceptors found that electron lucent vesicles accumulated around the base of the connecting cilium and along an adjacent structure known as the periciliary region. These vesicles, later shown to contain rhodopsin, between the cilium and periciliary regions were also observed to fuse with the plasma membrane, suggesting that rhodopsin bearing vesicles fuse with the plasma membrane before the rhodopsin is delivered to the outer segment. Consistent with these data, subsequent studies successfully immunolocalized rhodopsin to the connecting cilium plasma membrane (Wolfrum and Schmitt, 2000). Thus, it appears as if IFT transports rhodopsin while it is embedded in the ciliary plasma membrane, similar to what has been described for the TRPV channel in *C. elegans* sensory neurons (Qin et al., 2005).

The first evidence to directly suggest a role for IFT in protein transport to outer segments was obtained through the analysis of a photoreceptor specific knockout of murine *Kif3A*, a kinesin II subunit. These mice exhibited opsin and membrane accumulation within the inner segment of photoreceptors that eventually underwent apoptosis (Marszalek et al., 2000). However, potential pleiotropic effects of the *Kif3A*

mutation on photoreceptors prevented any direct link between IFT and protein trafficking in photoreceptors. Subsequently, the TG737^{orpk} mouse, a mutant that was a model for polycystic kidney disease (Moyer, 1994), was shown to disrupt the *ift88* gene, reducing expression of *ift88* by 90% (Pazour et al., 2000). A following study showed TG737^{orpk} mutants exhibited progressive photoreceptor degeneration and defects in opsin transport (Pazour et al., 2002a). This work provided the first direct evidence for the role of IFT in protein transport in photoreceptors. Further study utilizing an ENU-induced mutation in zebrafish *ift88* found that IFT was essential for outer segment formation, opsin transport and photoreceptor survival (Tsujikawa and Malicki, 2004). These studies all noted mislocalized opsins and defective outer segment morphogenesis when anterograde IFT was compromised, yet the role of retrograde IFT in photoreceptors was less clear. The cytoplasmic dynein-2 heavy chain and light intermediate chain are both expressed in photoreceptors and localize to the connecting cilium, implying that retrograde IFT occurs in photoreceptors (Mikami et al., 2002). However, the only study that investigated the effects of loss of retrograde IFT noted that knockdown of *ift140* did not affect photoreceptor survival to the extent of mutation of *ift88* (Tsujikawa and Malicki, 2004)

Golgi to Cilium Rhodopsin Trafficking

Ciliary transport of cargoes to the photoreceptor outer segment is an essential process for photoreceptor survival, however, these cargoes must first be properly targeted to the base of the cilium before the process of IFT can deliver them to the outer segment. Rhodopsin is the predominant protein in the outer segment and appears to be

the most important outer segment protein from the perspective of human disease, so the intracellular trafficking of rhodopsin will be discussed here. Rhodopsin contains a sorting sequence at its C-terminus consisting of a VXPX motif, where X is any amino acid (Deretic et al., 2005; Mazelova et al., 2009). Newly synthesized rhodopsin in the Golgi directly binds to ADP-ribosylation factor 4 (ARF4), which mediates the incorportation of rhodopsin into specialized post-Golgi rhodopsin transport carriers (RTCs). Without ARF4, rhodopsin remains trapped in the Golgi. The intracellular targeting of these rhodopsin-bearing vesicles is through Rab6 and Rab8, as expression of mutant forms of Rab8 causes accumulation of rhodopsin-bearing vesicles and the base of the cilium (Deretic et al., 1995; Moritz et al., 2001). Ezrin and Moesin, proteins involved in apical membrane trafficking may also play a role in targeting of rhodopsin, because they localize to post-golgi rhodopsin vesicles (Deretic et al., 2004). The physical movement of RTCs is likely mediated by cytoplasmic dynein-1, as the C-terminus of rhodopsin physically interacts with the cysoplasmic dynein-1 light chain tctex-1 and expression of mutant tctex-1 causes rhodopsin mislocalization (Tai et al., 1999; Yeh et al., 2006). Consistent with a general role for cytoplasmic dynein-1 in apical trafficking of vesicles, inhibition of cytoplasmic dynein-1 function caused mislocalization of RPGR, the retinitis pigmentosa GTPase regulator protein that localizes to the basal body and cilium of photoreceptors (Khanna et al., 2005). These data are consistent with the orientation of microtubules between the Golgi and basal body. However, the delivery of RTCs by cytoplasmic dynein-1 remains controversial because addition of microtubule

depolymerizing agents did not result in mistargeted rhodopsin bearing vesicles (Vaughan et al., 1989)

Once at the basal body, rhodopsin bearing vesicles likely associate with the IFT particle via Rab8 through its interaction with the endocytic regulator Rabaptin 5. Rabaptin 5 also interacts with *elipsa*, the zebrafish homologue of *C. elegans* Dyf-11, and a putative IFT protein (Bacaj et al., 2008; Kunitomo and Iino, 2008; Li et al., 2008; Omori et al., 2008). Elipsa also interacts with *Ift20*, illustrating a direct sequence of protein-protein interactions between the IFT particle and rhodopsin bearing vesicles. Additionally, *Ift20* localizes to the Golgi, suggesting it may also play a role in targeting of post-Golgi RTCs to the photoreceptor cilium, just as it does for the transmembrane protein Pkd2 (Follit et al., 2008; Follit et al., 2006a). Interestingly, Rab8 has recently been shown to be essential for cilium formation and to play a role in promoting ciliary membrane biogenesis (Nachury et al., 2007; Omori et al., 2008). This suggests that rhodopsin trafficking may be through a cilium-specific post-Golgi mechanism, and that other GPCRs localized to cilia may utilize this pathway as well.

Defective Protein Trafficking and Human Disease

Retinitis Pigmentosa (RP) is the most common genetic disease that causes blindness, affecting approximately 1 in 4000 individuals. RP is a broadly defined genetic disease, characterized by progressive degeneration of photoreceptors and the RPE (Heckenlively, 1988). Those affected initially report night blindness, followed by progressive loss of the peripheral visual field, and eventually complete loss of vision for some. The genetic lesions that can cause RP occur at numerous loci, though the most

common locus is that of the visual pigment rhodopsin, of which about 150 different mutations have been described (Garriga and Manyosa, 2002). In fact, some of the most severe forms of RP have been mapped to lesions at the C-terminus of rhodopsin including P347L and S344Ter, indicating that this region is especially important in this disease. In fact, the C-terminal tail of rhodopsin contains a sorting sequence that is necessary and sufficient for transport to the outer segment (Perkins et al., 2002; Tam et al., 2000). Mutations in this region result in protein accumulation in the inner segment and at the base of the connecting cilium in mice, rats, and frogs (Green et al., 2000; Li et al., 1996; Sung et al., 1994; Tam et al., 2000), leading to photoreceptor degeneration. Rhodopsin mislocalization, and consequently retinal degeneration, also occurs in animals with mutations in the molecular motors kinesin II (Marszalek et al., 2000) and the dynein light chain Tctex-1 (Tai et al., 1999). It is imperative, therefore, that cargo targeted for the outer segment reach its destination or retinal degeneration will occur. Thus, both mutations within the opsin gene and mutations in the transport machinery can cause retinal degenerative diseases.

Choroideremia

One human disease resulting from defective intracellular protein trafficking is choroideremia (CHM). CHM is an X-linked retinal degenerative disease caused by mutation of the Rab escort protein 1 (REP1) gene (Cremers et al., 1990a; Seabra et al., 1992). This disease presents in early adulthood as night blindness, and the vision of those affected continues to progress until complete blindness is reached in middle age.

Clinically, CHM patients show patchy depigmentation of the RPE, abnormal vasculature of the choroid, and degeneration of photoreceptors and RPE.

Humans have two REP genes, REP1 and REP2, that are expressed ubiquitously and are partially functionally redundant, interacting with many shared substrates (Seabra, 1996). REPs are essential for the maturation of Rab proteins, the small GTPase proteins that are required for targeting of post-Golgi vesicles and thus, proper intracellular transport. Briefly, REP binds to a newly synthesized Rab protein in the cytosol and escorts it to an enzymatic protein complex called geranyl geranyl transferase II, which catalyzes the addition of a geranyl geranyl group to a double Cys motif on the Rab C-terminus. The REP subsequently transfers the modified Rab to its appropriate target membrane where the geranyl geranyl group embeds into the cytosolic face of the appropriate membrane. Membrane localization is required for Rab function, thus, without REP function, Rab proteins are rendered nonfunctional and intracellular vesicular trafficking is compromised.

Exactly how REP1 dysfunction leads to CHM is currently unclear. Though both photoreceptors and RPE degenerate in this disease, it is unknown if the primary defect is in photoreceptors or the RPE. Rab6 and Rab8 play an essential role in targeting post-Golgi vesicles to the outer segment, therefore, one explanation for photoreceptor death in CHM is that Rab6 and Rab8 dysfunction leads to opsin mislocalization, which kills the photoreceptor. However, opsin mislocalization is not typically observed in CHM patients or animal models, though it has been documented in one female carrier of this disease (Bonilha et al., 2008). Alternatively Rab27a, a known target of REP1,

facilitates melanosome transport and may mediate phagocytosis of shed outer segment disks (Gibbs et al., 2004; Gibbs et al., 2003; Seabra et al., 1995). Thus, RPE degneneration could be explained by defective phagocytic function of the RPE. A third possibility is that defective RPE creates a toxic environment for photoreceptors, resulting in photoreceptor cell death. Consistent with this, previous studies have noted that the severity of degeneration of the RPE does not always correlate with that of photoreceptors, suggesting that these two tissues degenerate independently (Syed et al., 2001; Tolmachova et al., 2006). Though it is clear that CHM is the result of defective intracellular protein trafficking, the primary tissue affected needs to be determined in order to design targeted therapies to treat this disease.

The Ciliopathies

The study of cilia has experienced an incredible surge in interest over the past several years, in large part due to the realization that cilia play a central role in a number of human diseases, now known collectively as ciliopathies. The basis for much of our understanding about the role of cilia in human disease comes from the Oak Ridge Polycystic Kidney (ORPK) mouse, reviewed in (Lehman et al., 2008). The ORPK mouse was originally identified through an insertional mutagenesis screen and later found to partially disrupt expression of the *ift88* gene (Moyer, 1994; Yoder et al., 1995). Several studies found these mutants exhibited polycystic kidneys, liver abnormalities, retinal degeneration, anosmia, hydrocephaly, skeletal abnormalities, polydactyly and *situs inversus* (Banizs et al., 2005; Haycraft et al., 2007; Murcia et al., 2000; Pazour et al., 2002a; Pazour et al., 2000; Serra, 2008; Zhang et al., 2005). Remarkably, several

human diseases display a similar constellation of phenotypes exhibited by this mutant, thereby providing the initial link between cilia and human disease. These diseases, or ciliopathies, include Bardet-Biedl syndrome, Senor-Loken syndrome, nephronophthisis, Meckel-Gruber Syndrome, Oral-Facial-Digital Syndrome, Joubert Syndrome, Jeune asphyxiating thoracic dystrophy, and Alstrom syndrome (Beales et al., 2007; Pazour and Rosenbaum, 2002; Snell et al., 2004). Many human genetics studies have begun to identify the genes responsible for these human diseases, expanding the number of cilia-related genes.

Jeune Asphyxiating Thoracic Dystrophy

It is known that cilia defects cause human diseases, but only one disease is known to be the direct result of a mutation in an IFT gene. Jeune asphyxiating thoracic dystrophy (JATD) is a genetically heterogeneous disease characterized by retinal degeneration, polydactyly, polycystic kidneys, and chondrodysplasia. A recent study found one subtype of JATD is cause by mutation of *IFT80*, validating the role of IFT in human disease (Beales et al., 2007).

Bardet-Biedl Syndrome

There are examples where identification of human disease genes has helped identify new genes involved in cilia biology. Bardet-Biedl Syndrome (BBS) is a rare genetic disease characterized by obesity, polydactyly, mental retardation, kidney abnormalities, hypogenitalism and diabetes (Blacque and Leroux, 2006; Mykytyn et al., 2004; Nishimura et al., 2004; Tobin and Beales, 2007). These phenotypes are variable, likely due to the genetic heterogeneity of the disease, as there are 14 genes known to

cause BBS, named BBS1-14. In fact, many of the BBS proteins form a multisubunit protein complex called the BBSome (Nachury et al., 2007). Though the exact function of many of these proteins is unclear, it is apparent that they are all involved in some aspect of cilia structure or function. For example, BBS7 and BBS8 have been shown to undergo IFT in *C. elegans* through functional interactions with the IFT particle. Interestingly, it appears as if BBS7 and BBS8 serve to coordinate the function of the anterograde IFT motors kinesin II and OSM-3 by tethering the IFT complex A and complex B together (Ou et al., 2005). In contrast, the G-protein coupled receptors that play a regulating feeding behavior, somatostatin receptor type 3 and melanin-concentrating hormone receptor 1 were mislocalized in BBS2 and BBS4 mutant neurons, which have apparently normal cilia (Berbari et al., 2008a). Taken together, these data suggest that BBS proteins tend to function in the trafficking of proteins to the basal body and perhaps regulation of IFT. Elucidating the functions of each BBS protein in cilia biology will provide valuable insights into the mechanisms underlying the human disease condition.

Cilia Disease Phenotypes Resulting from Impaired Cellular Signaling

Though the number of different ciliopathies known to clinicians is impressive, it is striking that only one IFT protein has been implicated as the cause of human disease. The mutations described for *IFT80* are amino acid substitutions, indicating these mutant forms of *IFT80* could retain some function. The paucity of IFT genes identified as disease genes can likely be explained by the lethal phenotype of mouse null mutations in IFT genes. For example, several chemically induced mutations that caused sonic

hedgehog (shh) signaling defects were mapped to IFT genes, including *ift88*, *ift172* and *dync2-h1* (Huangfu and Anderson, 2005; Huangfu et al., 2003; May et al., 2005). Subsequent studies have shown IFT proteins are necessary for correct processing and function of the transcription factors *Gli2* and *Gli3*, effectors of shh signaling. Additionally, the shh receptor smoothened localizes to the primary cilium when ligand is present, suggesting this too, plays an important role in shh signal transduction. (Corbit et al., 2005; Haycraft et al., 2005; May et al., 2005).

Similarly, cilia have also been shown to be involved in planar-cell-polarity signaling, PDGF signaling, and possibly BMP signaling. The integral role of cilia in diverse signaling pathways has led many to consider the primary cilium to function as a "cellular antennae" of sorts, an area of the cell where extracellular cues are detected and integrated. Thus, it is likely that null mutations in IFT genes have not been identified as disease genes because these embryos are inviable. Instead, human diseases are caused by mutations that only affect one aspect of cilia function, or represent hypomorphic alleles that result in cilia that are partially functional.

Dissertation Objectives

The goal of my work is to understand how proteins are trafficked within a photoreceptor and the functional consequences resulting from dysfunction of these processes. By using a combination of genetics, cell biology, biochemistry and molecular biology I model the pathology of a human disease and make contributions to the understanding of molecular mechanisms behind ciliary protein trafficking, the conclusions of which are broadly applicable to other types of cilia.

Chapter II is a study designed to address two competing hypotheses in the field of choroideremia research regarding the primary tissue defect that causes retinal degeneration in this disease. Using the technique of blastomere transplantation and a zebrafish line with a mutation in the zebrafish *rep1* gene, I demonstrate that *rep1* mutant photoreceptors do not degenerate when placed opposite a wild type RPE. In contrast, *rep1* mutant RPE is sufficient to cause degeneration of wild type photoreceptors. These studies show that photoreceptor degeneration in CHM is non-cell autonomous and is caused by defective RPE. Additionally, this study indicates that human therapies designed to treat CHM should target the RPE.

Chapter III utilizes a combination of cell biology, biochemistry and genetics to elucidate the role of the *Ift57* protein within photoreceptors and the intraflagellar transport particle. A phenotypic analysis reveals that, unlike previously described IFT mutants, the process of IFT is partially functional when *Ift57* is lost in photoreceptors. I go on to show, using a series of co-immunoprecipitation experiments, that kinesin II fails to dissociate from the IFT particle, while *Ift20* does not associate with the IFT particle in *Ift57* mutants. I therefore conclude that *Ift57* is only required for efficient IFT, because it mediates the ATP-dependent dissociation of kinesin II from the IFT particle, likely through *Ift20*.

Chapter IV addresses the function of retrograde IFT in the context of photoreceptors, an aspect of IFT in photoreceptor biology that has, until now, remained uninvestigated. Utilizing morpholinos directed against the heavy chain, light intermediate chain and intermediate chain subunits of cytoplasmic dynein-2, the

retrograde IFT motor, I show that retrograde IFT is necessary for outer segment extension, organization and the recycling of IFT protein subunits. Addtionally, I show that dynein morphants have defects in retinal electrophysiology, suggesting these proteins may play a greater role in retinal physiology. Furthermore, I provide the first functional data that show the intermediate chain subunit of cytoplasmic dynein-2 is required for retrograde IFT function. Overall, this study provides the first functional evidence that retrograde IFT plays an important role in photoreceptor structure and function.

CHAPTER II

NONCELL-AUTONOMOUS PHOTORECEPTOR DEGENERATION IN A ZEBRAFISH MODEL OF CHOROIDEREMIA*

OVERVIEW

This study analyzes the cause of photoreceptor degeneration in zebrafish *rep1* mutants. Joe Bilotta of Western Kentucky University is a collaborator who performed the ERG analysis on *rep1* mutants.

SUMMARY

Choroideremia is an X-linked hereditary retinal degeneration resulting from mutations in the Rab escort protein-1 (*REP1*). The Rep1 protein facilitates post-translational modification of Rab proteins, which regulate intracellular trafficking in the retinal pigment epithelium (RPE) and photoreceptors and are likely involved in the removal of outer segment disk membranes by the RPE. A critical question for potential treatment of choroideremia is whether photoreceptor degeneration results from autonomous defects in opsin transport within the photoreceptor or as a non-autonomous and secondary consequence of RPE degeneration. To address this question, we have characterized the retinal pathology in zebrafish *rep1* mutants, which carry a recessive nonsense mutation in the *REP1* gene. Zebrafish *rep1* mutants exhibit degeneration of

---

the RPE and photoreceptors and complete loss of visual function as measured by electroretinograms. In the mutant RPE, photoreceptor outer segment material was not effectively eliminated and large vacuoles were observed. However, opsin trafficking in photoreceptors occurred normally. Mosaic analysis revealed that photoreceptor degeneration was non-autonomous and required contact with the mutant RPE as mutant photoreceptors were rescued in wild type hosts and wild type photoreceptors degenerated in mutant hosts. We conclude that mutations in *REP1* disrupt cellular processes in the RPE, which causes photoreceptor death as a secondary consequence. These results suggest that therapies that correct the RPE may successfully rescue photoreceptor loss in choroideremia.

INTRODUCTION

Choroideremia (CHM) is an X-linked form of retinal degeneration caused by mutations in the gene for Rep1 (Rab escort protein 1) (Cremers et al., 1990b; Seabra et al., 1992), a protein found in all tissues and highly expressed in the outer retina and retinal pigment epithelium (RPE). CHM causes night-blindness in children and progresses to complete loss of vision in adults. CHM is one of the few hereditary blindness disorders that can be clinically identified before significant loss of visual function (Sorsby et al., 1952), suggesting that diagnosis and intervention during childhood may prevent further loss of vision.

Rep proteins play an essential role in the post-translational modification of Rab proteins, the small GTP-binding proteins that are essential for many aspects of intracellular transport. Rep proteins bind newly synthesized Rab proteins and facilitate

the addition of geranyl-geranyl groups, a modification essential for Rab function in intracellular trafficking (reviewed in (Preising and Ayuso, 2004). In humans, Rep1 and its homolog Rep2, are ubiquitously expressed and exhibit overlapping substrate specificity (Cremers et al., 1994). Mutations in Rep1 prevent the modification of Rab proteins, thereby disrupting Rab-mediated intracellular trafficking in photoreceptors and the RPE. As patients with CHM only experience age-related blindness, Rep2 appears to effectively compensate for the loss of Rep1 in all tissues except the eye (Seabra, 1996). Interestingly, zebrafish do not contain a Rep2 ortholog and the loss of Rep1 results in lethality at larval stages (Starr et al., 2004).

The development and survival of photoreceptors requires effective intracellular trafficking in both photoreceptors and the RPE. In the photoreceptor, proteins destined for the outer segment (e.g. opsin) travel from the Golgi to the connecting cilium via vesicular transport that is regulated by Rab8 and Rab6 (Deretic et al., 1995; Deretic and Papermaster, 1993). In *Xenopus laevis* expressing dominant negative forms of Rab8, rapid photoreceptor degeneration and defects in outer segment morphogenesis were observed (Moritz et al., 2001). It has been proposed that mutations in Rep1 may lead to defects in opsin trafficking that contribute to photoreceptor degeneration (Alory and Balch, 2001). In the RPE, intracellular trafficking controls the phagocytosis and degradation of disk membranes shed from the apical tips of photoreceptor outer segments. Failure of the RPE to clear outer segment debris leads to a toxic environment surrounding the photoreceptors and causes death. It is believed that Rab proteins function during phagocytosis by the RPE, although the mechanism is not clear. It is

known that Rab27a is target of Rep1 and that Rab27a interacts with myosin VIIA in the transport of melanosomes (Gibbs et al., 2004; Seabra et al., 1995). Furthermore, cultured RPE cells that lack myosin VIIA exhibit defects in the phagocytosis of outer segment membranes (Gibbs et al., 2003). A tempting hypothesis states that loss of Rep1 disrupts the function of a Rab27a/myosinVIIA complex and causes defects in phagocytosis by the RPE. As all retinal cells express Rep1, it is unknown if CHM reflects a cell-autonomous degeneration by photoreceptors, a non-cell-autonomous effect caused by RPE dysfunction, or a combination of both. Development of appropriate therapies requires a clear understanding of the tissue-specific contributions to disease. Here we report that zebrafish carrying a recessive nonsense mutation in *rep1* (Starr et al., 2004) exhibit retinal phenotypes consistent with CHM. Using histological, functional, and embryonic manipulations, we found that *rep1* mutants experience photoreceptor degeneration, loss of visual function, and defects in RPE pigmentation and outer segment phagocytosis. By producing genetically mosaic animals, we show that the loss of Rep1 in the RPE is sufficient to induce degeneration of wild type photoreceptors. These findings provide novel insight into the pathology of the disease and have implications for the design of future therapies.

RESULTS

The morphological phenotypes of *rep1* mutants are described elsewhere (Starr et al., 2004), but retinal defects have not been studied extensively. Mutants had slightly smaller eyes and the loss of pigment in the RPE could be observed through the lens as a cloudy coloration in the posterior part of the eye (data not shown). As patients with

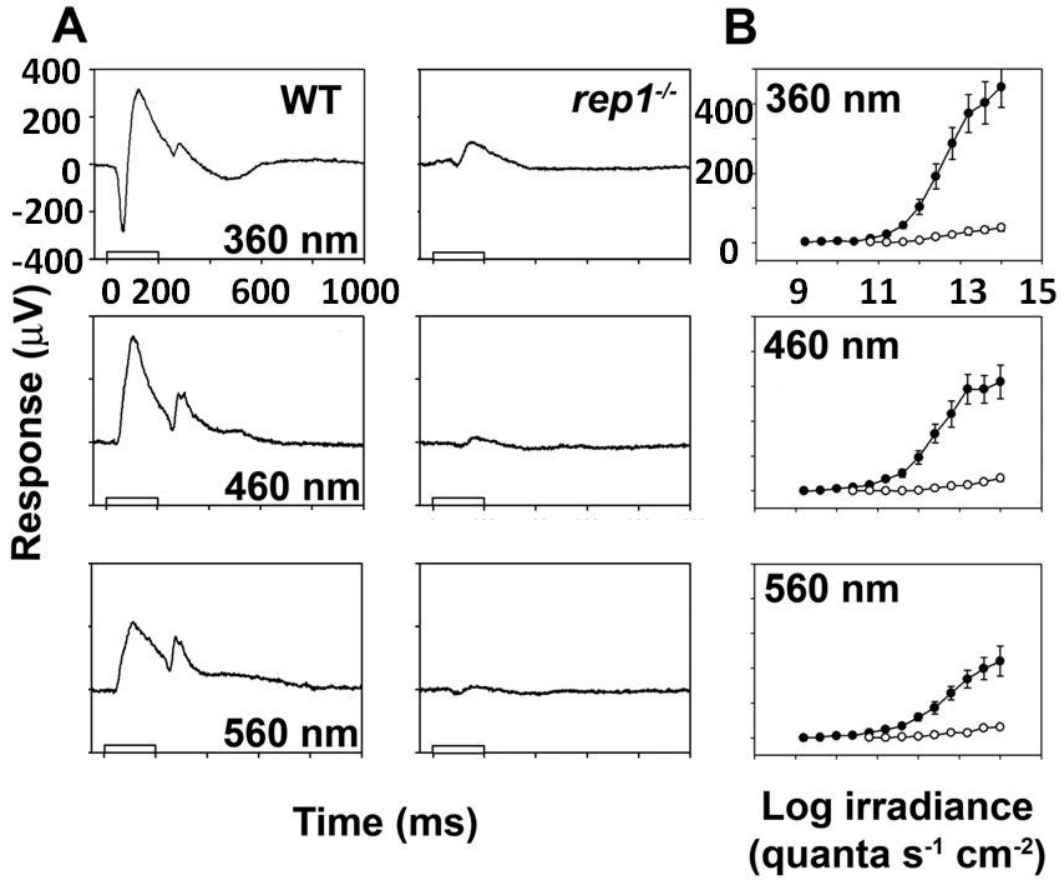

Fig. 5. ERG analysis of *rep1* mutant larvae. (A) ERG responses from 5 dpf wild type (*left*) and mutant (*right*) to 200 msec flashes of light at the designated wavelengths. Each waveform was based on the average response from ten stimulus presentations. Stimulus irradiance (15 log quanta s^{-1} cm^{-2}) was the same across all panels. Bars represent the light stimulus. (B) Graph of the average irradiance-response functions from wild type (filled circles; n=11) and mutant (open circles; n = 14) subjects based on the b-wave amplitude at three different wavelengths. Error bars represent ± 1 SEM. A mixed design Analysis of Variance (ANOVA) found a significant difference ($p \leq .05$) between the wild type and mutant responses at the last five irradiances tested.

CHM lose vision, an animal model of CHM should also exhibit visual defects. We used full field electroretinogram (ERG) recordings to determine if the *rep1* mutation also results in loss of visual function. We recorded the ERG at 5 days post fertilization (dpf) using stimuli at three different wavelengths (Fig. 5A). When presented with a long-flash (≥200 msec), the vertebrate ERG is characterized by a hyperpolarizing a-wave, a depolarizing b-wave, and a depolarizing d-wave, which reflect photoreceptor cell and on and off activity of second-order cells, respectively. Above 360 nm the amplitude of the b-wave masks the a-wave signal. Compared to wild type animals, all components of the mutant ERG were significantly reduced at 360 nm, 460 nm and 560 nm. The minimum light intensity required to produce the smallest detectable ERG response was almost two orders of magnitude higher in the mutants, depending upon the wavelength tested (Fig. 5B). The b-wave amplitude of *rep1* mutants was reduced across a range of stimuli intensities at all three wavelengths. These data indicate that *rep1* mutants exhibit severe loss of outer retina function.

CHM is characterized by degeneration of the choroid, RPE and photoreceptors, so we investigated the retinal histology of *rep1* mutants. Retinal lamination of *rep1* mutants was not affected and all major cell types were present (Fig. 6). The RPE maintains a consistent thickness in wild type animals; however, RPE thickness was highly irregular in the mutants. Hypertrophic areas extended into the photoreceptor layer and other areas possessed few or no observable melanosomes. The morphology of the mutant photoreceptor layer was disorganized. Mutant photoreceptor outer segments

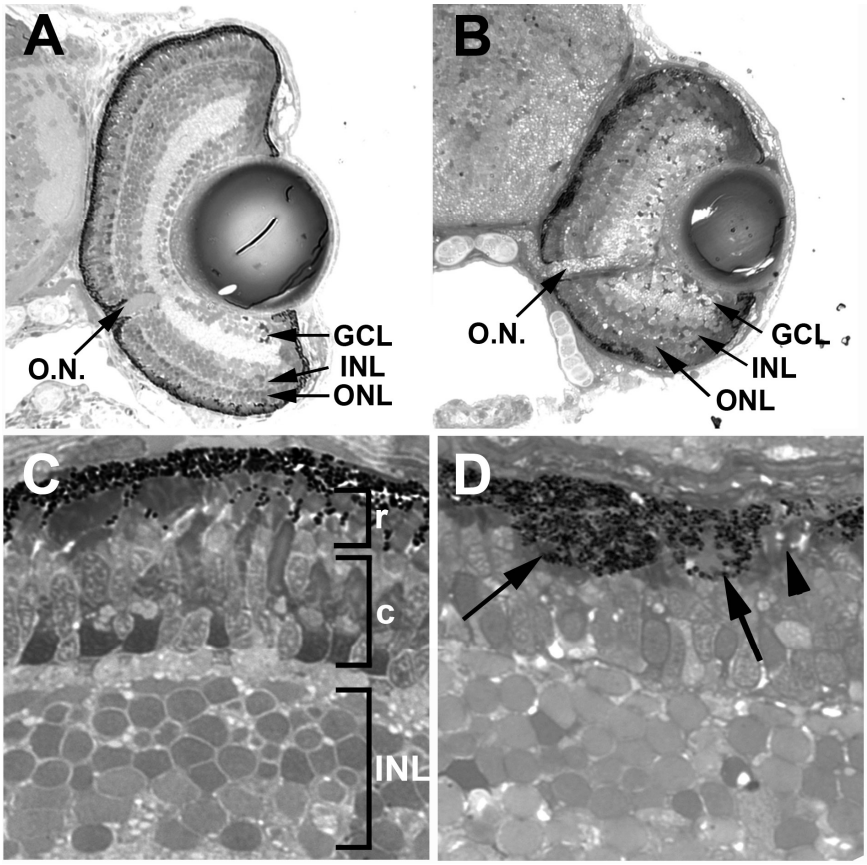

Fig. 6. Histological sections of 4.5 dpf wild type and *rep1* mutant retinas. (A) Wild type retinas at 4.5 dpf have fully laminated and retinal ganglion cells (GCL), amacrine and bipolar interneurons (INL) and photoreceptors (ONL) have differentiated and the optic nerve (O.N.) is apparent. (B) Lamination and cellular differentiation is not affected in *rep1* mutants but eye size is reduced and the RPE layer appears irregular. (C) High magnification of sections from light-adapted wild type retinas showing the rod (r) outer segments positioned distally from the cone (c) outer segments. (D) Sections of *rep1* mutants showing areas of RPE hypertrophy (arrows) into the photoreceptor layer and other regions where the RPE is almost devoid of pigmentation (arrowhead). Rod and cone outer segments are not normally positioned and are shorter than wild type.

were compressed against hypertrophic regions of RPE. In wild type retinas, rod and cone photoreceptors are tiered, with UV cones located basally and rods located apically. In *rep1* mutant retinas, no discernable tiering could be observed, perhaps due to hypertrophy of the RPE into the photoreceptor layer.

Ultrastructural analysis of *rep1* mutants by transmission electron microscopy revealed additional defects of the photoreceptors and RPE (Fig. 7). In *rep1* mutants, photoreceptor outer segments were disheveled and degenerating. Melanosomes in the RPE cells were smaller and more immature than those found in wild type animals. Large vacuoles and undigested outer segment disk membranes were observed within the RPE of the mutants. The results from light microscopy and electron microscopy indicate that loss of Rep1 disrupts maturation of melanosomes and the elimination of photoreceptor disk membranes within the RPE and leads to degeneration of the RPE and photoreceptors.

It is well established that defects in opsin trafficking can lead to photoreceptor death. As Rab proteins function in opsin trafficking (Deretic et al., 1995; Deretic and Papermaster, 1993; Moritz et al., 2001), we tested the hypothesis that loss of Rep1 results in opsin mislocalization and therefore contributes to degeneration in CHM. Retinal sections labeled with an antibody that recognizes rhodopsin (1D1) showed little to no mislocalization in wild type or mutant rods (Fig. 8A, E). During development, small amounts of rhodopsin can be seen around the plasma membrane in wild type rods (Morris and Fadool, 2005; Perkins et al., 2005) and this was occasionally observed in

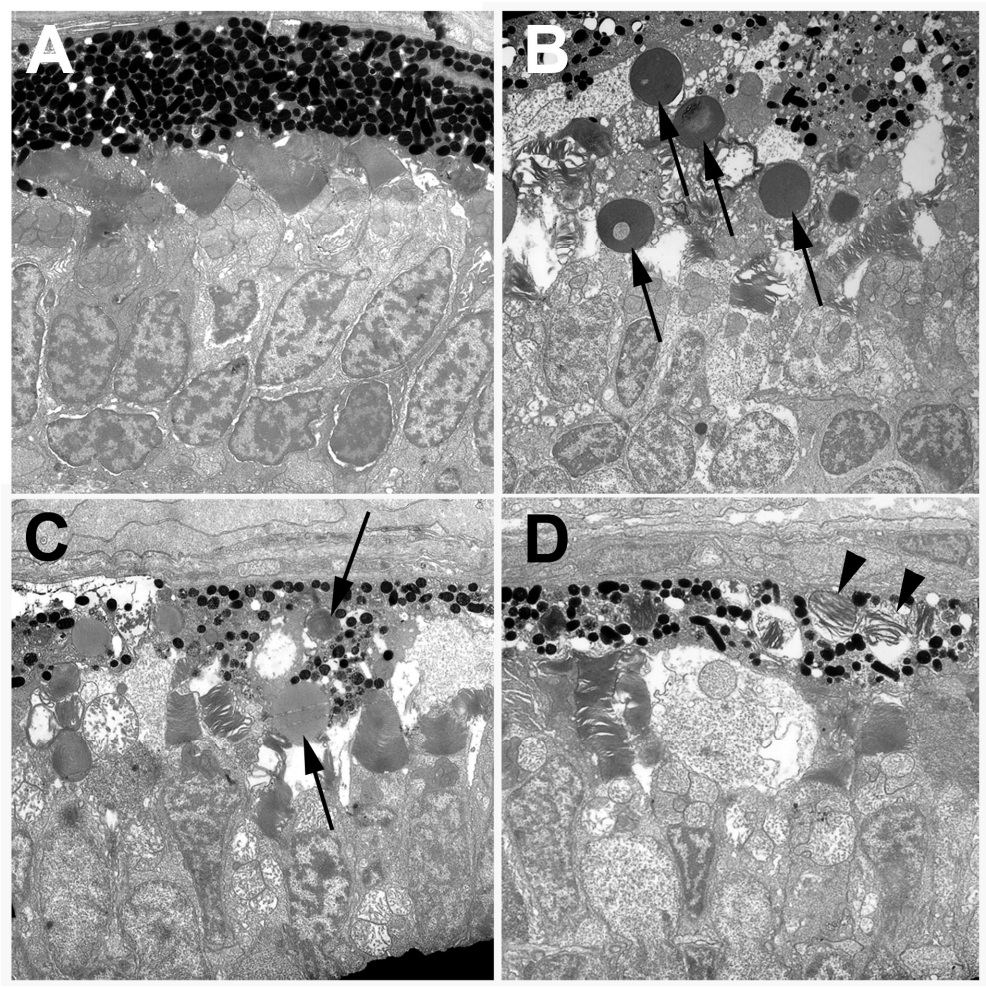

Fig. 7. Transmission electron microscopy of 4.5 dpf wild type and *rep1* mutant retinas. (A) Electron micrographs of wild type retinas reveal an orderly array of photoreceptor outer segments and the uniform thickness of the RPE. Melanosome maturation within the RPE is normal. (B-D) Electron micrographs from multiple *rep1* retinas showing degeneration of the RPE and photoreceptors. Arrows in *B* and *C* indicate large vacuoles observed in the RPE of *rep1* mutants. Arrowheads in *D* indicate outer segment material that is not digested by the RPE. Melanosome size and maturation varies more dramatically and is less dense than what is seen in wild type.

rep1 mutants, although this was not interpreted as an effect of Rep1 loss. In addition, both blue and green cone opsin proteins localized exclusively to the cone outer segments in wild type and mutant animals (Fig. 8B, C, F, G). Taken together, these data indicate that opsin mislocalization is not responsible for photoreceptor degeneration.

As the larval ERG is cone-dominated, we used additional immunohistochemical markers to specifically investigate cone morphology. In wild type animals, the red/green double cones are regularly spaced and columnar in appearance (Fig. 8D, H). In *rep1* mutants, these cones are irregularly shaped, appear disheveled, and have lost their columnar organization. To investigate synapse integrity of *rep1* mutants, retinas were stained with antibodies for a glutamate transporter, GLT-1, which is stains cone pedicles and bipolar cell terminals in goldfish, and the outer plexiform layer of zebrafish (Vandenbranden et al., 2000; Yazulla and Studholme, 2001). We found that GLT-1 labeling was missing from the outer plexiform layer and strongly reduced in the inner plexiform layer, suggesting that cone degeneration disrupts synapse formation and may have deleterious effects on inner retinal cells such as bipolar cells (Fig. 9). Although correlative, loss of GLT-1 immunoreactivity agrees with the loss of activity by inner retinal cells seen in the ERG of *rep1* mutants.

In *rep1* mutant zebrafish, the degenerating RPE fails to eliminate photoreceptor disk membranes yet transport of opsin within the photoreceptors is normal. We therefore addressed the hypothesis that photoreceptor degeneration is non-cell autonomous and directly caused by the RPE. We produced genetically mosaic eyes in *rep1* and wild type animals by transplanting cells from blastula stage embryos

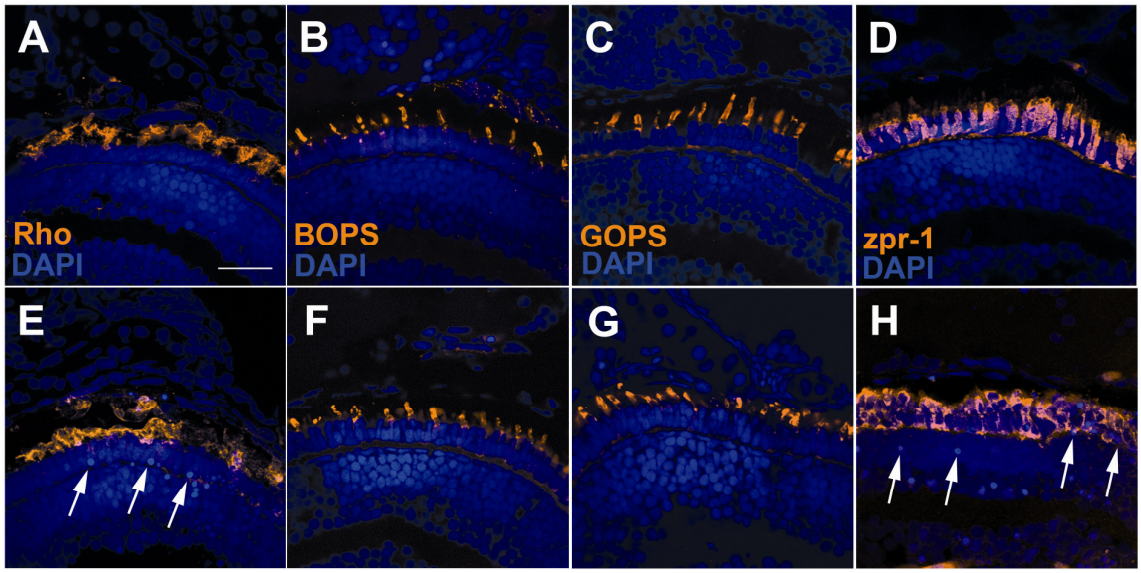

Fig. 8. Opsin trafficking is unaffected in *rep1* mutants. Retinal cryosections were stained with markers for rod and cone photoreceptors in wild type (*A-D*) and *rep1* mutants (*E-H*). The 1D1 marker labels rhodopsin (Rho) whereas antibodies against blue opsin (BOPS) and green opsin (GOPS) in the photoreceptor outer segments of wild type and *rep1* mutants. The zpr-1 antibody labels the red/green double cones and reveals the disheveled morphology of the photoreceptors. All sections were counterstained with DAPI to visualize nuclei. Pyknotic nuclei, a hallmark of cell death, are seen in *rep1* mutants and indicated by arrows. Bar = 20 µm.

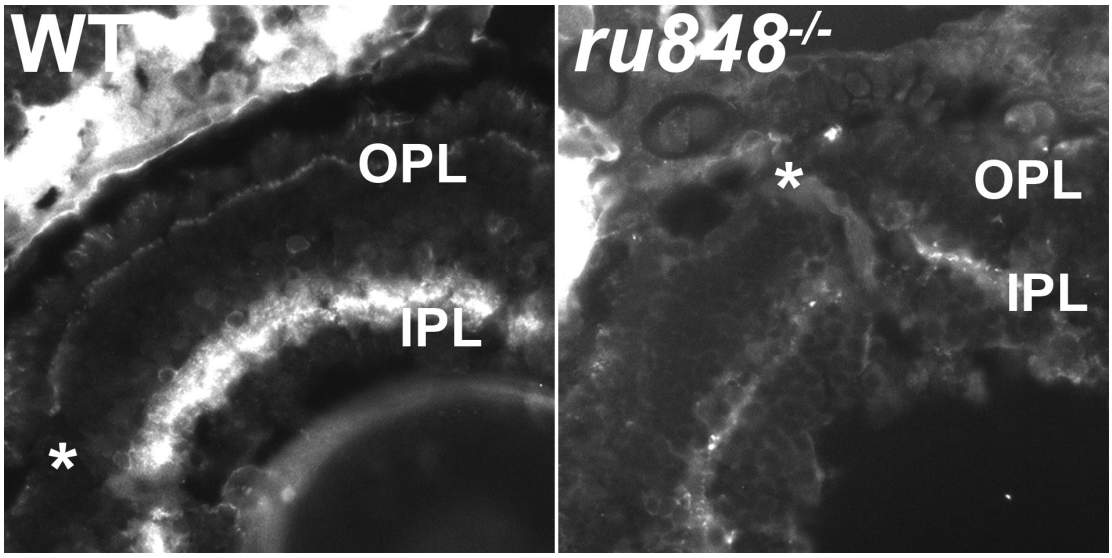

Fig. 9. Loss of *rep1* disrupts photoreceptor termini. Retinal cryosections of (A) wild type and (B) *rep1* mutant retinas were stained with an antibody against the glutamate transporter (GLT-1). Staining in the OPL and IPL is greatly reduced in *rep1* mutants. The asterisks mark the optic nerve.

(Ho and Kane, 1990). Cells from donor embryos that had been injected with a lineage tracing dye (rhodamine-dextran) were transplanted into unlabeled hosts. Transplanted cells gave rise to clones of varying size that were assessed for cone morphology and cell death. Wild type cells transplanted into wild type hosts produced cones with normal morphology with no evidence of cell death (Fig. 10A-D). When *rep1* mutant cells were transplanted into *rep1* mutant hosts, the photoreceptors produced by the clones lacked the columnar organization and were similar in morphology to cells outside the clone (Fig. 10M-P). In addition, cell death was often observed within and outside the clone as small, round pyknotic nuclei that stained brightly with DAPI. When mutant cells were transplanted into wild type hosts, the photoreceptor morphology was rescued and cell death was rarely observed anywhere within the clone (Fig. 10E-H). Conversely, when wild type cells were transplanted into mutant hosts, cell death was observed within the clone and the morphology of photoreceptors within the wild type clone resembled that of the surrounding mutant cells (Fig. 10I-L). Quantification of clones exhibiting cell death revealed that almost all clones of mutant photoreceptors (94%) could be rescued when placed opposite wild type RPE (Table 2). Importantly, most clones of wild type cells (71%) exhibited some cell death and acquired an abnormal morphology when placed opposite RPE from mutant animals.

To directly test the role of mutant RPE in photoreceptor dysfunction, we transplanted cells from wild type or *rep1* mutant donors into albino hosts (Fig. 11). As donor cells were pigmented, the location of RPE clones was easily identified in the

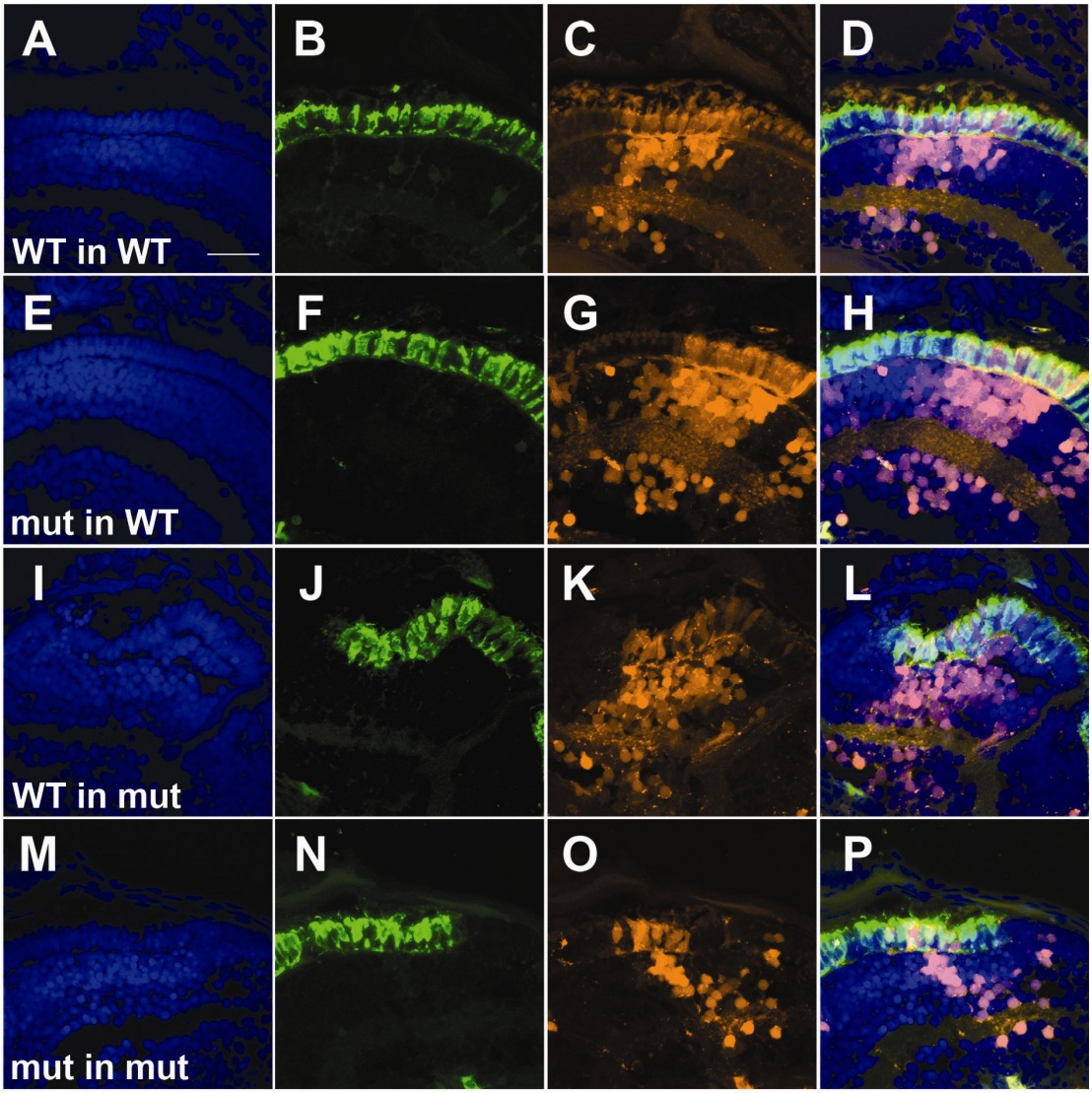

Fig. 10. Analysis of photoreceptor morphology and survival in mosaic animals. Genetically mosaic animals were created by blastomere transplantation. Shown are retinal cryosections of 4.5 dpf mosaic animals. Cryosections were stained with DAPI to visualize nuclei (blue; A, E, I, M), and the zpr-1 antibody to label the red-green double cones (green; B, F, J, N). Donor cells were labeled by the lineage-tracer rhodamine-dextran (red cells; C, G, K, O). Composite images (D, H, L, P) show all markers and labels. Bar = 20 µm.

Table 2. Cell death within mosaic clones.

	Clones analyzed	Clones with pyknotic nuclei
WT-WT	12	0 (0%)
mut-WT	16	1 (6%)
WT-mut	17	12 (71%)
mut-mut	6	5 (83%)

albino hosts. Photoreceptor morphology remained unaffected by the presence of wild type RPE and no differences could be seen in photoreceptors in contact with the RPE clone and those outside the clone (Fig. 11A-E). In contrast, RPE cells from *rep1* mutant donors disrupted the morphology of the host photoreceptors. The host photoreceptors were shorter, disheveled, and more disorganized than those photoreceptors not in contact with the mutant RPE clone (Fig. 11F-J). Taken together, the mosaic experiments show that photoreceptor degeneration in CHM is non-cell autonomous and that RPE cells lacking Rep1 are both necessary and sufficient for photoreceptor cell death.

DISCUSSION

The purpose of this study was to investigate the retinal pathology of a zebrafish model of CHM and to test various hypotheses regarding the mechanism of photoreceptor degeneration. The results point to four significant findings. First, mutation of the zebrafish *rep1* gene caused degeneration of the RPE and photoreceptors in a manner that closely resembled the degeneration seen in human cases of CHM (Syed et al., 2001). Similar to what is observed in human cases of CHM (Flannery et al., 1990; Jacobson et al., 2006), zebrafish *rep1* mutants exhibit variable thickness of the RPE with areas of depigmentation and accumulation of outer segment material in the RPE. Mutant photoreceptors became much shorter and visual function was highly reduced or absent. Thus, the zebrafish represents a suitable animal model for this disease. Second, the RPE of *rep1* mutant zebrafish failed to properly eliminate photoreceptor disk membranes, which can be a cause of non-autonomous photoreceptor death (Vollrath et al., 2001). The failure to effectively digest phagosomes carrying disk membranes is hypothesized to

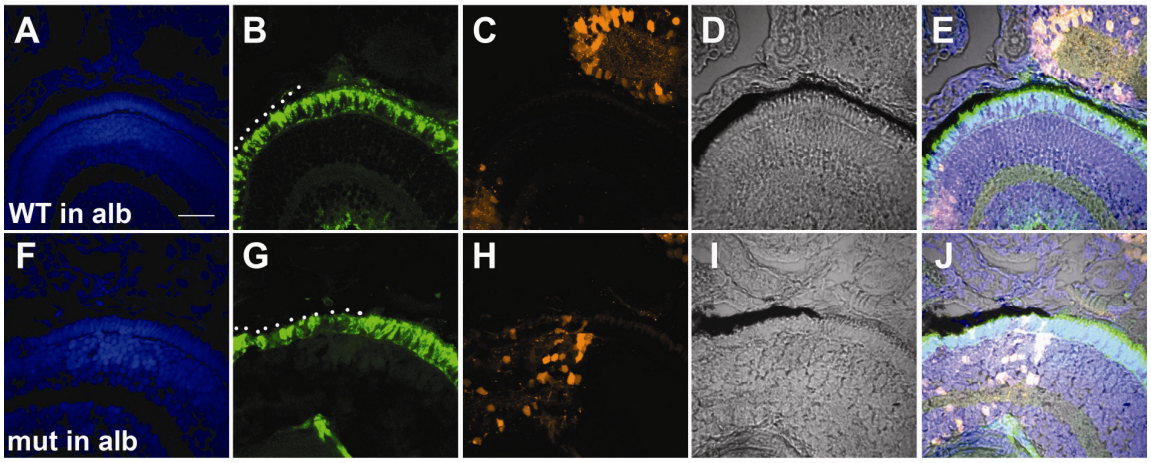

Fig. 11. Effects of RPE clones on wild type photoreceptor morphology. Donor cells from wild type or *rep1* mutant embryos were transplanted into albino hosts in order to visualize transplanted RPE clones. Retinal cryosections of 4.5 dpf mosaic animals were stained with DAPI to visualize nuclei (blue; A, F), and the zpr-1 antibody to label the red-green double cones (green; B, G). Donor cells were labeled by the lineage-tracer rhodamine-dextran (red cells; C, H). Brightfield images using Nomarski optics (D, I) were used to visualize and distinguish pigmented RPE (donor) from albino RPE (host). Composite images (E, J) show all markers and labels. The dotted line (B, G) denotes the location of donor RPE. Bar = 20 µm.

cause the accumulation of lipofuscin within the RPE, which is a clinical feature of CHM and other forms of retinal degeneration (Kolb and Gouras, 1974; Syed et al., 2001; Weng et al., 1999). Third, opsin mislocalization was not observed in intact rod or cone photoreceptors. Mislocalization of opsin was observed in a single case study of a female carrier of CHM in which photoreceptor degeneration was variable (Syed et al., 2001). While mutations that affect rhodopsin folding and trafficking can cause autonomous photoreceptor cell death (Li et al., 1996; Moritz et al., 2001; Pazour et al., 2002a; Sung et al., 1993), opsin mislocalization can also occur when the RPE fails to phagocytize shed disk membranes, as in the RCS rat (Dowling and Sidman, 1962; Nir and Papermaster, 1989) and possibly in the Myo7a mouse (Gibbs et al., 2003). Finally, genetic mosaic analysis indicated that the RPE of *rep1* zebrafish was both necessary and sufficient to cause photoreceptor degeneration (Figs. 10-11).

Perhaps the most debated question regarding the pathology of CHM is the primary site of the disease. Our results strongly suggest that photoreceptor death in CHM is secondary to defects in the RPE, which differs from previous studies. In reports of a human female carrier of CHM (Syed et al., 2001) and of CHM mouse models (Tolmachova et al., 2006), the authors argue that the severity of degeneration of photoreceptors and RPE does not always correlate, suggesting that the tissues degenerate independently. To address the autonomy of the disease, Tolmachova et al. (Tolmachova et al., 2006) bred mice carrying a Chm^{flox} gene with mice carrying a *six3-Cre* transgene to generate a tissue-specific knockout of the mouse *CHM* gene. During development, however, both *six3* and the *six3-Cre* transgene are expressed in the anterior neural plate

and the optic vesicle, which are tissues that give rise to both neural retina and RPE (Furuta et al., 2000; Oliver et al., 1995). Thus, autonomy could not be directly tested in these experiments because the *CHM* gene was likely missing from both photoreceptors and RPE. Our results and methodology are similar to those of Mullen and LaVail (Mullen and LaVail, 1976), who used chimeric animals to identify the RPE as the primary site of disease in RCS rats. It should be noted that the long-term fate of mutant photoreceptors in our mosaic animals is not known and we cannot rule out the possibility that a slow, progressive degeneration may occur. Furthermore, as zebrafish lack an ortholog to the human Rep2 protein, the effects observed in this study may be more severe than what occurs in human CHM patients. Nevertheless, our results show that loss of Rep1 from the RPE is sufficient for early photoreceptor degeneration in zebrafish. These results have significant implications for development of appropriate RPE-specific therapies to treat and correct CHM. As this disease can be diagnosed during childhood while symptoms are mild (Sorsby et al., 1952), effective intervention of the RPE at early ages may prevent the loss of vision later in life.

MATERIALS AND METHODS

Zebrafish Care and Maintenance

The *rep1*^{ru848} allele, which contains a nonsense mutation (Q32X) in the second exon, was obtained from Dr. James Hudspeth (Starr et al., 2004). Albino animals were obtained from the Zebrafish International Resource Center (ZIRC). All fish were maintained according to standard methods (Westerfield, 1995).

Histology: Light Microscopy and Transmission Electron Microscopy (TEM)

Embryos were processed for histology as previously described (Schmitt and Dowling, 1999). For transmission electron microscopy, transverse sections (60-80 nm) of the central retina were stained with lead citrate and uranyl acetate. Photographs were obtained with a JEOL transmission electron microscope and image processing performed using Adobe Photoshop.

Immunohistochemistry

Immunohistochemistry was performed as previously described (Perkins et al., 2005). Images were obtained with an Olympus FV1000 confocal microscope. The following is a list of primary antibodies used, dilution, and cell types that possess the antigens: 1D1 (1:500) rods (Fadool, 1999), Zpr1 (1:100) red-green double cones (Larison and Bremiller, 1990), cone opsin antibodies (1:200) (Vihtelic et al., 1999), and glutamate transporter (1:100; AB1783, Chemicon)(Yazulla and Studholme, 2001). The appropriate fluorescently conjugated antibodies (Jackson ImmunoResearch) were used at 1:500 dilutions. Slides were counterstained with DAPI (Molecular Probes) to label DNA.

Electroretinographic (ERG) Recording

Details of the optical system and embryo preparation can be found elsewhere (Bilotta et al., 2001; Hughes et al., 1998; Saszik and Bilotta, 1999). All experiments were performed on light-adapted animals at 5 dpf. Animals were given a 200-ms stimulus at a range of irradiances (10 to 15 log quanta s^{-1} cm^{-2}) at 360 nm, 460 nm and 560 nm wavelengths.

Mosaic Analysis

Mosaic retinas were produced by blastomere transplantation (Ho and Kane, 1990). Clutches of embryos from *rep1* heterozygous matings were dechorionated and injected at the 1-to 4-cell stage with a lineage-tracing label (1:9 mix of lysine fixable rhodamine-dextran (Molecular Probes) at a total concentration of 5% w/v). At the 1000-cell stage, 10-40 donor cells were transplanted to the animal pole of the dechorionated wild-type hosts, the region fated for eye and forebrain (Kimmel et al., 1995). Donor embryos were phenotyped at 4 dpf and host embryos were fixed in 4% paraformaldehyde at 4.5 dpf. Donor cells in host embryos were assessed by immunohistochemistry and confocal microscopy as described above.

CHAPTER III

THE INTRAFLAGELLAR TRANSPORT PROTEIN *Ift57* IS REQUIRED FOR CILIA MAINTENANCE AND REGULATES IFT-PARTICLE-KINESIN-II DISSOCIATION IN VERTEBRATE PHOTORECPTORS*

OVERVIEW

This work analyzes the photoreceptor phenotypes of the zebrafish *ift57* mutants and investigates the function of *Ift57* protein within the IFT particle.

SUMMARY

Defects in protein transport within vertebrate photoreceptors can result in photoreceptor degeneration. In developing and mature photoreceptors, proteins targeted to the outer segment are transported through the connecting cilium via the process of Intraflagellar Transport (IFT). In studies of vertebrate IFT, mutations in any component of the IFT particle typically abolish ciliogenesis, suggesting that IFT proteins are equally required for IFT. To determine if photoreceptor outer segment formation depends equally on individual IFT proteins, we compared the retinal phenotypes of *ift57* and *ift88* mutant zebrafish. *ift88* mutants failed to form outer segments, while *ift57* mutants formed short outer segments with reduced amounts of opsin. Our phenotypic analysis revealed that *ift57* is not essential for IFT, but is required for efficient IFT. In co-immunoprecipitation experiments from whole animal extracts, we determined that

---

*Reprinted with permission from "The Intraflagellar transport protein *Ift57* is required for cilia maintenance and regulates IFT-particle-kinesin-II dissociation in vertebrate photoreceptors." by B.L. Krock and B.D. Perkins, 2008. *J. Cell Science* **121**, 1907-15.

kinesin II remained associated with the IFT particle in the absence of *Ift57*, but *Ift20* did not. Additionally, kinesin II did not exhibit ATP-dependent dissociation from the IFT particle in *ift57* mutants. We conclude that *ift20* requires *ift57* to associate with the IFT particle and that *Ift57/Ift20* mediate kinesin II dissociation.

INTRODUCTION

Vertebrate photoreceptors are highly specialized neurons that possess a modified sensory cilium known as the outer segment. The outer segment develops as an extension of a nonmotile primary cilium (De Robertis, 1960). As the outer segment lacks the machinery for protein synthesis, all protein destined for the outer segment must pass through the connecting cilium. Large amounts of protein synthesized in the inner segment must be efficiently transported to the outer segment to replenish material lost from the distal tips each day. Estimates from mammalian systems have calculated ~2000 rhodopsin molecules per minute must be transported to the outer segment to compensate for lost material (Besharse, 1990). Hence, both the development and survival of the photoreceptor require this continual transport of protein to the outer segment (Marszalek et al., 2000).

Studies of rhodopsin trafficking in several species have linked defects in protein transport to photoreceptor degeneration and the disease retinitis pigmentosa. The C-terminal tail of rhodopsin contains a sorting sequence that is necessary and sufficient for transport to the outer segment (Perkins et al., 2002; Tam et al., 2000). Mutations in this region result in protein accumulation in the inner segment and at the base of the connecting cilium in mice, rats, and frogs (Green et al., 2000; Li et al., 1996; Sung et al.,

1994; Tam et al., 2000), leading to photoreceptor degeneration. Indeed, mutations in the C-terminus of human rhodopsin, such as P347L and S344Ter, can cause retinitis pigmentosa (Berson et al., 1991). Rhodopsin mislocalization also occurs in animals with mutations in the molecular motors kinesin II (Marszalek et al., 2000) and the dynein light chain Tctex-1 (Tai et al., 1999), both of which show severe retinal degeneration. It is imperative, therefore, that cargo targeted for the outer segment reach its destination or retinal degeneration will occur. Thus, both mutations within the opsin gene and mutations in the transport machinery can cause retinal degenerative diseases.

Protein transport along a ciliary axoneme, such as the connecting cilium, occurs via the process known as Intraflagellar transport (IFT) (Rosenbaum and Witman, 2002). Both the assembly and maintenance of cilia require IFT and defects in ciliogenesis have been linked to retinal degeneration, polycystic kidney disease, Bardet-Biedl syndrome, Jeune asphyxiating thoracic dystrophy, respiratory disease and defective left-right axis determination (Beales et al., 2007; Pazour and Rosenbaum, 2002; Snell et al., 2004). IFT refers to movement of the IFT particle, a multisubunit protein complex which consists of at least 17 IFT proteins that form two subcomplexes: complex A and complex B (Cole et al., 1998). The IFT particle associates with heterotrimeric kinesin II, which is composed of two motor subunits and an accessory subunit, known as *Kif3A*, *Kif3B* and *KAP*, respectively (reviewed in (Cole, 1999). Kinesin II cooperates with a homodimeric kinesin II known as OSM-3 to mediate transport of the IFT particle and its associated cargo toward the ciliary tip (Cole et al., 1998; Orozco et al., 1999; Ou et al., 2005; Snow et al., 2004). The process of IFT is highly conserved, as mutations in IFT

proteins perturb ciliary assembly and/or maintenance in organisms as diverse as *Chlamydomonas*, *C. elegans*, *Drosophila*, mouse, humans and zebrafish (Beales et al., 2007; Cole et al., 1998; Han et al., 2003; Murcia et al., 2000; Pazour et al., 2000; Pedersen et al., 2005; Sun et al., 2004; Tsujikawa and Malicki, 2004).

Recent biochemical studies, predominantly in *Chlamydomonas*, have started to reveal the structural composition of the IFT particle and specific interactions between individual IFT proteins, particularly within complex B. Eleven proteins constitute the *Chlamydomonas* complex B, a subset of these form a core consisting of an *Ift*72/74-*Ift80* tetramer along with *Ift88*, *Ift81*, *Ift52* and *Ift46* (Lucker et al., 2005). The outer surface of complex B is composed of *Ift20*, *Ift57*, *Ift80* and *Ift172*. Data from yeast two-hybrid experiments indicate direct interactions between *Ift72/74* and *Ift81* and between *Ift57* and *Ift20*. Similar approaches indicated interactions between *Ift20* and the *Kif3B* subunit of kinesin II (Baker et al., 2003; Lucker et al., 2005). While the *Ift72/74-Ift80* interaction likely forms the structural core of complex B, the functional nature of the interactions described for the outer surface IFT proteins remains unclear.

Previous studies investigating mutations in IFT genes have revealed few phenotypic differences in ciliated structures of any tissue. In *Chlamydomonas*, mutations in genes coding for complex B proteins, such as *ift52*, *ift88* and *ift172*, result in a complete absence of flagella (Cole, 2003). *Ift88* mutations have been shown to abolish cilia in the sensory neurons of *C. elegans and Drosophila* (Han et al., 2003; Haycraft et al., 2001). In zebrafish, mutants of *ift88* and *ift172* lack outer segments entirely and *ift88* mutants lack all sensory cilia at 4 days post fertilization (dpf) (Gross et

al., 2005; Tsujikawa and Malicki, 2004). In mice, all null alleles of *Ift88* and *Ift172* cause embryonic lethality before E12, thereby preventing analysis of photoreceptor structure, though nodal cilia are completely absent in these animals (Huangfu et al., 2003; Murcia et al., 2000). In $Tg737^{orpk}$ mutants, a hypomorphic mutation in murine *ift88*, photoreceptors display aberrant outer segment disk stacking, accumulation of vesicles, and progressive photoreceptor degeneration (Pazour et al., 2002a; Pazour et al., 2000). Recent evidence suggests, however, that loss of individual IFT proteins may not completely abolish ciliogenesis. While not completely normal, cilia do remain in *Chlamydomonas* cells lacking *Ift27*, which plays a role in cell cycle regulation (Qin et al., 2007), or *Ift46*, which facilitates transport of outer dynein arms (Hou et al., 2007). Phenotypic differences have not yet been described in other tissues or species.

While the photoreceptor phenotypes associated with the partial or complete loss of function of *ift88* have been well characterized in both mouse and zebrafish, no such analysis has been done for most of the remaining 16 or so IFT peptides. Loss of function studies with zebrafish *ift140* and *ift81* did not reveal a retinal phenotype, though the *ift81* mutation did cause cystic kidneys (Gross et al., 2005; Sun et al., 2004; Tsujikawa and Malicki, 2004). Morpholino knockdown of the zebrafish *ift52* and *ift57* genes resulted in a loss of photoreceptors (Tsujikawa and Malicki, 2004); however, the ultrastructure, development and morphology of photoreceptors in these animals were not analyzed. Although photoreceptors clearly require the IFT process for proper outer segment biogenesis, the composition of the IFT particle functioning in the photoreceptor may be different than the one in *Chlamydomonas*. Many cargo molecules destined for

the outer segments, such as rhodopsin, are unique to photoreceptors. Vertebrate photoreceptors also have a simpler axonemal structure (9+0 microtubule arrangement) than the one found in the *Chlamydomonas* flagellum or vertebrate motile cilia (9+2 arrangement).

Herein we analyze zebrafish with an insertional mutation in the *Ift57* gene, which have a photoreceptor phenotype that is distinct from *ift88* mutant zebrafish. Our data show that the process of IFT can occur, albeit inefficiently, in the absence of *Ift57*. Our data also attribute specific functions to *Ift57* and *Ift20* within the IFT complex and provide novel insights into how kinesin II dissociates from the IFT particle. This work has implications in both the molecular mechanism of IFT and the molecular requirements for photoreceptor outer segment formation.

RESULTS

To determine the effects different IFT mutations have on photoreceptor development, we examined the phenotypes of zebrafish *ift57* and *ift88* mutants. In a screen for photoreceptor defects, we previously identified a mutation in the zebrafish *ift57* homolog (Gross et al., 2005). The hi3417 allele is a retroviral insertional mutation (Amsterdam and Hopkins, 1999) in the first exon of the *ift57* gene. This mutant has been reported to form kidney cysts (Sun et al., 2004), but the retinal phenotype of *ift57* mutants has yet to be fully characterized. Zebrafish *oval* mutants carry an ENU induced point mutation in the *ift88* gene that introduces a premature stop codon, thereby eliminating function (Tsujikawa and Malicki, 2004).

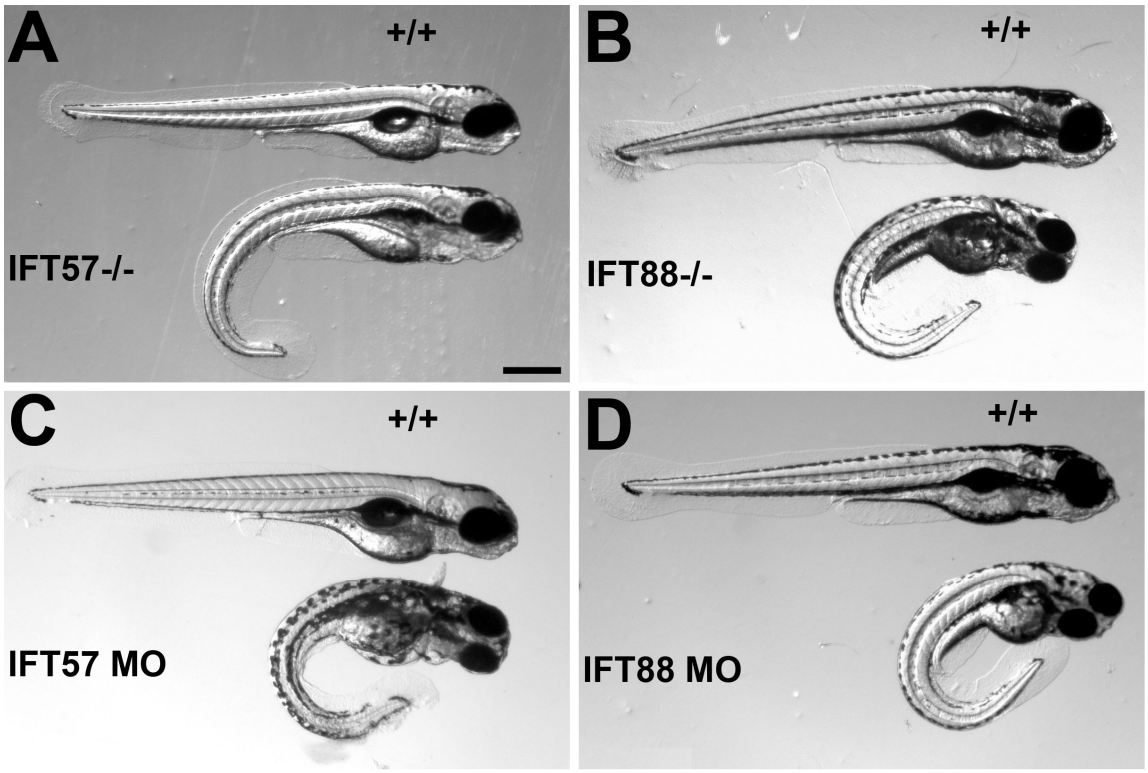

Fig. 12. Morpholinos phenocopy *ift57*and *ift88* mutant zebrafish. (A) Wild type (top) and *ift57* mutant larvae (bottom) at 4 dpf. (B) Wild type (top) and *ift88* mutant larva (bottom) at 4 dpf. (C-D) Uninjected control (top) and zebrafish larva injected with a splice-blocking morpholino (MO) against *ift57* (bottom) or a translation blocking morpholino against *ift88* (D – bottom). Bar = 200μm

At 4 days post fertilization, both *ift57* and *ift88* mutants exhibited a ventral body curvature, had slightly smaller eyes, and developed kidney cysts (Fig. 12). To confirm that the retroviral insertion in *ift57* causes the observed phenotype, we injected splice site-directed morpholino oligonucleotides into wild type embryos. Injection of gene-specific morpholinos phenocopied the morphological and kidney phenotypes of both *ift57* and *ift88* mutants (Fig. 12). These results show that the general phenotype of both mutants is highly similar and suggest that the *ift57* mutation represents a functional null allele.

To compare the retinal anatomy of *ift57* and *ift88* mutants, we analyzed histological sections of 4 dpf animals by light microscopy. Retinal lamination and normal cellular differentiation was unaffected in *ift57* and *ift88* mutants at 4 dpf (Fig. 13A-C). Both i*ft57* and *ift88* mutants exhibited holes within the photoreceptor layer, which is indicative of cell death, while other cell types within the retina were unaffected. Cell death specifically within the outer nuclear layer indicated that photoreceptors are the only cell type within the retina whose survival was affected by the loss of IFT proteins. Consistent with previous findings (Doerre and Malicki, 2002; Tsujikawa and Malicki, 2004), higher magnification images (Fig. 13D-F) revealed no photoreceptor outer segments in *ift88* mutants. In contrast, *ift57* mutant photoreceptors retained short outer segments in both the periphery and central regions of the retina. Morpholino-injected animals (morphants) were phenotypically identical to the mutants at 4 dpf (Fig. 13E-F compared with H-I). To test if the *ift57* mutant phenotype reflected a hypomorphic mutation, we performed western blots on lysates of 4 dpf *ift57* mutant

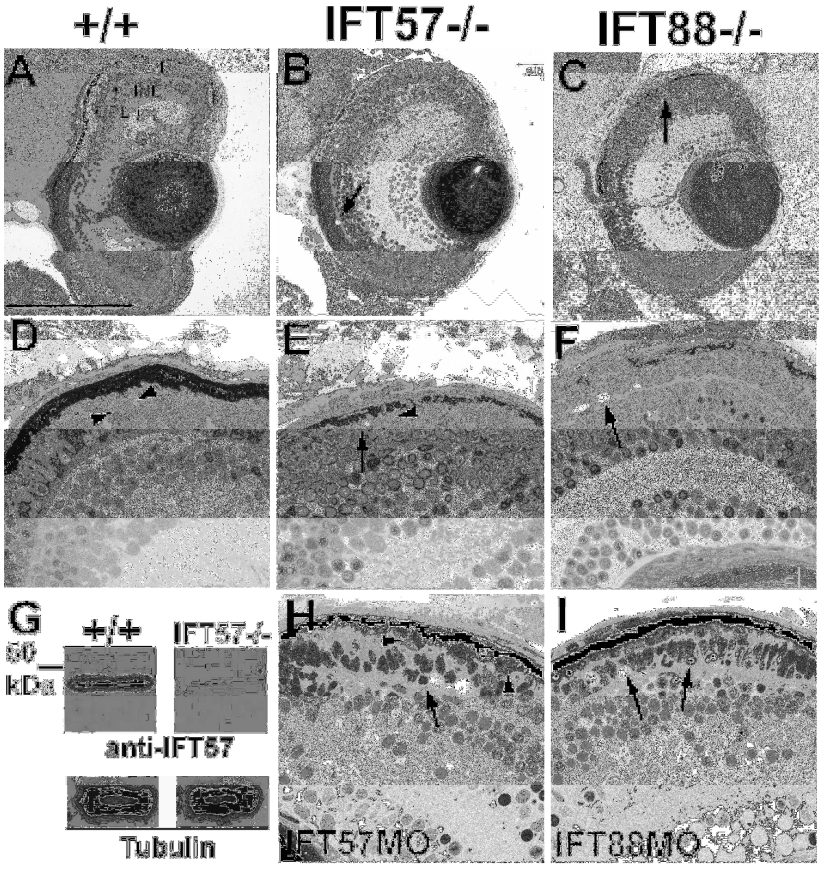

Fig. 13. Histology of 4 dpf wild type and IFT mutant retinas. (A) The outer nuclear layer (ONL), inner nuclear layer (INL) and retinal ganglion cells (RGC) are present in wild type and the outer plexiform layer (OPL), and inner plexiform layer (IPL) are easily observable. (B,C) In both *ift57* and *ift88* mutants acellular holes (arrows) in the ONL are observed. (D) Wild type retinas have photoreceptor outer segments (arrowhead), (E,F) but *ift88* mutants do not, while *ift57* mutants have short outer segments (arrowhead). (G) Western blot analysis of *ift57* mutants at 4dpf. No *Ift57* protein is observed in *ift57* mutants (upper blot lane 2). Lower blot shows loading control. (H, I) Histological analysis of *ift57* and *ift88* morphants phenocopy the *ift57* and *ift88* mutations, respectively. Scale bar: 100µm in (A-C), 20µm in (D-F, H,I).

embryos with a polyclonal antibody against the C-terminus of zebrafish *Ift57* (See materials and methods). We did not detect any *Ift57* protein in mutant lysates (Fig 13G), and concluded that the hi3417 allele caused a null mutation in the *ift57* gene. These results demonstrate phenotypic differences resulting from mutations in two different IFT complex B proteins.

As *ift57* mutants produced outer segments, we hypothesized that components of the phototransduction cascade would be transported to the outer segments. Immunohistochemical analysis with an antibody against rhodopsin, 1D1, and an antibody against blue cone opsin revealed both rhodopsin and blue cone opsin were present within the outer segments of *ift57* mutant rods and blue cones, respectively (Fig. 14A-F). Opsin mislocalized to the inner segment in *ift57* mutant photoreceptors, although transport to the outer segments did occur (Fig. 14B,E). Both rhodopsin and blue opsin were completely mislocalized throughout the plasma membrane of *ift88* mutant photoreceptors (Fig. 14C, F). These data indicate that transport to the outer segment via IFT was disrupted but not abolished in the absence of *Ift57* but did not occur in the absence of *Ift88*. To address the question of whether *ift57* mutants generated connecting cilia, we stained retinal sections with anti-acetylated tubulin (Fig. 14J-L). Consistent with the observation that outer segment formation and opsin transport occurs in *ift57* mutants, we found cilia projecting apically from the inner segment of wild type and *ift57* mutants. Ciliary projections were not observed in *ift88* mutants. However, when stained with ZPR1, a marker for red-green double cone

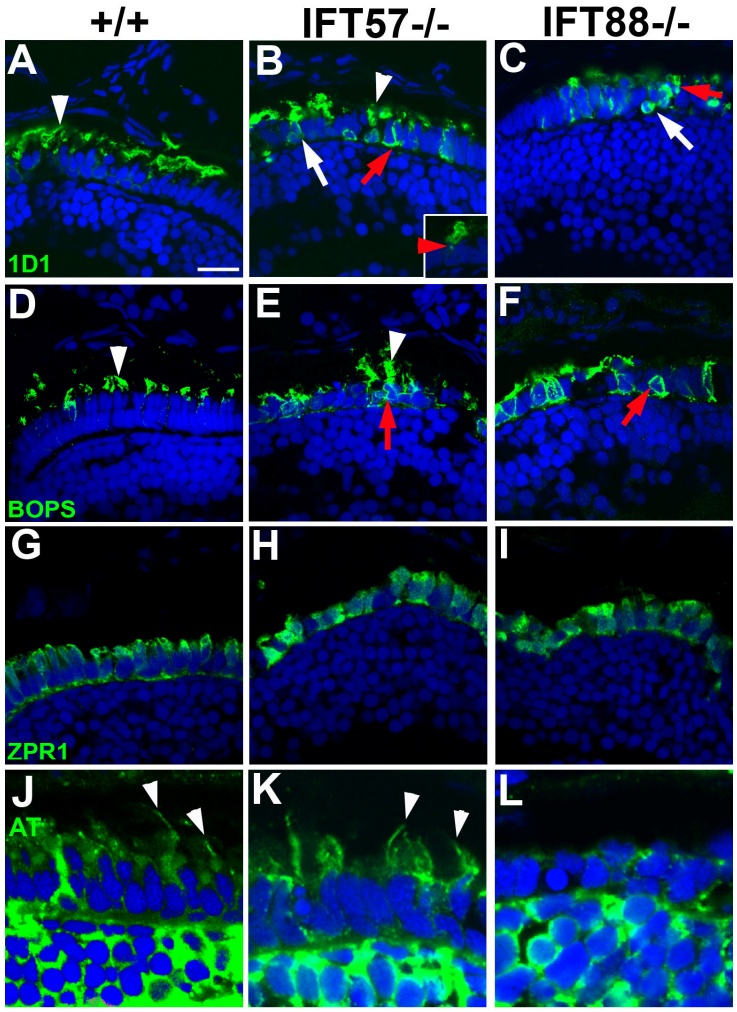

Fig. 14. Immunohistochemical analysis of wild type and IFT mutants. Retinal cryosections of 4 dpf larvae were stained for rhodopsin (1D1), blue cone opsin (BOPS), ZPR1, which labels cones and acetylated tubulin to label cilia. In all panels, immunolabel is shown in green and nuclei are counterstained with DAPI (blue). (A-F) White arrowhead indicates outer segment, red arrow indicate mislocalized opsin, white arrow indicates pyknotic nuclei, red arrowhead indicates opsin mislocalized around basal body. (G-I) ZPR1 labeling indicates red-green double cone morphology at 4 dpf. (J-L) Anti-acetylated tubulin labels the connecting cilia (arrowheads). Bar = 10µm

morphology, we found that *ift57* and *ift88* mutant photoreceptor morphology was abnormal (Fig. 14G-I).

As mislocalization of opsin can cause photoreceptor degeneration, and defects in opsin transport are associated with disorganized outer segments (Pazour et al., 2002a), we used transmission electron microscopy (TEM) to examine the photoreceptor morphology of 4 dpf *ift57* and *ift88* mutants (Fig. 15A-C). Wild type photoreceptors had elongated outer segments, while *ift88* mutants exhibited no photoreceptor outer segments. In contrast, both rod and cone outer segments were seen in *ift57* mutants. Consistent with results from immunohistochemistry, basal bodies and connecting cilia were observed in *ift57* mutant photoreceptors. We observed vesicle membranes accumulating near the connecting cilium in *ift57* mutants. These vesicles were similar to those seen in photoreceptors expressing a dominant-negative *Rab8*, which disrupted transport of vesicular cargo through the connecting cilium (Moritz et al., 2001). These membranes were likely post-Golgi vesicles that reflect inefficient protein transport through the outer segment, which is consistent with results of opsin mislocalization in the inner segment. Although the outer segments were shorter and ciliary transport was affected, the disk membranes remained well ordered and tightly stacked in the *ift57* mutants. Upon quantification, *ift57* mutants were found to have photoreceptor outer segments that were reduced in length by 75% compared to wild type photoreceptors (Fig. 16A). To quantify how the loss of *Ift57* and *Ift88* affected rhodopsin transport, we performed immunogold analysis on *ift57* and *ift88* mutants using the anti-rhodopsin antibody 1D1 (Fig. 15F-H). Although the rhodopsin immunogold label localized

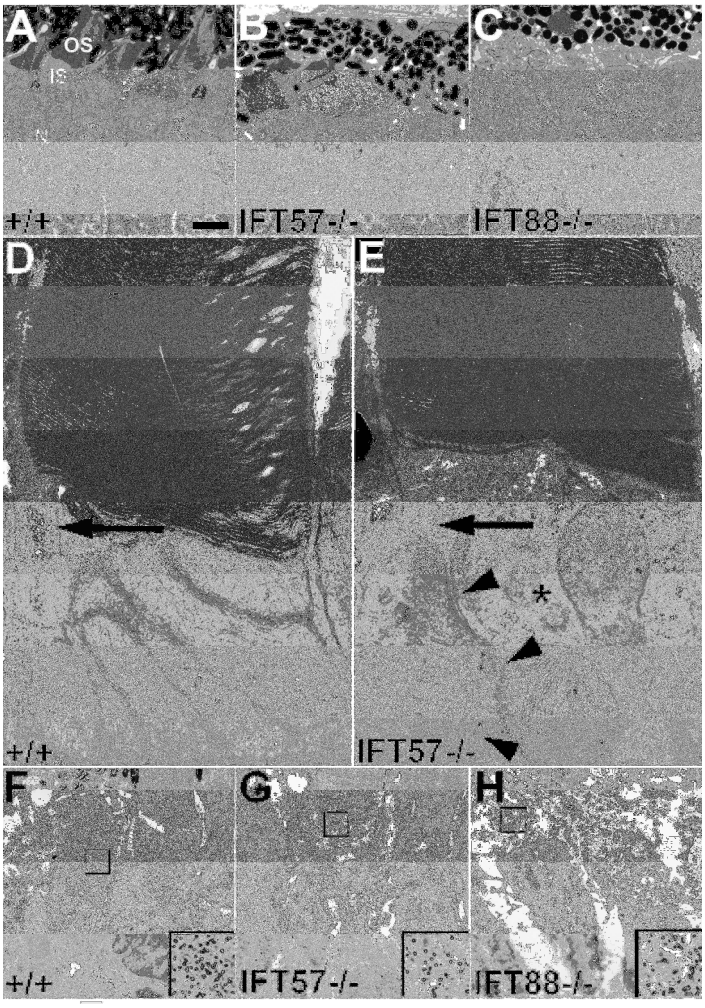

Fig. 15. Transmission electron microscopy of 4 dpf wild type and IFT mutant retinas. (A-C) Low magnification micrographs of retinas illustrate the outer segment (OS), inner segment (IS) and nucleus (N). (D, E) High magnification micrographs of wild type and *ift57* mutant retinas. *ift57* mutants have accumulated vesicles (black arrowheads). An asterisk denotes centrioles. (F-H) Immunogold labeling of rhodopsin, outer segments are outlined by broken line and insets are magnified views of the boxed area in each panel, which illustrate gold particle density. Bar = 2µm (A-C), 200nm (D, E), 0.75 µm (F), 1µm (G,H).

primarily to the rod outer segments in *ift57* mutants (Fig. 15G), gold particle density was reduced by 59% when compared to age-matched wild type controls (Fig. 16B). In *ift88* mutants, gold-labeled rhodopsin localized predominantly to the apical part of the inner segment but was also distributed in the plasma membrane (Fig. 15H), indicating that vesicular trafficking from the Golgi to the apical surface is unaffected by loss of *Ift88*. These data demonstrate that outer segment formation and opsin transport requires *Ift88*, whereas IFT can function at reduced efficiency without *Ift57*.

Biochemical studies have shown that *Ift57* directly interacts with *Ift20* and that *Ift20* directly interacts with the *Kif3B* subunit of kinesin II (Baker et al., 2003). Baker and colleagues (2003) proposed a model wherein *Ift57* recruits *Ift20* to the IFT particle and *Ift20* serves as the link between kinesin II and the IFT particle. To investigate the nature of the *Ift57-Ift20* interaction *in vivo*, we analyzed the localization of *Ift20* in *Ift57* mutant photoreceptors. In immunohistochemical analysis, the polyclonal antibodies we generated against *Ift20* failed to label with sufficient specificity for conclusive results. We therefore injected 1-cell embryos with a plasmid containing an *Ift20*-GFP fusion protein under the control of a *Xenopus laevis* rhodopsin promoter to transiently express *Ift20*-GFP in a subset of zebrafish rod photoreceptors. In transgenic rods of 4 dpf wild type embryos, *Ift20*-GFP was observed at the base of the connecting cilium, as demonstrated by colocalization with anti-acetylated tubulin (Fig. 17A). *Ift20*-GFP also localized to the base of the cilium in *ift57* mutant rods, indicating that ciliary localization of *Ift20* does not require *Ift57* (Fig. 17B). Consistent with recent reports that *Ift20* also localized to the Golgi apparatus (Follit et al., 2006b), we observed that *Ift20*-GFP

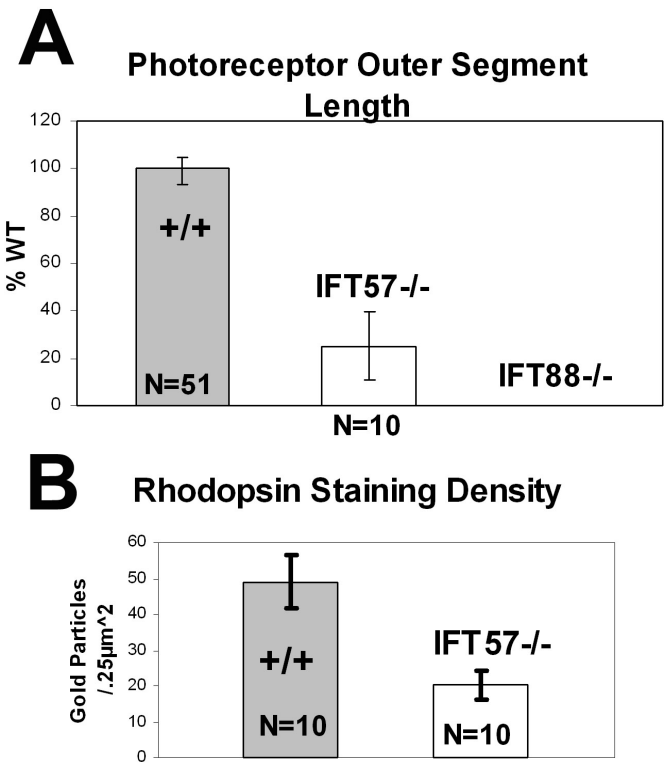

Fig. 16. Quantification of outer segment length and rhodopsin staining density within the outer segments of wild type and *ift57* mutants. (A) *ift57* mutant photoreceptor outer segments are reduced in length by 75% when compared to age-matched wild type photoreceptors. Data was taken from retinas of four animals for both wild type and IFT mutants. (B) Photoreceptor outer segments in *ift57* mutants contain 59% less rhodopsin. Staining density was determined by counting colloidal gold particles in a random $0.25\mu m^2$ region of rod outer segments with each data point obtained from a unique outer segment. Data was obtained from retinas of four animals for both wild-type and *Ift57* mutants. (A) $P<0.01$, (B) $P<0.0001$, as determined by a Students t-test.

fluorescence colocalized with antibodies against syntaxin-6, a marker for the trans-Golgi network, in both wild type and *ift57* mutants (Fig. 17C-D). As mutation of *ift88* completely abolishes IFT and our *ift57* mutant exhibits some functional IFT, we predicted that loss of *Ift57* would not affect the localization of *Ift88* to the connecting cilium. When we immunolabeled *ift57* mutant retinal sections with an anti-*Ift88* antibody, we observed *Ift88* staining that colocalized with acetylated tubulin. The pattern of localization of *Ift88* also indicated that *Ift88* was present within the connecting cilium itself, consistent with our assertion that *ift57* mutants retain some functional IFT. Taken together, these results indicate that *Ift57* is not required for the normal localization of *Ift20* or *Ift88* to the base of the connecting cilium.

We next analyzed the composition of the IFT particle in *ift57* mutants in order to understand how the process of IFT could occur in the absence of the *Ift57* protein. We first performed western blotting experiments on wild-type and *ift57* mutant larval lysates (Fig. 18A). Protein blots probed with antibodies against *Kif3A*, *Ift88*, *Ift52* and *Ift20* showed that IFT protein levels were present at levels that would likely be sufficient for biological activity. As shown previously, we did not detect measurable levels of *Ift57* protein in mutant lysates. These results suggested that loss of *Ift57* did not significantly alter the expression of other IFT components. We next performed co-immunoprecipitation experiments on 4 dpf wild type and *ift57* mutant lysates. Briefly, 4 dpf zebrafish larvae were homogenized and IFT proteins co-immunoprecipitated using a polyclonal antibody against zebrafish *Ift88* (Fig. 18B). We found that *Ift52*, *Ift20* and the *Kif3A* subunit of kinesin II could be co-precipitated from wild-type zebrafish lysates.

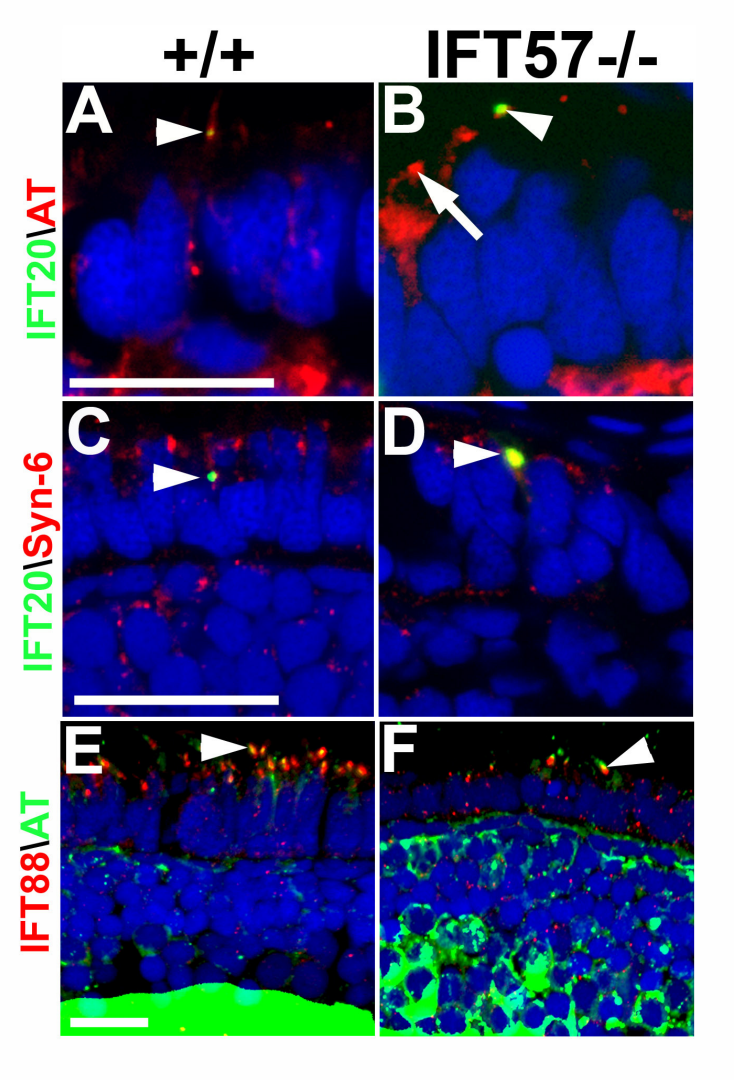

Fig. 17. *Ift20*-GFP localization in wild type and *ift57* mutant photoreceptors. (A,B) Arrow points to the connecting cilia in a neighboring cell that does not express the *Ift20*-GFP transgene. (C-D) In the presence or absence of *Ift57*, *Ift20*-GFP localized to the Golgi apparatus where it colocalizes with syntaxin-6 (arrowhead). (E) *Ift88* localizes to the base of the connecting cilium (arrowhead) in wild type and *Ift57* mutant photorecptors (F). AT = acetylated tubulin. Syn-6 = syntaxin-6 Bar = 10µm (A,B,E,F); 40 µm (C, D).

When these experiments were performed on *ift57* mutant lysates, we found that *Kif3A* and *Ift52* co-precipitated, but *Ift20* did not. We were surprised to find that *Kif3A* also co-precipitated in the absence of *Ift20*, indicating that kinesin II can interact with the IFT particle independent of *Ift20*. When we performed the co-immunoprecipitation experiments on *ift57* mutant lysates, we noticed that significantly more *Kif3A* was present in our precipitates from *ift57* mutant lysates than from wild type lysates. Given that the process of IFT is defective in *ift57* mutants, but still occurs, we hypothesized that kinesin fails to dissociate from the IFT particle in the absence of *Ift57*. The interaction between kinesin II and the IFT particle is salt-sensitive and ATP-dependent, such that addition of 1 mM ATP to lysates blocks precipitation of kinesin II with the IFT particle (Baker et al., 2003). Consistent with these results, we found that kinesin II did not co-precipitate from wild type lysates in the presence of 1 mM ATP (Fig. 18C). When *ift57* mutant lysates were incubated with 1 mM ATP, however, the association between kinesin II and the IFT particle is maintained (Fig. 18C). However, if protein lysates were incubated with 10 mM ATP, the association between kinesin II and the IFT particle is lost in both wild type and *ift57* mutants (Fig. 18D). These data show that the ATP-dependent dissociation of kinesin II from the IFT particle is impaired, and suggest a role for *Ift57* and *Ift20* in mediating motor dissociation from the IFT particle.

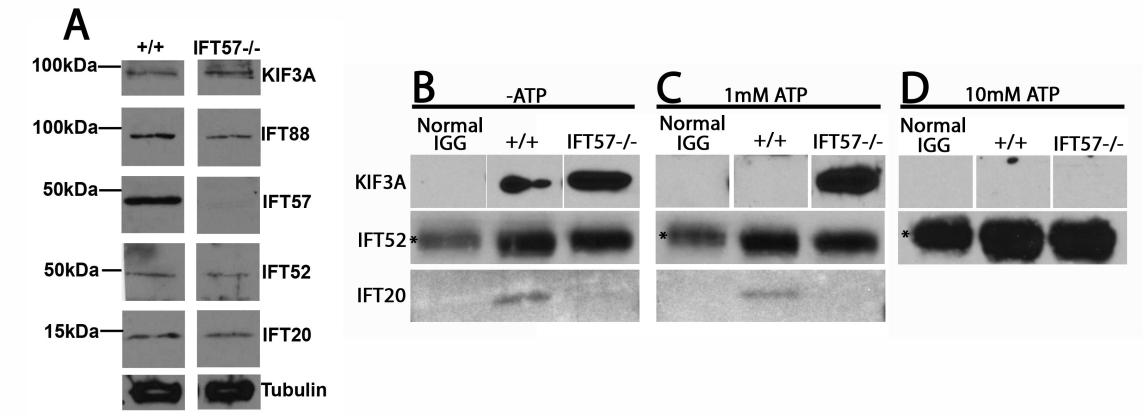

Fig. 18. Biochemical analysis of *ift57* mutants. (A) Western blot of lysates generated from the larval heads of 4dpf wild type and *ift57* mutants. Mutation of *ift57* does not significantly alter the abundance of any other IFT protein other than *Ift57*. (B) Lysates of wild type (+/+) or *ift57* mutants (IFT57-/-) were incubated with rabbit antibodies against zebrafish *Ift88* or normal rabbit IGG as a negative control. Immunoprecipitates were subsequently blotted with antibodies against *Kif3A*, *Ift52* and *Ift20*. In *ift57* mutants, *Ift20* is not precipitated along with the IFT complex, while more *Kif3A* is precipitated. (C) The addition of 1mM ATP to lysates blocks the association of *Kif3A* with the IFT particle in wild-type lysates but not ift*57* lysates. Lysates were prepared as described above, and then ATP was added to a final concentration of 1 mM prior to the addition of *Ift88* antibody and precipitation. (D) The addition of 10mM ATP blocks the association of *Kif3A* with the IFT particle in both wild-type and mutant lysates. Asterisk indicates IGG heavy chain band from precipitating antibody on immunoblots.

DISCUSSION

In this study we investigated and compared the roles of *Ift57* and *Ift88* in vertebrate photoreceptor development. Unlike the mouse Tg737^{orpk} allele of *ift88*, which forms outer segments, the zebrafish *ift57* mutant phenotype is not the result of a hypomorphic allele. Although a genome duplication occurred during the evolution of the lineage leading to zebrafish, only about 30% of these genes were retained (Postlethwait et al., 2000). *ift57* paralogs have not been identified in the zebrafish genome databases that might compensate for its function and generate a hypomorphic phenotype (Sun et al., 2004), and this study). Our western blotting analysis of *ift57* mutants also excludes maternal contribution of protein or mRNA as an explanation for the ciliary phenotype of *ift57* mutants at 4 dpf. Even if an undetectable amount of *Ift57* protein exists in *ift57* mutants, the stoichiometric composition of the IFT particle would be perturbed, likely resulting in a null phenotype. Taken together, these results demonstrate that the loss of *Ift57* and *Ift88* can produce distinct phenotypes that reflect functional roles for these proteins within the IFT complex, as discussed below.

Many studies of loss-of-function phenotypes in vertebrate IFT genes focus attention on phenotypic similarities and rarely emphasize differences, which implies that all IFT mutant phenotypes should be identical. Mutations in the mouse *Ift52, -57, -88* and *-172* orthologs all lead to identical defects in cilia formation, sonic hedgehog signaling and motor neuron differentiation (Houde et al., 2006; Huangfu et al., 2003; Liu et al., 2005). A mouse knockout of *ift57* reported loss of nodal cilia, however their analysis does not exclude the possibility of cilia formation and subsequent degeneration

(Houde et al., 2006). Morpholinos that disrupt zebrafish *ift88* and *ift57* gene expression produce similar defects in left-right asymmetry, kidney function and cilia motility, although subtle differences in cilia length and phenotypic outcomes were mentioned but not elaborated (Bisgrove et al., 2005; Kramer-Zucker et al., 2005). In zebrafish, a retroviral insertion mutation in the complex B gene *ift81* did not affect photoreceptor development (Gross et al., 2005) but did cause kidney cysts (Sun et al., 2004), while morpholino knockdown of a complex A protein, *ift140*, did not affect photoreceptor survival (Tsujikawa and Malicki, 2004). Our results provide the first *in vivo* comparative study of photoreceptor structure and function in two null IFT mutants and demonstrate that mutations in *ift57* and *ift88* affect different aspects of photoreceptor development.

Our data also indicate that ciliary transport and outer segment morphogenesis requires *Ift88*, whereas *Ift57* is required for effective transport and outer segment maintenance. Transport is also eliminated in *ift88* mutants of *Chlamydomonas*, mice and worms (Haycraft et al., 2001; Pazour et al., 2000; Qin et al., 2001). In contrast, the presence of connecting cilia and opsin labeling of outer segment structures indicate ciliary transport does occur in *ift57* mutants. It is important to note, however, that transport remains compromised in *ift57* mutants, as indicated by opsin mislocalization to the inner segment, vesicle accumulation at the base of the cilium, and an overall reduction in outer segment length.

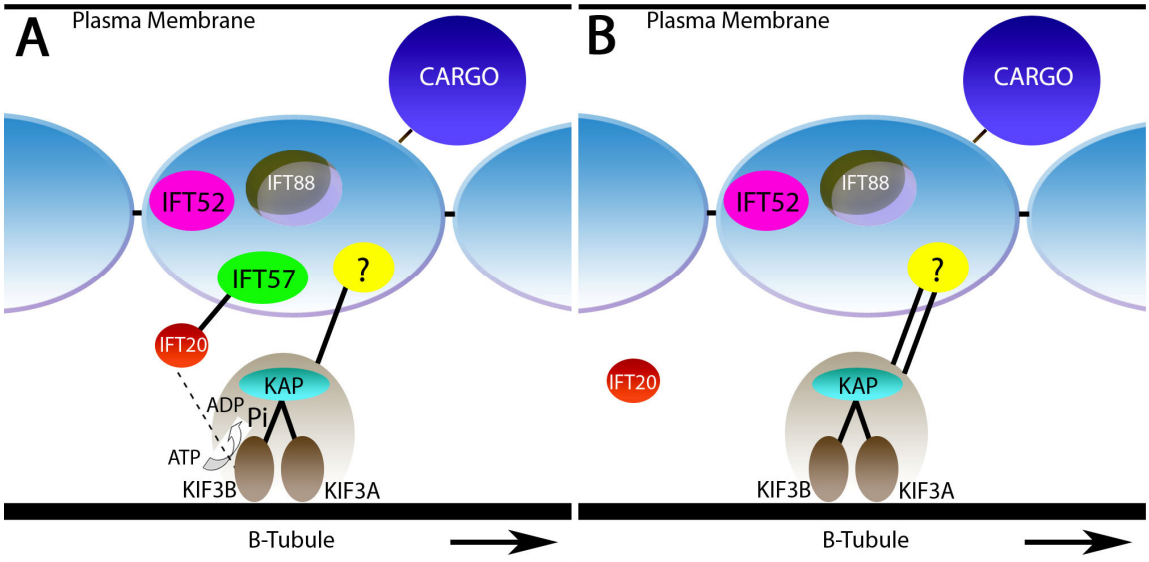

Fig. 19. *Ift57* and *Ift20* mediate the ATP-dependent dissociation of kinesin. (A) A model describing the nature of protein interactions within the IFT complex. *Ift57* tethers *Ift20* to the IFT particle, while kinesin binds to the IFT particle through an unknown entity. *Ift20* physically interacts with *Kif3B* and mediates the ATP-dependent dissociation of kinesin. (B) In the absence of *Ift57*, *Ift20* can no longer associate with the IFT particle. However, kinesin's interaction with the IFT particle is stabilized by loss of *Ift57* and *Ift20* from the IFT particle.

A previous analysis of a mutation in *CHE-13*, the *C. elegans* orthologue of *ift57*, noted that the *CHE-13* phenotype was identical to that of a previously characterized *ift88* mutation (Haycraft et al., 2003). Our analysis, however, indicates that mutation of these two genes results in different outcomes. This may be due to inherent differences in the mechanism of IFT between these two systems. Also, the authors did not exclude the possibility of formation of these structures and subsequent degeneration, which is what we observed in our study. Although transport is compromised, disk stacking in *ift57* mutant outer segments was unaffected. Opsin is believed to play an important role in the formation and stabilization of disk membranes within the outer segment (Nathans, 1992). Studies of rhodopsin heterozygous knockout mice found that reducing opsin by approximately 50% causes disorganization of outer segments and disk stacking, with some abnormally oriented membranes and a complete loss of outer segments in homozygous rhodopsin knockout mice (Humphries et al., 1997; Lem et al., 1999). Rhodopsin levels were reduced by almost 60% in *ift57* mutant photoreceptors yet no such disorganization of the outer segment was observed. One explanation is that opsin mislocalization kills the photoreceptor before outer segment disorganization occurs. Alternatively, zebrafish outer segments may require less opsin for disk membrane organization and outer segment integrity than do mammalian systems.

Our phenotypic and biochemical analyses of i*ft57* mutants support a model for protein interactions within the IFT particle that facilitate ciliary transport and anterograde motor dissociation. We show that *Ift20* does not bind the IFT particle in the absence of *Ift57*, indicating that *Ift57* mediates the interaction between *Ift20* and the

particle. Additionally, kinesin II co-precipitates with the IFT particle in *ift57* mutant lysates. These results indicate that the previously described *Ift20*-kinesin II interaction (Baker et al., 2003) is not the primary link between kinesin II with the IFT particle. We suggest that kinesin II binds to the IFT particle through an interaction with an unidentified IFT protein. Finally, we have shown that the ATP-dependent dissociation of kinesin II from the IFT particle is inhibited by loss of *Ift57*. Consistent with this, we also observe a greater quantity of *Kif3A* in *Ift57* mutant precipitates than in wild type precipitates. It is important to note, however that kinesin II has the ability to dissociate from the IFT particle in *Ift57* mutants, as addition of super-physiological levels of ATP (10 mM) can cause dissociation of kinesin II.

We propose that *Ift57* mediates the interaction between *Ift20* and the IFT particle, while an undefined IFT protein or adaptor protein serves as the primary bridge between kinesin II and the IFT particle (Fig. 19). Our data indicate this bridge must be independent of both *Ift57* and *Ift20*. Additionally, we propose that *Ift57* and/or *Ift20* mediates dissociation of heterotrimeric kinesin II from the IFT particle, potentially by enhancing the ATPase activity of *Kif3B*. As *Ift20* is the only IFT protein known to interact with kinesin II, loss of *Ift20* from the IFT particle is the likely explanation for the observed kinesin II dissociation defect. However, we cannot rule out a direct role for *Ift57* in this process, though yeast 2-hybrid analysis showed no interaction between *Ift57* and any of the kinesin II subunits (Baker et al., 2003). Others have shown that the ATP-mediated dissociation of kinesin II from the IFT particle is independent from the ATP-dependent dissociation of kinesin II from microtubules, illustrating that our data reflect a

novel mechanism for motor dissociation and are not a result of impaired microtubule association. According to our model neither the assembly of the IFT particle nor the recruitment of kinesin II requires *Ift57*.

Knockdown of *ift20* has been shown to abolish cilia in cultured mammalian cells, indicating that *Ift20* is essential for IFT. Our data indicate that *Ift20* is not essential for IFT but does play a vital role in effective transport. The more severe phenotype described in cultured cells may reflect additional roles of *Ift20* in post-Golgi to cilium trafficking of proteins. Consistent with this, Follit et al. (2006) observe a reduction in the amount of polycystin-2 that is trafficked to the cilium. As we show that loss of *Ift57* abolishes the interaction between *Ift20* and the IFT particle, we are able to separate the Golgi and ciliary functions of *Ift20* and demonstrate its role within the IFT particle and that *Ift20* is necessary only for efficient IFT.

In conclusion, we have provided novel details about IFT function in vertebrate photoreceptors that likely have broader implications for IFT function in a wide variety of tissues. First, we have demonstrated that *Ift57* is not absolutely required for ciliogenesis and transport in photoreceptors but is required for ciliary elongation (e.g. outer segment growth) and the long-term maintenance of photoreceptor survival. Combined with previous results demonstrating that loss of *Ift81* or *Ift140* does not affect photoreceptor development, it is likely that most, but not all, IFT proteins are required for ciliogenesis in all vertebrate tissues and the composition of the IFT particle varies from tissue to tissue. Second, we have provided evidence that presents novel insights into how *Ift20* associates with the IFT particle, and the mechanism by which kinesin II dissociates from

the IFT particle. These data illustrate how proper dissociation of kinesin II is necessary for efficient IFT and show the functional nature of two previously described interactions within the IFT particle. Additional biochemical studies are necessary to elucidate which IFT subunit(s) mediate the particle's interaction with kinesin II, the mechanism by which the IFT particle assembles and the mechanisms that mediate kinesin II dissociation from the IFT particle. Finally, the structure and function of cilia varies with different tissues and the composition of the IFT particle may reflect this diversity. Identification of IFT genes required for photoreceptor development may help predict whether mutations in specific IFT genes will lead to retinal disease.

MATERIALS AND METHODS

Zebrafish Care and Maintenance

The *oval* allele is an ENU induced point mutation that caused a T-A transition, resulting in a premature stop codon in exon 11 and a null mutation in the *ift88* gene. The *ift88* mutant line was a gift from Jarema Malicki (Doerre and Malicki, 2002) and the *ift57* mutation was previously described (Gross et al., 2005). Zebrafish were maintained according to standard procedures (Westerfield, 1995).

Morpholino Knockdown

Morpholino knockdown of *ift57* was carried out using morpholinos directed against the splice site, sequence 5' GTTATCGCCTCACCAGGGTTCGAAG 3'. A morpholino designed against the 5'UTR of *ift88*, sequence 5' TTATTAAACAGAAATACTCCCA 3' was used to knock down *ift88* gene expression.

Both morpholinos used have been described previously (Tsujikawa and Malicki, 2004) and were synthesized by Gene Tools, LLC.

Transient Expression of *Ift20*-GFP

An *Ift20*-GFP fusion construct driven by the zebrafish opsin promoter was obtained from Dr. Joe Besharse (Medical College of Wisconsin). Transgenic photoreceptors were generated as described (Perkins et al., 2002) and analyzed by immunohistochemistry as described below.

Histology: Light Microscopy and Transmission Electron Microscopy (TEM)

Embryos were processed for light microscopy and TEM histology as previously described (Schmitt and Dowling, 1999). Histological sections were stained with a solution of 1% azure blue, 1% methylene blue and 1% sodium borate (Electron Microscopy Sciences). For immunogold labeling, staged embryos were fixed in 4% paraformaldehyde, 0.5% glutaraldehyde and 1% tannic acid in 0.1M sodium cacodylate buffer (pH 7.4) overnight at 4°C. Embryos were washed in 0.15M sodium cacodylate buffer at 4°C and dehydrated in a graded ethanol series with 1% p-phenylenediamine. Specimens were embedded in LR-White resin (Electron Microscopy Sciences) and polymerized overnight at 55°C. For immunolocalization, incubations were done in a PELCO Biowave (Ted Pella Inc) at low wattage, at 30°C. Grids were incubated in blocking solution (PBST + 4% cold water fish gelatin), then in primary antibody (1D1 1:50) diluted in blocking solution. Grids were washed with PBS then incubated in secondary antibody, donkey anti-mouse 18nm colloidal gold (Jackson Immuno Research 1:30) diluted in TBST (TBST+2% normal donkey serum +4% coldwater fish gelatin).

Grids were washed with TBS and then fixed with 1% glutaraldehyde and post stained with 2% uranyl acetate. Photographs were obtained on a JEOL 1200EX transmission electron microscope and images processed using Adobe Photoshop.

Antibody Production

Rabbit polyclonal antibodies were generated against synthetic peptides corresponding to the C-terminus of *Ift88*, *Ift57*, *Ift52* and *Ift20*. The antigens were LEFADGELGDDLLPE, CMHATHLLEPNAQAY, CKKLNEEHDVDTAEARFSMY and CEAEQSEFIDQFILQK, respectively. The *Ift88*, *Ift57* and *Ift20* antibodies were generated and affinity purified by Bethyl Labs, while the *Ift52* antibody was generated and affinity purified by Open Biosystems.

Immunohistochemistry

Immunohistochemistry was performed as previously described (Perkins et al., 2005). Images were obtained on an Olympus FV1000 confocal microscope or a Zeiss ImagerZ1 fluorescence microscope fitted with an ApoTome. Images were prepared using Adobe Photoshop software. The following list of primary antibodies were used, followed by the dilution used: 1D1 (1:200)(Fadool, 1999), cone opsin antibodies (1:200)(Vihtelic et al., 1999), ZPR1 (Zebrafish International Resource Center 1:200), anti-acetylated tubulin (Sigma 1:500), anti-syntaxin6 (BD Bioscience 1:200) anti-*Ift88* (1:5000). The appropriate fluorescently conjugated antibodies (Jackson Immunological) were used at 1:500 dilutions. Slides were counterstained with DAPI (Invitrogen) to label DNA.

Immunoprecipitation

4 dpf wild-type and *ift57* mutants were collected and homogenized using 200-250 larvae per reaction in IP lysis buffer (PBS + 1% Triton + 5mM EDTA) supplemented with a cocktail of protease inhibitors (Complete-mini EDTA Free, Roche). Samples were lightly sonicated and lysates subsequently clarified by centrifugation at 13,200 RPM at 4°C for 15 minutes. Lysates were then precleared with ExactaCruz F preclearing matrix (Santa Cruz Biotechnology) according to manufacturer's instructions. Polyclonal rabbit anti-*Ift88* antibody was bound to ExactaCruz F IP matrix per instructions. An equivalent amount of normal rabbit IGG (Santa Cruz Biologicals) was bound to ExactaCruz F IP matrix as a negative control. Lysates were then pooled and normalized for total protein concentration before incubation overnight at 4°C with antibody-IP matrix on a rocking platform. The IP matrix was pelleted by low speed centrifugation and washed 2X with cold PBS and then 5X with cold IP lysis buffer. Samples were eluted from IP matrix by boiling 5 minutes in 45µl of 2X laemmli buffer and then 20µl loaded on an SDS-PAGE gel for analysis. For ATP experiments, prior to addition of antibody-IP matrix to the lysates, ATP (Roche) was added to achieve either 1 or 10mM final concentration. The lysates were incubated with ATP at 4C for 1h prior to the addition of antibody-IP matrix to the lysates.

SDS-PAGE and Immunoblot Analysis

4 dpf zebrafish heads were homogenized in IP lysis buffer at a volume of 3µl per head, then lightly sonicated. 4x SDS sample buffer was added to the lysate and the

samples were then boiled for 5min. prior to centrifugation at 13,200 rpm for 10min and subsequent loading on a 10% PAGE gel. Following electrophoresis, proteins were blotted onto PVDF membranes (Bio-Rad) and subjected to immunodetection using standard protocols. The following dilutions of primary antibodies were used: K2.4 (mouse anti-*Kif3A*, Covance 1:10,000), Rabbit anti-*Ift88* (1:5000), Rabbit anti-*Ift52* (1:5000), Rabbit anti-*Ift20* (1:5000), Rabbit anti *Ift57* (1:5000), mouse anti-acetylated tubulin (Sigma, 1:10,000).

CHAPTER IV

RETROGRADE INTRAFLAGELLAR TRANSPORT BY CYTOPLASMIC DYNEIN-2 IS REQUIRED FOR OUTER SEGMENT EXTENSION IN VERTEBRATE PHOTORECEPTORS BUT NOT ARRESTIN TRANSLOCATION

OVERVIEW

This chapter assesses the role of retrograde intraflagellar transport in vertebrate photoreceptor cell biology and physiology. It reflects a collaboration with John Dowling's Lab in the Department of Molecular and Cellular Biology at Harvard University, as Ishara Mills-Henry performed the electroretinograms in this study.

SUMMARY

Anterograde Intraflagellar Transport (IFT) is essential for photoreceptor outer segment formation and maintenance, as well as for the proper intracellular trafficking of opsins. However, the role of retrograde IFT in vertebrate photoreceptors remains unclear. Some proteins in photoreceptors, such as arrestin, move in a retrograde direction through the photoreceptor cilium, and retrograde IFT is a candidate to mediate this process. The purpose of this study was to evaluate the cell biology and physiology of photoreceptor lacking the retrograde IFT motor, cytoplasmic dynein-2. We utilized morpholino oligonucleotides against the heavy chain (*dync2-h1*), light intermediate chain (*dync2-li1*) and intermediate chain (*dync2-i1*) subunits of cytoplasmic dynein-2 to compromise retrograde IFT function in larval zebrafish. These zebrafish morphants were subjected to immunohistochemical and ultrastructural analyses to determine the

effects of cytoplasmic dynein-2 dysfunction on photoreceptors and other ciliated cells. Additionally, whole field electroretinograms (ERGs) were performed on 5 and 6 dpf dynein morphants in order to assess the effect of cytoplasmic dynein-2 dysfunction of retinal electrophysiology. Analyses of zebrafish lacking cytoplasmic dynein-2 function revealed morphants had small eyes, kidney cysts, and short photoreceptor outer segments, some of which were disorganized and accumulated vesicles. Morphant photoreceptor connecting cilia were swollen, but neither opsin nor arrestin was mislocalized, while IFT88 accumulated in the distal region of the connecting cilium. Nasal cilia were severely shortened and displayed cytoplasmic swelling along the axoneme. Our ERG analysis revealed electrophysiology is affected by cytoplasmic dynein-2 dysfunction. This study shows that retrograde IFT is essential for outer segment extension, organization and IFT protein recycling in vertebrate photoreceptors. We show for the first time that the *dync2-i1* subunit of cytoplasmic dynein-2 is necessary for retrograde IFT. Additionally, the retrograde movement of visual arrestin is not mediated by retrograde IFT. Finally, our ERG results suggest cytoplasmic dynein-2 may play a previously unappreciated role in retinal electrophysiology.

INTRODUCTION

Vertebrate photoreceptors detect light through the phototransduction cascade, which occurs in the outer segment. The outer segment is a modified sensory cilium (De Robertis, 1960), and as all other cilia, lacks the cellular machinery for protein synthesis. Thus, all of the protein components used in phototransduction and that make up the outer segment, such as opsins, must pass through the narrow connecting cilium. Failure to

transport opsins efficiently to the outer segment leads to photoreceptor degeneration and death (Grimm et al., 2000; Portera-Cailliau et al., 1994), as opsins play an important structural role in the outer segment (Lem et al., 1999). Thus, the effective transport of proteins through the connecting cilium is critical to both the function and survival of photoreceptors.

The process of intraflagellar transport (IFT) is the mechanism by which some proteins move through the connecting cilium to the outer segment (Marszalek et al., 2000; Pazour et al., 2002a). Studies of zebrafish IFT mutants have shown that the initial stages of outer segment formation require IFT and that IFT is also necessary for outer segment maintenance (Krock and Perkins, 2008; Sukumaran and Perkins, 2009b; Tsujikawa and Malicki, 2004). Similarly, loss of IFT function causes mislocalization of opsins, a phenotype that is accompanied by photoreceptor cell death. These studies, along with similar studies in mouse (Marszalek et al., 2000; Pazour et al., 2002a), reinforce the premise that the outer segment is, in fact, a modified cilium (Marszalek et al., 2000). As several diseases affecting cilia and ciliary trafficking, such as Jeune asphyxiating thoracic dystrophy (JATD) and Bardet-Biedl Syndrome (BBS), result in blindness and retinal degeneration, understanding the process of IFT in the context of vertebrate photoreceptors is of great importance.

In photoreceptor cell biology, anterograde IFT has received the most scrutiny, while the role of retrograde IFT in photoreceptors remains largely unexplored. Kinesin-II (Kozminski et al., 1995), and OSM-3 (Snow et al., 2004) cooperate to drive anterograde IFT, while cytoplasmic dynein-2 (Pazour et al., 1999) mediates retrograde

IFT. The retrograde IFT motor is composed of an ATP-dependent homodimeric heavy chain, *Dync2-h1* (previously termed DHC-1b) (Pazour et al., 1999; Porter et al., 1999; Signor et al., 1999; Zhang et al., 1993), a cytoplasmic dynein-2 light intermediate chain, *dync2-li1* (Hou et al., 2004; Mikami et al., 2002; Perrone et al., 2003), an intermediate chain, *dync2-i1* (Rompolas et al., 2007), and light chain known as LC8 (Pazour et al., 1998; Rompolas et al., 2007). Importantly, *dync2-h1* and *dync2-li1* are expressed in bovine photoreceptors and localize to the connecting cilium (Mikami et al., 2002), suggesting the process of retrograde IFT occurs in photoreceptors.

Retrograde IFT is indeed necessary in other vertebrate cilia, as mouse *Dync2-h1* and *Dync2-li1* mutants have stumpy nodal cilia with swollen ciliary tips that contain disorganized microtubules, IFT proteins and cellular debris (May et al., 2005; Rana et al., 2004). The ciliary phenotype resulting from *dync2-i1* dysfunction remains unknown, though knockdown of the *Trypanosome dync2-i1* homologue resulted in flagellar dysfunction (Baron et al., 2007). So, what then, is the potential role form retrograde IFT in photoreceptors?

The established function for retrograde IFT is to recycle IFT proteins and other ciliary components by returning them to the basal body from the tip of the cilium (Pazour et al., 1999; Qin et al., 2004). This function has not been formally tested in phororeceptors. The movement of some proteins through the connecting cilium is indeed unidirectional, (e.g. opsins), however, is clear that some proteins move in a retrograde fashion, such as arrestin and transducin, reviewed in (Calvert et al., 2006)).

During light adaptation, arrestin moves from the photoreceptor inner segment to the outer segment through the connecting cilium, while transducin moves in a complementary fashion. During dark adaptation, arrestin translocates back to the photoreceptor inner segment, while transducin moves into the outer segment (Brann and Cohen, 1987; Philp et al., 1987; Whelan and McGinnis, 1988). Although most current models suggest arrestin and transducin translocate via passive diffusion, there remains a possibility that an active transport mechanism plays a role. First, the kinetics of arrestin movement during light adaptation are estimated move at a rate 100-1000 times that of rhodopsin, suggesting an active transport mechanism would be incapable of moving cargoes this quickly (Calvert et al., 2006). However, the movement of arrestin during dark adaptation is much slower. This raises the possibility that anterograde and retrograde arrestin movement are mediated by different processes and that molecular motor-driven transport could account for this phenomenon. Second, both the actin and microtubule cytoskeletons are required for the retrograde movements of arrestin and transducin, which is consistent with an active transport model (Broekhuyse et al., 1985). As cytoplasmic dynein-2 is a microtubule minus-end motor, and IFT is a known mechanism that mediates retrograde protein movement, retrograde IFT is a prime candidate to mediate retrograde arrestin translocation through the photoreceptor connecting cilium.

In this study, we utilize antisense-morpholino oligonucleotides to abrogate expression of *dync2-h1*, *dync2-li1* and *dync2-i1* in order to understand the function of retrograde IFT in vertebrate photoreceptors. Additionally, we describe robust light-

dependent translocation of visual arrestin in larval zebrafish rods. We have found that retrograde IFT is necessary for outer segment extension, organization, and recycling of IFT proteins in photoreceptors. We provide the first functional evidence to show that the cytoplasmic dynein-2 intermediate chain is required for the process of retrograde IFT, and that retrograde IFT plays an essential role in both sensory and motile cilia. Finally, we show that the electrophysiological response of dynein morphant retinas is compromised, suggesting a greater role for cytoplasmic dynein-2 in retinal physiology.

RESULTS

To identify the zebrafish *dync2-h1* orthologue, we search performed a BLAST search of the zebrafish genome for sequences with homology to mouse *Dync2-h1*. Two partial mRNA sequences were recovered, which represented 6.3kb of the 5' end and 11.4kb of the 3' end of *dync2-h1* (accession numbers XR_029028 and XR_029028.2, respectively), these two sequences combined yielded a predicted protein product of 4266 amino acids, which was 69% identical to mouse *Dync2-h1*, but only 26% identical to mouse *Dync1-h1* and 24.5% identical to zebrafish *dync1-h1*. To verify this as the true zebrafish orthologue of previously described *dync2-h1* genes, we performed a phylogenetic analysis of zebrafish *dync2-h1* using the Neighbor-Joining method (Fig. 20) and found that this zebrafish *dync2-h1* sequence is most closely related to other vertebrate dync2-h1 genes. Sequence data for *dync2-li1* and *dync2-i1,* the zebrafish orthologue of *Chlamydomonas FAP133* were identified using Ensembl. In zebrafish, previous studies have shown IFT genes are most highly expressed in the CNS and

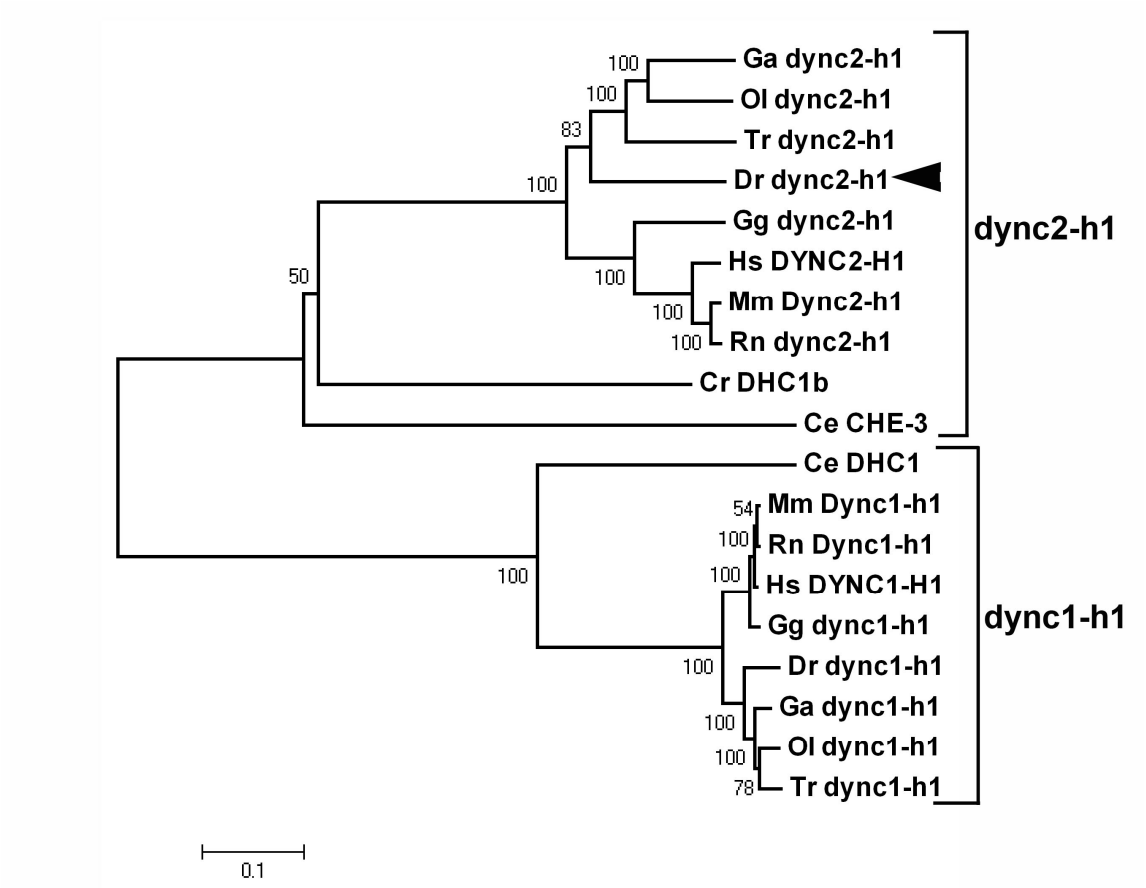

Fig. 20. Phylogenetic analysis of zebrafish *dync2-h1*. A neighbor-joining tree was generated based on Clustal W protein sequence alignments of Cr, *Chlamydomonas reinhardtii*, Ce, *C. elegans*, Ga, *Gasterosteus aculeatus,* Gg, *Gallus gallus,* Hs, *Homo sapiens,* Mm, *Mus musculus,* Ol, *Orzius latipes* Rn, *Rattus norvegicus,* and Tr, *Takifugu rubripes dync1-h1* and *dync2-h1* genes. The bootstrap percentages (500 iterations) are shown at the branch points. Note how the *dync2-h1* gene identified in this study (arrow) lies closest to other vertebrate *dync2-h1* genes. Scale bar, 0.1 substitutions/amino acid.

pronephros (Bisgrove et al., 2005). As cytoplasmic dynein-2 genes have not been investigated previously in this system, we first wanted to assess the expression pattern of *dync2-h1*, *dync2-li1* and *dync2-i1* via *in situ* hybridization on 72 hpf zebrafish embryos. Consistent with cytoplasmic dynein-2 being involved in IFT, we observed expression of *dync2-h1*, *dync2-li1* and *dync2-i1* most strongly in the CNS and pronephros (Fig. 21A-C). Though *dync2-h1* and *dync2-li1* have previously been shown to be expressed in photoreceptors (Mikami et al., 2002), others have suggested that *dync2-i1* is only expressed in motile cilia (Rompolas et al., 2007). To address this question, we sectioned embryos following *in situ* hybridization and observed that *dync2-h1*, *dync2-li1* and *dync2-i1* genes were all expressed throughout the retina, including in photoreceptors (Fig. 21D-F). The identical expression patterns of dync2-h1, *dync2-li1* and *dync2-i1* are consistent with these being part of the same molecular complex.

In order to disrupt retrograde IFT, we injected antisense morpholino oligonucleotides against the *dync2-h1*, *dync2-li1* and *dync2-i1* genes into one-cell stage zebrafish embryos. Zebrafish IFT mutants all exhibit a specific constellation of phenotypes due to ciliary dysfunction, these phenotypes include ventral curvature of the body axis, kidney cysts and small eyes. Remarkably, *dync2-h1* morphants look very similar to previously described IFT mutants, such as *ift88* ^{oval} and *ift57*^{hippi} (Kramer-Zucker et al., 2005; Tsujikawa and Malicki, 2004). The *dync2-h1* morphants have a distinctive ventral curvature of the body axis, small eyes and 100% penetrance of kidney cysts at 4 dpf (Fig. 21F). *dync2-li1* morphants similarly exhibit small eyes and a high

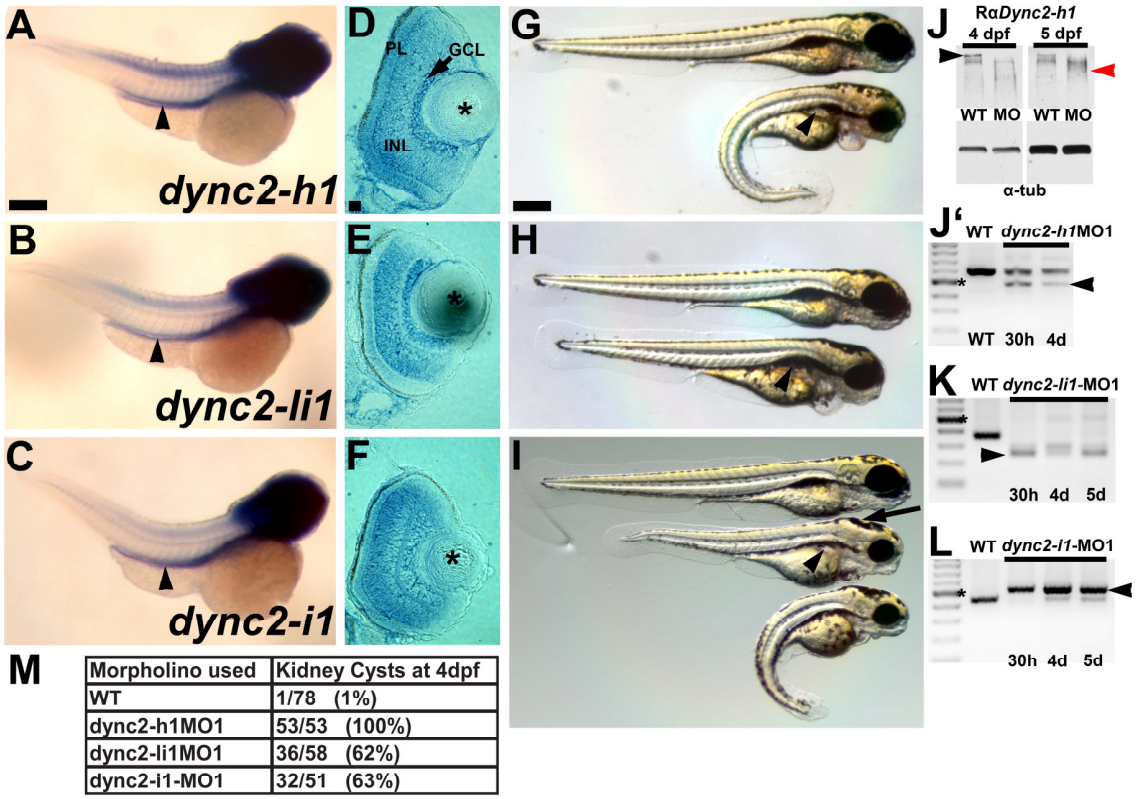

Morpholino used	Kidney Cysts at 4dpf
WT	1/78 (1%)
dync2-h1MO1	53/53 (100%)
dync2-li1MO1	36/58 (62%)
dync2-i1-MO1	32/51 (63%)

Fig. 21. Dynein gene expression and morphant phenotypes. (A-C) *In situ* hybridization performed on 72 hpf zebrafish. (D-F) Transverse retinal sections of *in situs* from A-C, dorsal is up. (G-I) Dynein morphant phenotypes, kidney cysts are indicated with arrowheads, hindbrain swelling (I, arrow) was observed for *dync2-i1* morphants. (J-L) Assessment of morpholino efficacy. (J) Western blot of cellular lysates from WT and *dync2-h1* morphants. Red arrowhead indicates 500kDa standard. (J'-L) RT-PCR of *dync2-h1, dync2-li1 and dync2-i1* morphants, arrowheads indicate RT-PCR products that are the result of defective splicing. (M) Table of penetrance of kidney cysts observed in dynein morphants at 4 dpf. Asterisks in (D-F indicates the lens) and in (K,L) indicate 500bp DNA standard. Scale bar: (A-C, G-I) 200µm; (D-F) 20µm

penetrance of kidney cysts (Fig 2H) though they do not exhibit ventral curvature of the body. Knockdown *dync2-i1* yielded morphants with small eyes, pronounced swelling in the hindbrain and kidney cysts, and a penetrance of kidney cysts similar to that of *dync2-li1* morphants (Fig. 21M). Some *dync2-i1* morphants had a ventral curvature of the body while others did not (Fig. 21I), and both *dync2-li1* and *dync2-i1* morphants were shorter than age-matched controls. Importantly, knockdown experiments with non-overlapping morpholinos designed against each gene resulted in phenotypes identical to those just described, strongly suggesting that the phenotypes observed in the dynein morphants are specific (data not shown). These phenotypes are consistent with ciliary defects and with the known function of cytoplasmic dynein-2 as the retrograde IFT motor. Western blots were performed on heads of 4 dpf and 5 dpf larvae using a polyclonal antibody against zebrafish *Dync2-h1* show it recognizes a high molecular weight band that is depleted in morphants at 4 and 5 dpf (Fig. 21J). RT-PCR analysis of *dync2-h1* morphants showed similar results (Fig. 21J'). Due to the absence of suitable antibodies against *dync2-li1* and *dync2-i1*, we performed RT-PCR to assess the efficacy of our morpholinos to interfere with splicing. Sequencing of two RT-PCR products revealed that the *dync2-li1* morpholino disrupted splicing through 5 dpf, and resulted in either exclusion of the 70 bp exon 4 or exclusion of both exon 4 and the 35 bp exon 3 (Fig. 21K). Exclusion of exon 4 resulted in a frameshift of the downstream message and introduction of a stop codon, while exclusion of exons 3 and 4 produced an in-frame deletion that removed 35 amino acids from the protein. This 35 amino acid region is highly conserved among *dync2-li1* sequences and likely results in a nonfunctional protein, based on the

phenotypic analysis. The *dync2-i1* morpholino caused production of a longer transcript containing frameshift mutations, which resulted from inclusion of the 71 bp intron 4. RT-PCR of *dync2-i1* morphants revealed full knockdown at 30 hpf, and nearly complete knockdown at 4 and 5 dpf. (Fig. 21K,L). Taken together, these data show cytoplasmic dynein-2 activity was effectively inhibited through 5 dpf.

As the function of cytoplasmic dynein-2 in photoreceptors is unknown, we first performed histology on 4 dpf morphant retinas to assess the effect of loss of cytoplasmic dynein-2 on retinal organization. Similar to previously described IFT mutants, overall retinal organization was normal in all three dynein morphants. However, dynein morphant eyes were smaller than controls (Fig. 22). We did not observe pyknotic nuclei or other evidence of cell death within the photoreceptor layer of dynein morphants, unlike previously described IFT mutants (Krock and Perkins, 2008; Tsujikawa and Malicki, 2004). As IFT plays a critical role in outer segment formation and maintenance, we hypothesized that retrograde transport would also be important for outer segment integrity. At 4 dpf, transmission electron microscopy (TEM) revealed that wild-type photoreceptors have robust outer segments that extend into the retinal pigmented epithelium (Fig 23A-B). In contrast, all of the dynein morphants exhibited very short outer segments, with some photoreceptors completely lacking these structures (Fig. 23C,E,G). Higher magnification images of the photoreceptor connecting cilium showed that all dynein morphant connecting cilia were swollen, likely due to accumulation of IFT particles and cellular debris (Fig. 23D,F,H arrow). Many *dync2-li1* morphant photoreceptors had outer segments composed of disordered membranes, some

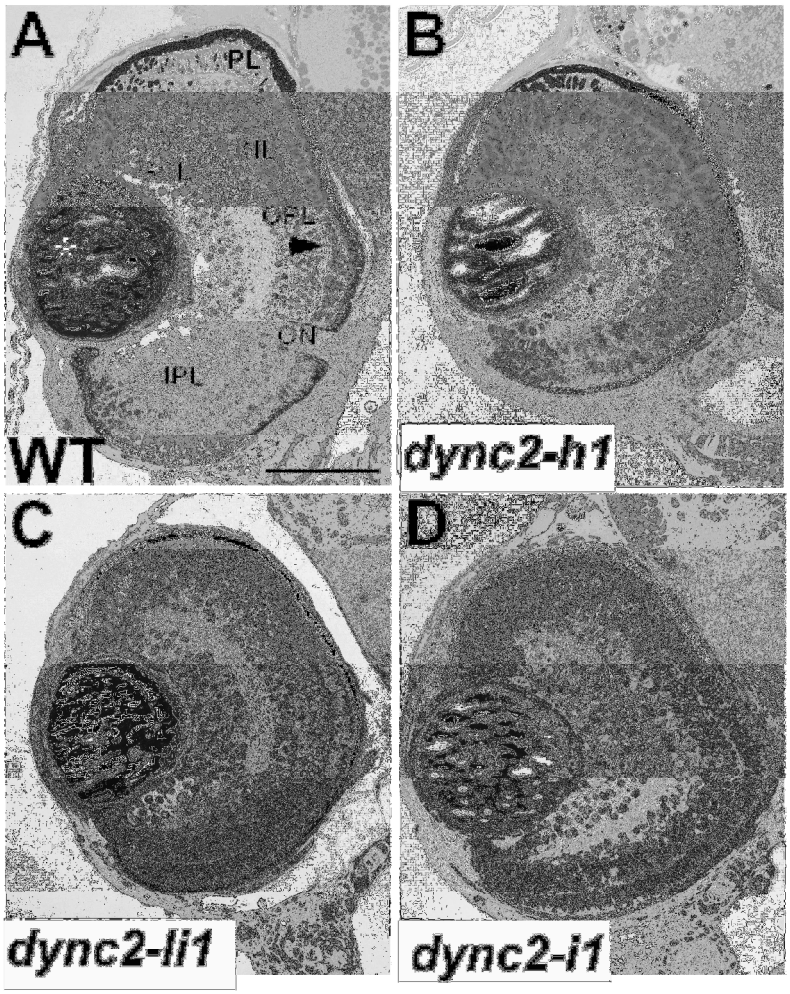

Fig. 22. Transverse histological sections through 4 dpf wild type and dynein morphant retinas (A-D). The wild-type zebrafish retina (A) is highly organized by 4 dpf with all cellular layers readily observable, including the ganglion cell layer (GCL), inner nuclear layer (INL), photoreceptor layer (PL) and retinal pigmented epithelium (RPE). The organization of dynein morphant retinas (B-D) is unaffected, though their eyes are smaller than wild-type. IPL(Inner plexiform layer), OPL (outer plexiform layer), ON (optic nerve) Scale bar, 100μm.

of which contained large vesicles within them (Fig. 23E-F). These structures are highly abnormal and were never observed in wild-type photoreceptors. We also observed accumulated vesicles within the outer segments of *dync2-i1* morphants (Fig. 23G,H). These data show that outer segment extension requires retrograde IFT and suggest that recycling of IFT proteins and retrograde movement of vesicular cargoes function in outer segment formation.

It is well established that retrograde IFT is essential for cilium formation and maintenance in *Chlamydomonas, C. elegans,* and mouse. If our dynein morphants lack retrograde IFT, we should observe defects in other ciliated tissues. Kidney cysts occurred with high penetrance in *dync2-h1, dync2-li1* and *dync2-i1* morphants, suggesting that pronephric cilia in these morphants were impaired (Fig. 21M). To test this directly, we performed whole-mount immunolabeling on 30 hpf zebrafish embryos with an antibody against acetylated tubulin, a marker for cilia. At 30 hpf, the anterior zebrafish pronephros is highly ciliated, with numerous monocilia extending into the pronephric lumen (Fig. 24A). *dync2-h1* morphants, however, possessed few cilia and the existing cilia were significantly shorter than wild type cilia (Fig. 24B). *dync2-li1* morphants displayed cilia that were shorter that wild type, but longer than *dync2-h1* morphants (Fig. 24C). Cilia density was lower in *dync2-i1* morphants, though their lengths were comparable to that of wild type (Fig. 24D). These data are consistent with the penetrance of kidney cysts observed at 4 dpf for all three morphants (Fig. 21M) and demonstrate pronephric cilia are compromised by *dync2-h1*, *dync2-li1* and *dync2-i1* dysfunction.

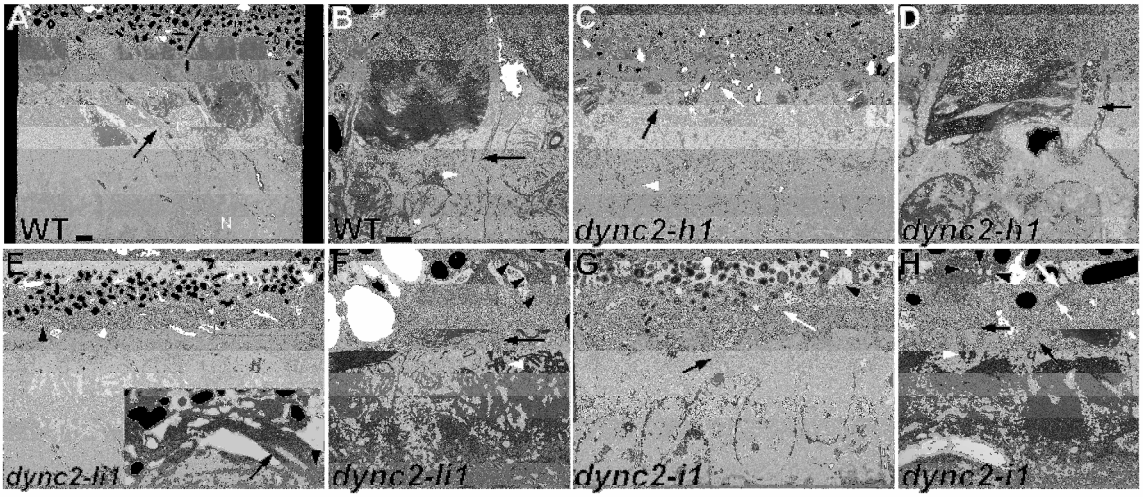

Fig. 23. Transmission electron microscopy of 4 dpf wild type and dynein morphant retinas. (A,C,E,F) Low magnification electron micrographs of wild-type and dynein morphant retinas. The wild-type retina (A) illustrates photoreceptor outer segments (OS), inner segments (IS), nuclei (N) and connecting cilia (black arrow). White arrows in (A,C,E,F) indicate cells lacking outer segments. *dync2-li1* morphants (E) had short outer segments and cells with abnormal membranous structures that had large electron lucent vesicles in them (arrowhead). Inset of (C) is the boxed area magnified 2.5x and illustrates a photoreceptor cilium that had disorganized membrane at its distal end. The basal body (arrowhead) and axoneme (arrow) are evident. (B,D,F,H) High magnification micrographs show connecting cilia (black arrow) and basal bodies (white arrowhead) and disorganized outer segment membranes with accumulated vesicles in them (black arrowheads) are evident in (H) In *dync2-i1* morphants electron-lucent vesicles (black arrowheads) are visible at the distal tip of an outer segment. White arrows indicated photoreceptor membranes that are improperly oriented in (H). Scale bar: (A,C,E,G) 1μm; (B,D,F,H) 500nm.

The canonical ciliary phenotype of disrupted retrograde IFT is swollen ciliary axonemes in which accumulated cytoplasm, IFT proteins and cellular debris are present (May et al., 2005; Pazour et al., 1999; Signor et al., 1999). If our dynein morphants truly reflect a state of compromised retrograde IFT, we expected to observe the phenotype in ciliated cells outside the retina. The zebrafish nasal epithelium is highly ciliated and provides a very accessible ciliated tissue for analysis at 4 dpf. We performed TEM on the nasal epithelium of 4 dpf larvae and found robust cilia in wild-type individuals (Fig. 24E). As expected, we observed very short nasal cilia with swollen axonemes in all three dynein morphants (Figs. 24F-H). These data indicate that *dync2-h1, dync2-li1* and *dync2-i1* morphants had compromised retrograde IFT and that retrograde IFT is essential for nasal cilium integrity.

Rod and cone opsins have been shown to be mislocalized in kinesin-II, *ift88* and *ift57* mutants, implying that opsins are cargo of IFT in photoreceptors (Krock and Perkins, 2008; Marszalek et al., 2000; Pazour et al., 2002a; Tsujikawa and Malicki, 2004). Indeed, others have reported that rhodopsin co-immunoprecipitated with the IFT complex (Insinna and Besharse, 2008). However, as opsins and most other known outer segment proteins are believed to move unidirectionally and not translocate back to the inner segment, it is unclear if retrograde IFT would affect opsin trafficking. We performed immunohistochemistry on 4 dpf dynein morphants using antibodies directed against zebrafish rhodopsin and blue cone opsin. At 4 dpf, both rod and blue cone opsins localized nearly exclusively to the outer segment (Fig. 25A). We obtained similar

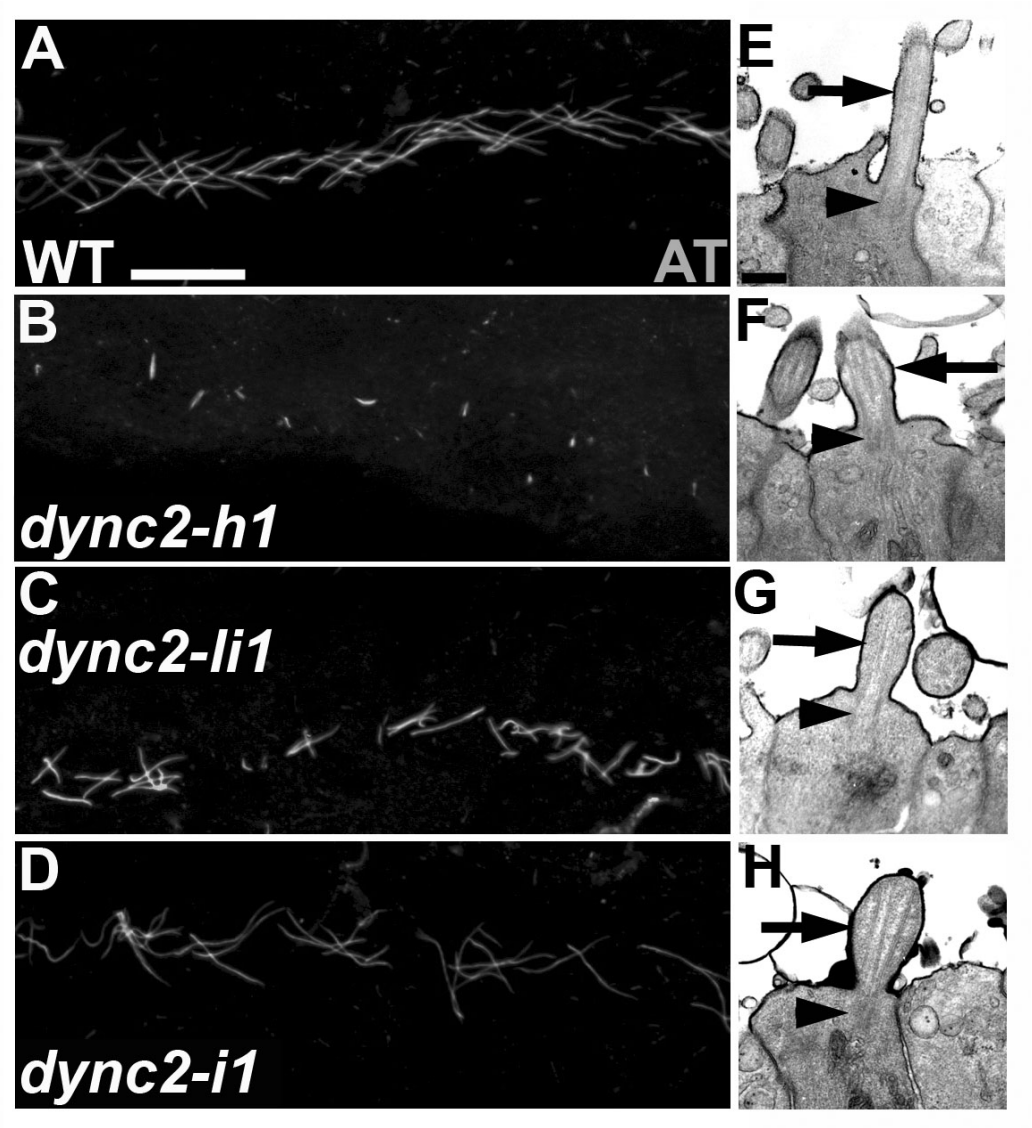

Fig. 24. Analysis of non-photoreceptor cilia. (A-D) 30 hpf wild-type and dynein morphant embryos were immunolabeled with an anti-acetylated tubulin antibody, a marker for cilia. Images were collected of the anterior pronephros, anterior is to the left dorsal is up. (E-H) Electron micrographs of 4 dpf wild-type and dynein morphant nasal cilia, nasal cilia (arrow) and basal bodies (arrowhead) are readily observable. Scale bar, (A-D) 20μm; (E-H) 500nm.

results with *dync2-h1, dync2-li1* and *dync2-i1* morphants (Figs. 25B-D), though occasionally we observed subtle mislocalization of opsins in these morphants. This phenotype was only observed in the most severely affected photoreceptors and likely reflects the cells inability to make an outer segment of normal size.

As disruption of retrograde IFT causes accumulation of IFT particles within cilia (Pazour et al., 1999; Pazour et al., 1998; Porter et al., 1999; Signor et al., 1999), we speculated that the accumulated debris we observed in photoreceptor cilia was IFT proteins. To test this, we immunolabeled 4 dpf retinal sections with antibodies against *Ift88* and acetylated tubulin. In wild-type photoreceptors, *Ift88* colocalized with acetylated tubulin at the connecting cilium, while acetylated tubulin staining often extended distally past the *Ift88* staining, likely representing the photoreceptor axoneme that extends to the tip of the outer segment (Fig. 25E). In the *dync2-h1* morphants, however, IFT88 and acetylated tubulin staining often colocalized in a small sphere and failed to elongate in the proximal-distal axis (Fig. 25F, arrowhead). In *dync2-li1* and *dync2-i1* morphants *Ift88* labeling was biased distally relative to the connecting cilium (Figs. 25G-H, arrows). This mislocalization of *Ift88* is consistent with the role of retrograde IFT in IFT protein recycling and suggests that some of the debris observed in dynein morphant outer was IFT proteins.

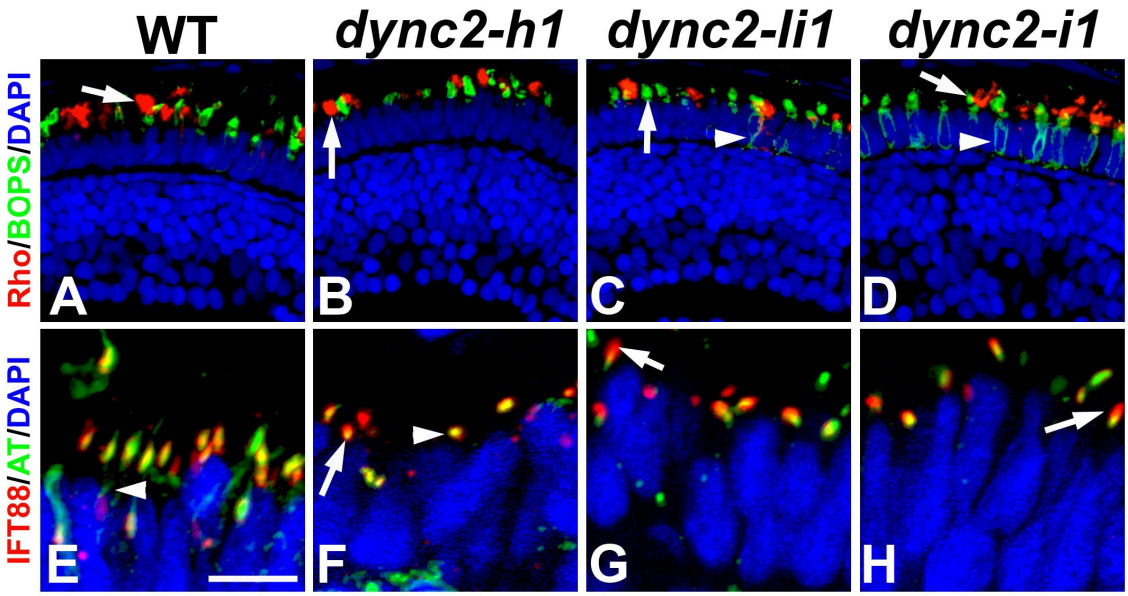

Fig. 25. Immunohistochemical analysis of 4 dpf wild type and dynein morphant photoreceptors. (A-D) Immunohistochemical labeling of rhodopsin (red) and blue cone opsin (green) in 4 dpf wild type and dynein morphant photoreceptors, arrows indicate outer segment localization of opsins and arrowheads indicated subtle mislocalization of opsins. (E-H) Immunolabeling with antibodies against *Ift88* (red) and acetylated tubulin (green), which marks the connecting cilium. *Ift88* is mislocalized at the distal tip of the connecting cilium in morphants (arrowhead). (E) In wild-type photoreceptors , there is show marked colocalization of acetylated tubulin and *Ift88* (yellow), though the acetylated tubulin staining often extends more distally than *Ift88* (arrowhead). DAPI (blue) labels nuclei. Scale bar, (A-D) 20µm; (E-H) 5µm.

Although cytoplasmic dynein-2 does not participate in anterograde opsin trafficking, studies of mammalian photoreceptors have shown that transducin and arrestin move in a retrograde fashion through the connecting cilium. Zebrafish cone transducin does not move to the inner segment during light adaptation (Kennedy et al., 2004), but the translocation of arrestin has not been tested in zebrafish. To first establish that arrestin moves in a light-dependent manner in zebrafish rods, we performed immunohistochemistry on 5 dpf zebrafish larvae with a monoclonal anti-rod arrestin antibody (Peterson et al., 2003). Briefly, larvae were dark adapted for three hours and then fixed at regular intervals after light exposure and assayed for arrestin localization. We observed robust light-dependent translocation of arrestin to the rod outer segment, with outer segment localization of rod arresting peaking at 15 minutes of light adaptation (Fig. 26B). With continued light exposure, arrestin progressively migrated back to the inner segment (Fig. 26C), with migration nearly complete after 60 minutes (Fig. 26D). This pattern of arrestin movement is similar to that previously described in *Xenopus* (Peterson et al., 2003). In order to evaluate arrestin movement in zebrafish dynein morphants, 5 dpf larvae were dark adapted for three hours and then light adapted for 15 minutes, the time at which arrestin concentrations peaked in the outer segment. Animals were returned to the dark to facilitate retrograde movement back to the inner segment and then fixed at regular intervals. Following light adaptation of wild-type animals, nearly all of the arrestin translocated to the inner segment within 15 minutes of dark adaptation (compare Figs. 26E and 26I). The timecourse of retrograde arrestin movement in *dync2-h1, dync2-li1,* and *dync2-i1* morphant rods was identical to that of

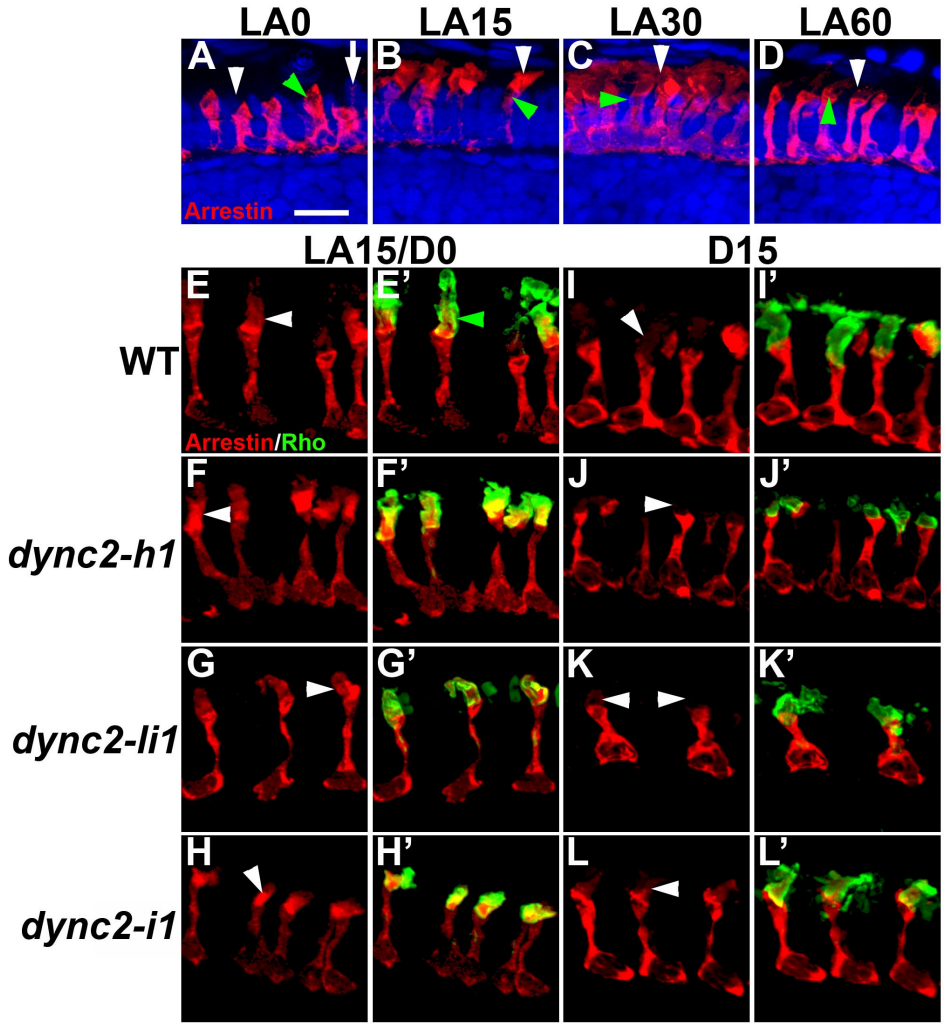

Fig. 26. Immunohistochemical analysis of arrestin translocation. (A-D) Arrestin (red) moves to the outer segment during light adaptation (white arrowhead), the apical part of the inner segment has a semicircular area of less intense staining, likely due to exclusion of cytoplasm by the mitochondria (green arrowhead). Staining along the photoreceptor cilium (white arrow) was apparent for some rods. DAPI (blue) labels the photoreceptor nuclei. (E-L) Retrograde arrestin movement is not affected in dynein morphants. Dark adapted rods (I-L) had little arrestin in outer segments (arrowheads). Rhodopsin labeling (green) marks the outer segments. Scale bar, 10μm.

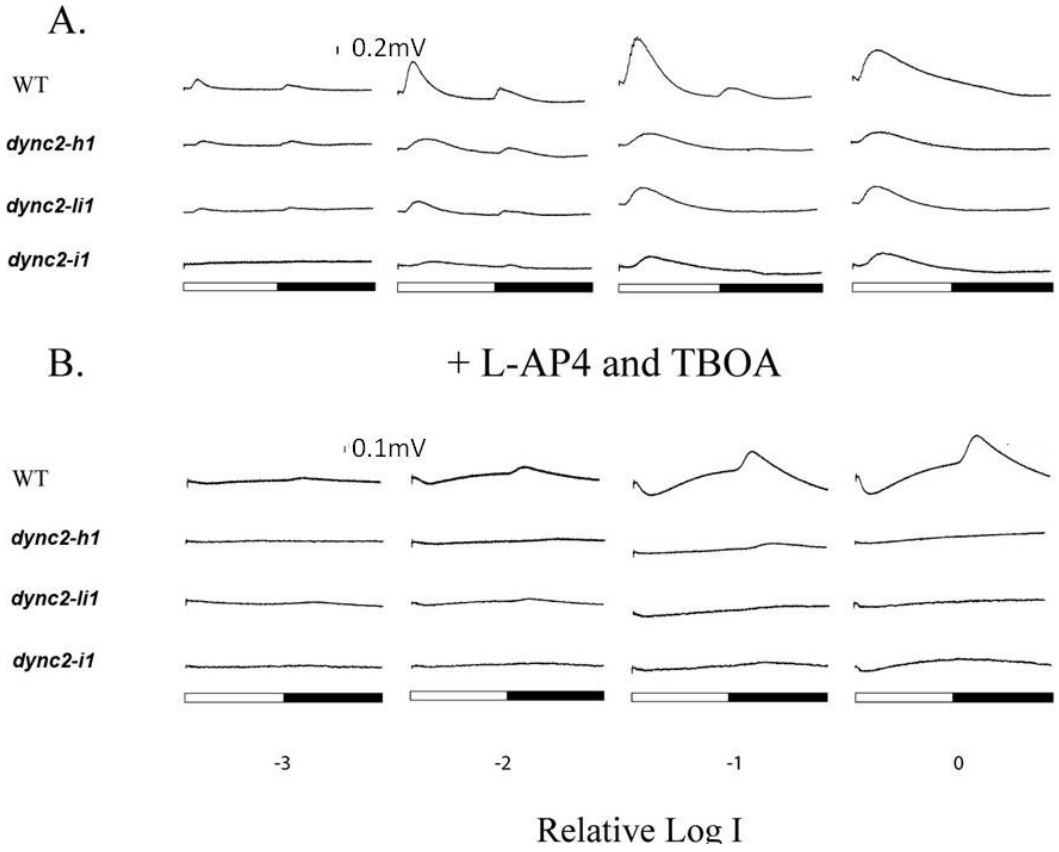

Fig. 27. Electrophysiological analysis of dynein morphants. Electroretinograms (ERGs) of wild-type (wt), *dync2-h1*, *dync2-li1*, and *dync2-i1* morphant 5-6 dpf larvae under photopic conditions. (A). ERGs at increasing light intensities (B) ERGs after incubation in pharmcological agents L-AP4 and TBOA to isolate the photoreceptor response, and increasing light intensities. The bars indicate light on (white bar) and light off (black bar) in 500 ms light stimulus.

wild-type rods (Figs. 26E-L). Additionally, we also observed retrograde arrestin movement was not affected in dynein morphants when these experiments were performed at 4 dpf (data not shown). These data indicate that cytoplasmic dynein-2, and by extension, retrograde IFT does not play a role in retrograde arrestin movement during dark adaptation.

In order to investigate the role of the retrograde IFT motor in photoreceptor physiology, we performed whole-field electroretinograms on 5 and 6 dpf dynein morphants (Fig. 27). Wild-type larvae have an ERG response characterized by a hyperpolarizing a-wave, and a depolarizing b- and d-wave, which reflect the response of photoreceptors and on and off-bipolar cells respectively. Dynein morphant ERGs exhibited decreased b- and d-wave amplitudes. Pharmacological isolation of the a-wave revealed dynein morphants also displayed reduced a-wave amplitudes. These data show that overall visual function of dynein morphants is significantly impaired.

DISCUSSION

In this study, we investigated the function of retrograde IFT in vertebrate photoreceptors and non-photoreceptor cilia through morpholino-mediated gene knockdown of three cytoplasmic dynein-2 subunits. The phenotype of photoreceptors lacking cytoplasmic dynein-2 differs from those described for mutations in anterograde IFT components. First, IFT88 and IFT172 mutants fail to make outer segments altogether (Tsujikawa and Malicki, 2004), while IFT57 mutants produce short outer segments (Krock and Perkins, 2008; Sukumaran and Perkins, 2009a). Though the outer segments in dynein morphants appear shorter than those described for IFT57 mutants,

they are not accompanied by significant opsin mislocalization or cell death, as was observed in IFT57 mutants. Second, the outer segments formed in IFT57 mutants had surprisingly normal ultrastructure, while we observed disorganized disk membranes and accumulated vesicles and debris in dynein morphant outer segments.

Our analysis revealed the accumulation of vesicles within the dynein morphant outer segments. We considered two possible explanations for these observations. First, the vesicles we observed may indicate that some vesicular traffic is recycled to the inner segment. As the outer segment sheds roughly 10% of its volume from the distal tips each day, it was assumed that most, if not all vesicles trafficked to the outer segment remained there. The composition of these vesicles remains unclear, as we are unaware of any vesicles that move from the outer segment to the inner segment. Alternatively, these vesicles could be the result of improper outer segment disk stacking. *Peripherin*/rds and *Rom-1* play essential roles in formation of new outer segment disks, and mutation of these genes causes severely disorganized outer segments that are composed of whorls of outer segment membrane, though accumulation of vesicles within the outer segments was not mentioned in these studies (Bascom et al., 1995; Kajiwara et al., 1994; Shastry, 1994). A FYVE domain protein SARA has recently been shown to play a role in fusion of rhodopsin bearing vesicles with nascent disk membranes. Importantly, RNAi mediated knockdown of SARA in rat photoreceptors caused accumulation of vesicles within the outer segment, the only previous documentation of this phenotype (Chuang et al., 2007). Additionally, SARA localizes to the photoreceptor axoneme in a pattern that is strikingly similar to that of IFT proteins

(Luby-Phelps et al., 2008). These data make it tempting to speculate that perhaps IFT, and specifically retrograde IFT, play a role in the fusion of rhodopsin bearing vesicles with nascent outer segment disks, potentially through interaction with SARA. Since IFT is the mechanism responsible for ciliary transport of rhodopsin, there must be a mechanism to mediate the hand off of membrane-bound cargo from the IFT machinery to its target membrane, either directly or through an intermediary.

Understanding the role of the accessory subunits of cytoplasmic dynein-2 is essential for a thorough understanding of the mechanism of retrograde IFT. Previous mutational studies in *Chlamydomonas*, *C. elegans*, and mouse have established a role for *dync2-h1*, *dync2-li1* and LC8 in retrograde IFT(Huangfu and Anderson, 2005; May et al., 2005; Pazour et al., 1999; Pazour et al., 1998; Porter et al., 1999; Signor et al., 1999). Our phenotypic analysis of *dync2-i1* morphants is the first, however, to show that the cytoplasmic dynein-2 intermediate chain is necessary for cytoplasmic dynein-2 function, as *dync2-i1* morphant photoreceptor and nasal cilia exhibit phenotypes characteristic of retrograde IFT dysfunction. We did not observe short pronephric cilia in *dync2-i1* morphants, even though they produced kidney cysts. This is likely explained by maternal contribution of *dync2-i1* compensating during early development.

To our knowledge, we are the first to describe light-dependent translocation of rod arrestin in zebrafish. The overall pattern of arrestin localization is similar to that described in *Xenopus*, where arrestin migrates to the outer segment during light adaptation and subsequently returns during prolonged light exposure (Peterson et al., 2003). This differs from murine systems where arrestin remains in the outer segment

with continued light adaptation (McGinnis et al., 1992; Philp et al., 1987; Whelan and McGinnis, 1988). This also suggests that retrograde arrestin translocation following continued light exposure a feature common to all teleosts and amphibians. Importantly, zebrafish rods display robust light-dependent movement of arrestin at 5dpf, and the utility of forward and reverse genetics in zebrafish could become a powerful tool for elucidating the mechanism underlying arrestin movements.

The mechanism underlying arrestin translocation has been the subject of several studies (Broekhuyse et al., 1985; McGinnis et al., 2002; McGinnis et al., 1992; Nair et al., 2005; Peterson et al., 2003; Philp et al., 1987). Although previous studies concluded that arrestin translocation occurs via simple diffusion (Nair et al., 2005), a direct test of retrograde IFT has not yet been performed. Although we observed several phenotypes consistent with disrupted retrograde IFT in dynein morphant photoreceptors, nasal cilia and pronephric cilia, we did not observe any defect in arrestin movements. While consistent with previous reports (Nair et al., 2005), our data directly show retrograde IFT does not participate in this process.

Finally, we observed reduced amplitude in dynein morphant ERG a, b and d waves. The a-wave reflects the hyperpolarizing photoreceptor response, and the presence of short outer segments in dynein morphants likely accounts for the reduced a-wave amplitudes observed in this study. A reduced photoreceptor response should reduce the electrical responses of the second order neurons, which is what we observed. Thus, the reduction in a- b- and d-wave amplitudes can be attributed to photoreceptor dysfunction.

MATERIALS AND METHODS

Fish Maintenance and Breeding

Wild-type zebrafish of the AB strain were housed, bred and staged according to standard procedures (Westerfield, 1995). Zebrafish were treated in accordance with the ARVO Statement for the Use of Animals in Ophthalmic and Vision Research.

Cloning of Dynein Genes and Phylogenetic Analysis of dync2-h1

5' RACE (Rapid Amplification of cDNA Ends) was performed on retinal cDNAs to clone the 5' end of *dync2-h1* using primer *dync2-h1* RACE1R: 5'TGCAGCAGGACGGGGCTGTAGACCTGA3' and the 5' end of *dync2-i1* using nested primers *dync2-i1* RACE 1R: 5'TTTGGCCGCTCTGGTCTTGTGTTTG3' and *dync2-i1*-nested-2R: 5'ATCGCCATCATCCACACGGCCAAAT3'. 5' RACE was done using the Gene Racer Kit (Invitrogen, Eugene, OR) according to manufacturers instructions. Initial *dync2-h1* sequence data was obtained from accession numbers: XR_029028 and XR_029028.2. The *dync2-h1* sequence was aligned against genomic contig NW_001514387 to annotate intron-exon boundries for the 5' 1.3kb of the coding sequence for morpholino design. Sequence data for *dync2-i1* and *dync2-li1* was obtained from Ensembl, numbers ENDSARG00000057635 and ENSDAR00000039770, respectively. Phylogenetic analysis was performed with MEGA software (www.megasoftware.net). Accession numbers and Ensembl numbers used are as follows: *C. reinhardtii dhc1b* (XP_001696428), *C. elegans DHC1* (NP_491363.1), CHE-3 (NP_492221.2), *D. rerio dync1-h1* (NP_001036210.1), *M. musculus Dync1-h1* (NP_084514.2), *Dync2-h1* (NP_084127.2), *R. norvegus* dync1-h1

(ENSNOG00000006178), *dync2-h1* (NP_075413.1), *G. gallus dync1-h1* (ENGALT00000037512), *dync2-h1* (ENSGALP00000027700), *O. latipes dync1-h1* (ENSORLP00000015944), *dync2-h1* (ENSORLT00000013451), *G. aculeatus dync1-h1* (ENSGALP00000014094), *dync2-h1* (ENSGALP00000010733), *T. rubripes dync1-h1* (ENSTRUP00000031697), *dync2-h1* (ENSTRUP00000010356).

***In situ* Hybridization**

Antisense riboprobes corresponding to *dync2-h1*, *dync2-li1* and *dync2-i1* were synthesized with SP6 RNA polymerase (Invitrogen) and *in situ* hybridizations performed as in (Jowett and Lettice, 1994). Probes for *in situ* hybridization were 5' RACE product corresponding to the 5'1.5kb of dync2-h1, a 1.2kb fragment of *dync2-li1* cloned via RT-PCR with PCR primers *dync2-li1*F: 5'GCAGGAGGCAAAACAACAAT3' and *dync2-li1*R: 5'GCTCTTTACGCTCCCTTGTG3', a 389bp fragment of *dync2-i1* cloned via RT-PCR with PCR primers *dync2-i1*F: 5'CCTTGGGATTTGGACACATT3' and *dync2-i1*R: 5' AGACTAGAGGGCGCGTAGGT3'. All RT-PCR products were ligated into pGEM T-Easy Vector (Promega, Madison, WI) for probe synthesis.

Morpholino Microinjection and Design

One to two cell stage zebrafish embryos were injected as described (Nasevicius and Ekker, 2000) . Morpholino were synthesized by Gene Tools, LLC. (Philomath, OR). The sequences were: *dync2-h1*MO1: 5'CTGCTGTGAATGCATGTACCTGCTG3', injected 8-9ng, *dync2-h1*MO2: 5'GACAGGTGTGCAGTCTGACCTCCTC3', injected 3.5ng. *dync2-li1*MO1sp:

5’GGACTGTCACTTTTACCGTATTATG3’, injected 13ng. *dync2-li1*MO2atg: 5’GCTTACTTTCGGCATTATTTTACCG3’, injected 3.5ng. *dync2-i1*MO1 5’ACAATAAACTGTTACCGGCCAAATC3’ , injected 5ng. *dync2-i1*MO2 5’CCACACTAATCCCAGAAATACAACA3’, injected 13ng.

Reverse Transcription-Polymerase Chain Reaction

RT-PCR was performed as in (Krock and Perkins, 2008). The primer sequences were as follows: *dync2-h1*MOF1: 5’TGTGGAAGCAGAATGAGCAC3’, *dync2-h1*MOR1: 5’TGCTAATTGTGGCTCGTTTG3’, *dync2-li1*MOF1: 5’GACACATTATGGGATATTGCT3’, *dync2-li1*MOR1: 5’GGTTTAGACAGATCCAAAACAA3’, *dync2-i1*MOF2: 5’GACCGAGATCTACAGACTTTC3’, *dync2-i1*MOR1: 5’AAACTACCACCTCACCACTGTA3’.

Immunohistochemistry and Immunocytochemisry

Whole mount immunostaining of 30 hpf zebrafish was performed as in (Riley et al., 1999) with an anti-acetylated tubulin antibody (Sigma, St. Louis, MO 1:50). Immunohistochemistry and imaging of frozen sections was performed as in (Krock and Perkins, 2008) using the following antibodies: anti-acetylated tubulin (1:500), anti-IFT88 (1:5000)(Krock and Perkins, 2008), 1d1 (monoclonal zebrafish rhodopsin antibody 1:100)(Fadool, 1999), rabbit anti-zebrafish rhodopsin and rabbit anti-zebrafish blue cone opsin (both 1:200) (Vihtelic et al., 1999). Staining with monoclonal anti-arrestin antibody (1:25) staining was performed as in (Peterson et al., 2003).

Antibody Generation

A rabbit polyclonal anti-*dync2-h1* antibody was generated against the synthetic peptide MAPGTDDPRK corresponding to the N-Terminus of zebrafish dync2-h1 and affinity-purified by Bethyl Laboratories (Montgomery, TX).

Histology and Electron Microscopy

Embryos were processed for histology and electron microscopy as described (Schmitt and Dowling, 1999)

SDS-PAGE and Western Blotting

Total protein from larval heads was generated as in (Krock and Perkins, 2008), electrophoresed on 5-15% gradient SDS-PAGE gels (Biorad, Hercules, CA), and transferred to PVDF. Rabbit anti-*dync2-h1* (1:5000) and anti-α-tubulin clone 12G10 (1:2000, Developmental studies hybridoma bank) were used and detected as in (Krock and Perkins, 2008).

Electroretinograms

Larval eyes were isolated using a tungsten wire loop according to (Wong et al., 2004) Ringer's solution as defined by (Emran et al., 2007), was added continuously through the preparation stage. This method prolongs the electrical responsiveness of the eye and improves the signal to noise ratio compared to whole animal recordings (Wong et al., 2004). A glass recording electrode with an 8-12 μm tip was placed below the cornea and above the lens to achieve the sum of the outer retinal cell responses. The reference electrode was placed in the 2% agarose pad covering the preparation stage.

Full-field light stimulation was prolonged for 500 ms under photopic conditions to ensure b- and d-wave separation. The light source utilized a 100W halogen bulb at the light intensity, log 0 = 13μW/cm^2. Three recordings are averaged to obtain the ERG trace. The response was amplified at 1,000 total gain and low-pass filtered at 300 Hz. L-AP4 (L-(+)-2-Amino-4-phosphonobutyric acid) and TBOA (DL-threo-b-Benzyloxyaspartic acid) were purchased from ToCris Biosciences (Ellisville, MA). Stock solutions of 100 mM were prepared by dissolving L-AP4 in 0.1 M NaOH and TBOA in DMSO. The stock solutions were added to fish water to a final concentration of 0.2mM TBOA and 0.4mM L-AP4. Larval fish at 5-6 dpf were incubated in TBOA and L-AP4 for 30 minutes.

CHAPTER V

SUMMARY AND FUTURE DIRECTIONS

SUMMARY

The purpose of my dissertation project was to investigate the mechanisms that mediate protein trafficking in the vertebrate retina, and how disruption of these processes leads to retinal degeneration.

In chapter II, I demonstrated that the phenotype zebrafish *rep1* mutants closely resembled that of human CHM patients, indicating it is a suitable animal model of this disease. Using this model, I subsequently showed that opsin mislocalization did not cause photoreceptor degeneration, but that defective RPE killed photoreceptors in a non-cell autonomous manner. The results of this study have specific implications for the design of human therapies, specifically that therapies should be targeted to the RPE.

In chapter III, I demonstrated that the photoreceptor phenotype of zebrafish *ift57* mutants was unique among previously described IFT mutants in that they formed short outer segments that contained a reduced amount of opsin. These data imply that the process of IFT occurred in *ift57* mutants, but at a reduced efficiency. In biochemical experiments, I utilized a co-immunoprecipitation assay and demonstrated that in *ift57* mutants, *Ift20* did not associate with the IFT particle, while *Ift88* and *Ift52* did. Most strikingly, I showed that kinesin II failed to dissociate from the IFT particle in *ift57* mutants, even in the presence of 1mM ATP. These results indicate that *Ift57* mediates the interaction between *Ift20* and the IFT particle, and that the interaction previously

described between *Ift20* and kinesin II facilitates the ATP-dependent dissociation of kinesin II. These results provide important details about a vital step in the process of IFT, anterograde motor dissociation.

In chapter IV, I evaluated the function of retrograde IFT in the context of photoreceptor cell biology, a previously unexplored area. I used a loss of function approach and showed that retrograde IFT was necessary for outer segment organization, extension, and possibly retrograde trafficking of vesicles from the outer segment to the inner segment. Additionally, retrograde IFT mediated return of IFT proteins to the base of the cilium, but did not mediate arrestin translocation. Additionally, I have shown for the first time that the intermediate chain subunit of cytoplasmic dynein-2 is necessary for retrograde IFT. Finally, an electrophysiological analysis of dynein morphants showed impaired retinal electrophysiology, suggesting a greater role for cytoplasmic dynein-2 in retinal physiology. This study was the first detailed analysis of retrograde IFT in vertebrate photoreceptors and provides a basis for further inquiry.

This dissertation provides valuable insights into the pathology of a human blindness disorder and the molecular mechanisms that drive ciliary protein trafficking in photoreceptors.

FUTURE DIRECTIONS

The field of IFT and the surge in interest in cilia biology are relatively recent occurrences, meaning there are many unexplored avenues to pursue in these fields. In the following section, I address future directions to build upon the work I have done and discuss a few interesting new directions for the study of IFT in the retina.

My work has shown that in a zebrafish model of CHM, photoreceptor degeneration is induced by the RPE. However, it is possible that over time, these photoreceptors may degenerate in a cell-autonomous manner. To address this shortcoming, repeating blastomere transplants with GFP-tagged *rep1* mutant donors would allow the assessment of long term survival of *rep1* mutant photoreceptors over a period of several months and into adulthood. Probing *rep1* mutant photoreceptors with markers for photoreceptor viability, and performing correlative electron microscopy would enable us to determine if photoreceptors require *rep1* and would conclusively determine the autonomy of photoreceptor degeneration in the zebrafish model of CHM.

My biochemical analysis showed that *Ift57* and *Ift20* are required for the ATP-dependent dissociation of kinesin II from the IFT particle. Exactly how the impaired dissociation of kinesin II affects the kinetics and mechanism of IFT, however, were not investigated. It is apparent that once IFT proteins are returned to the base of the cilium, the IFT particles themselves dissociate into IFT subunits, after which they are presumably re-integrated into new IFT particles (Cole et al., 1998; Iomini et al., 2001). This is probably an important step in the IFT cycle, and in *Ift57* mutants, the inability of kinesin II to dissociate from the IFT particle could perturb this. Perhaps the kinesin II bound IFT proteins are sequestered from re-integration into new IFT particles, thereby depleting the pool of free IFT subunits and kinesin II at the base of the cilium. This would create unfavorable conditions for the assembly of new IFT particles and likely lower the frequency of IFT particles entering the cilium. This hypothesis could be tested using a combination of biochemistry and ex vivo imaging. First, assessment of the

hydrodynamic properties of *ift57* mutant IFT particles using sucrose density centrifugation would enable comparison of the relative abundances of IFT particle-bound IFT subunits versus free IFT proteins. Second, ex-vivo imaging of *ift57* deficient photoreceptors expressing a *Ift88*-GFP construct would enable the evaluation of the effects of loss of *Ift57* on IFT kinetics. Since *ift57* mutant photoreceptors die, these experiments would be done on adult animals. *In-vivo* electroporation of *ift57* morpholinos into adult retinas would facilitate these studies.

In my analysis of cytoplasmic dynein-2 morphants, I observed accumulated vesicles within the outer segments. There are three plausible explanations for the origins of these vesicles; first, these may represent vesicular cargoes that are trafficked from the outer segment to the inner segment. However, there have been no descriptions of membrane bound cargoes or vesicles that move in a retrograde fashion in photoreceptors. Initial experiments to determine the composition of these vesicles is in order, with rhodopsin a likely candidate. Second, these vesicles may reflect improper formation of new disks at the base of the outer segment. Genetic interaction studies with cytoplasmic dynein-2 genes and *Peripherin/rds* and *Rom-1*, two proteins known to play a role in formation and organization of new outer segment disks, would effectively evaluate this potential connection between cytoplasmic dynein-2 and outer segment organization. Third, some believe rhodopsin bearing vesicles fuse with the nascent outer segment disks at the base of the outer segment, and defects in this process should cause vesicle accumulation within the outer segment. It is thought that a protein called Smad anchor for receptor activation (SARA) mediates this process (Chuang et al., 2007).

When SARA expression was perturbed in rat photoreceptors, they accumulated vesicles at the base of the outer segment, which is the only other description of this phenotype in the literature. Additionally SARA localizes to the photoreceptor connecting cilium in a pattern that is strikingly similar to IFT proteins. Therefore, genetic interaction studies with cytoplasmic dynein-2 and SARA are in line in order to determine if these similar phenotypes are due to a common mechanism.

Classic studies performed by Richard Young in the 1960s investigating where newly synthesized proteins were integrated into outer segments provided much of the foundation for how we currently view outer segment protein trafficking. His seminal studies determined that newly synthesized proteins were incorporated into the base of rod outer segments, however, this was not observed in cone outer segments (Young, 1967; Young, 1969). Instead, new proteins were integrated diffusely throughout cone outer segments. These data, typically overlooked by much of the vision community, suggest that cone opsins are not deposited in the same manner as rhodopsin is in rods. Intriguingly, when I immunolabeled adult zebrafish retinas with antibodies against *Ift88* and *Ift52*, I found that cones express IFT proteins at much higher levels than rods; others have mentioned this observation as well (Luby-Phelps et al., 2008). Taken together, these data suggest that the deposition of cargo by IFT occurs differently in cones, and that, perhaps cones utilize IFT in a slightly different way than rods. A first step in understanding these differences would be to image IFT *ex vivo* in both adult rods and cones expressing an *Ift88*-GFP fusion construct to evaluate the kinetics of IFT and

frequency of IFT particles entering the cilium. *in vivo* morpholino electroporation could be utilized in order to determine if IFT dysfunction differentially affects rods and cones.

Though it is now clear that IFT proteins play an integral role in the photoreceptor outer segment, there are recent data that show IFT proteins also localize to the photoreceptor synapse (Sloboda and Rosenbaum, 2007). The function of IFT proteins in this region of the cell is unclear, though bioinformatic analysis of IFT proteins indicated that these polypeptides are evolutionarily related to protein components of coat protein I (COPI) and clatharin-coated vesicles (Jekely and Arendt, 2006). These data make it tempting to speculate that IFT proteins may be involved in synaptic vesicle dynamics at the vertebrate synapse. This possible non-ciliary transport role of IFT proteins is an exciting new development worthy of further scientific inquiry. Specifically, it would be informative to determine if IFT proteins localize to the synaptic regions of other neurons. It is possible that this is a common feature of all neurons, or potentially only of a subset of neurons, possibly sensory neurons.

Additionally, we have found that IFT proteins are expressed throughout the entire retina, and it is becoming increasingly evident that essentially all vertebrate cells are ciliated. Without IFT proteins photoreceptors die, but it is unknown what the effect of IFT protein dysfunction is on cells of the inner nuclear layer or ganglion cell layer. Working in the zebrafish model, we are uniquely situated to address this question. An interesting set of experiments to address this would be to breed H2AX-GFP into our IFT mutant line and transplant the GFP tagged cells from their offspring into wild-type hosts. These experiments would enable the evaluation of survival of these cells, and more

interestingly, permit electrophysiological analyses via single-cell recordings. These studies would help evaluate the role of IFT proteins and cilia in non-photoreceptor retinal cells, an currently unexplored topic.

REFERENCES

Ahmed, N. T., Gao, C., Lucker, B. F., Cole, D. G. and Mitchell, D. R. (2008). ODA16 aids axonemal outer row dynein assembly through an interaction with the intraflagellar transport machinery. *J Cell Biol* **183**, 313-322.

Alory, C. and Balch, W. E. (2001). Organization of the Rab-GDI/CHM superfamily: the functional basis for choroideremia disease. *Traffic* **2**, 532-43.

Amsterdam, A. and Hopkins, N. (1999). Retrovirus-mediated insertional mutagenesis in zebrafish. *Methods Cell Biol.* **60**, 87-98.

Avidor-Reiss, T., Maer, A. M., Koundakjian, E., Polyanovsky, A., Keil, T., Subramaniam, S. and Zuker, C. S. (2004). Decoding cilia function: defining specialized genes required for compartmentalized cilia biogenesis. *Cell* **117**, 527-39.

Bacaj, T., Lu, Y. and Shaham, S. (2008). The conserved proteins CHE-12 and DYF-11 are required for sensory cilium function in *Caenorhabditis elegans. Genetics* **178**, 989-1002.

Bae, Y. K., Qin, H., Knobel, K. M., Hu, J., Rosenbaum, J. L. and Barr, M. M. (2006). General and cell-type specific mechanisms target TRPP2/PKD-2 to cilia. *Development* **133**, 3859-70.

Baker, S. A., Freeman, K., Luby-Phelps, K., Pazour, G. J. and Besharse, J. C. (2003). IFT20 links kinesin II with a mammalian intraflagellar transport complex that is conserved in motile flagella and sensory cilia. *J. Biol. Chem.* **278**, 34211-8.

Baker, S. A., Haeri, M., Yoo, P., Gospe, S. M., 3rd, Skiba, N. P., Knox, B. E. and Arshavsky, V. Y. (2008). The outer segment serves as a default destination for the trafficking of membrane proteins in photoreceptors. *J Cell Biol* **183**, 485-98.

Banizs, B., Pike, M. M., Millican, C. L., Ferguson, W. B., Komlosi, P., Sheetz, J., Bell, P. D., Schwiebert, E. M. and Yoder, B. K. (2005). Dysfunctional cilia lead to altered ependyma and choroid plexus function, and result in the formation of hydrocephalus. *Development* **132**, 5329-39.

Baron, D. M., Ralston, K. S., Kabututu, Z. P. and Hill, K. L. (2007). Functional genomics in *Trypanosoma brucei* identifies evolutionarily conserved components of motile flagella. *J Cell Sci* **120**, 478-91.

Bascom, R. A., Liu, L., Heckenlively, J. R., Stone, E. M. and McInnes, R. R. (1995). Mutation analysis of the ROM1 gene in retinitis pigmentosa. *Hum. Mol. Genet.* **4**, 1895-1902.

Baylor, D. A., Lamb, T. D. and Yau, K. W. (1979). Responses of retinal rods to single photons. *J Physiol (Lond)* **288**, 613-634.

Beales, P. L., Bland, E., Tobin, J. L., Bacchelli, C., Tuysuz, B., Hill, J., Rix, S., Pearson, C. G., Kai, M., Hartley, J. et al. (2007). IFT80, which encodes a conserved intraflagellar transport protein, is mutated in Jeune asphyxiating thoracic dystrophy. *Nat Genet* **39**, 727-9.

Berbari, N. F., Johnson, A. D., Lewis, J. S., Askwith, C. C. and Mykytyn, K. (2008a). Identification of ciliary localization sequences within the third intracellular loop of G protein-coupled receptors. *Mol Biol Cell* **19**, 1540-7.

Berbari, N. F., Lewis, J. S., Bishop, G. A., Askwith, C. C. and Mykytyn, K. (2008b). Bardet-Biedl syndrome proteins are required for the localization of G protein-coupled receptors to primary cilia. *Proc Natl Acad Sci U S A* **105**, 4242-6.

Berson, E. L., Rosner, B., Sandberg, M. A., Weigel-DiFranco, C. and Dryja, T. P. (1991). Ocular findings in patients with autosomal dominant retinitis pigmentosa and rhodopsin, proline-347-leucine. *Am. J. Ophthalmol.* **111**, 614-623.

Besharse, J. C., Hollyfield, J. G. and Rayborn, M. E. (1977a). Photoreceptor outer segments: accelerated membrane renewal in rods after exposure to light. *Science* **196**, 536-8.

Besharse, J. C., Hollyfield, J. G. and Rayborn, M. E. (1977b). Turnover of rod photoreceptor outer segments. II. Membrane addition and loss in relationship to light. *J. Cell Biol.* **75**, 507-27.

Besharse, J. C. and Pfenninger, K. H. (1980). Membrane assembly in retinal photoreceptors I. Freeze-fracture analysis of cytoplasmic vesicles in relationship to disc assembly. *J. Cell Biol.* **87**, 451-63.

Besharse, J. C. and Horst, C. J. (1990). *The photoreceptor connecting cilium. A model for the transition zone.* New York: Plenum Publishing Corp.

Bilotta, J., Saszik, S. and Sutherland, S. E. (2001). Rod contributions to the electroretinogram of the dark-adapted developing zebrafish. *Dev. Dyn.* **222**, 564-70.

Bisgrove, B. W., Snarr, B. S., Emrazian, A. and Yost, H. J. (2005). Polaris and Polycystin-2 in dorsal forerunner cells and Kupffer's vesicle are required for specification of the zebrafish left-right axis. *Dev Biol* **287**, 274-88.

Blacque, O. E. and Leroux, M. R. (2006). Bardet-Biedl syndrome: an emerging pathomechanism of intracellular transport. *Cell Mol Life Sci* **63**, 2145-61.

Bonilha, V. L., Trzupek, K. M., Li, Y., Francis, P. J., Hollyfield, J. G., Rayborn, M. E., Smaoui, N. and Weleber, R. G. (2008). Choroideremia: analysis of the retina from a female symptomatic carrier. *Ophthalmic Genet* **29**, 99-110.

Brann, M. R. and Cohen, L. V. (1987). Diurnal expression of transducin mRNA and translocation of transducin in rods of rat retina. *Science* **235**, 585-7.

Broekhuyse, R. M., Tolhuizen, E. F., Janssen, A. P. and Winkens, H. J. (1985). Light induced shift and binding of S-antigen in retinal rods. *Curr Eye Res* **4**, 613-8.

Calvert, P. D., Strissel, K. J., Schiesser, W. E., Pugh, E. N., Jr. and Arshavsky, V. Y. (2006). Light-driven translocation of signaling proteins in vertebrate photoreceptors. *Trends Cell Biol* **16**, 560-8.

Chuang, J. Z., Zhao, Y. and Sung, C. H. (2007). SARA-regulated vesicular targeting underlies formation of the light-sensing organelle in mammalian rods. *Cell* **130**, 535-47.

Cole, D. G. (1999). Kinesin-II, coming and going. *J Cell Biol* **147**, 463-6.

Cole, D. G. (2003). The intraflagellar transport machinery of *Chlamydomonas reinhardtii. Traffic* **4**, 435-42.

Cole, D. G., Diener, D. R., Himelblau, A. L., Beech, P. L., Fuster, J. C. and Rosenbaum, J. L. (1998). *Chlamydomonas* kinesin-II-dependent intraflagellar transport

(IFT): IFT particles contain proteins required for ciliary assembly in *Caenorhabditis elegans* sensory neurons. *J. Cell Biol.* **141**, 993-1008.

Corbit, K. C., Aanstad, P., Singla, V., Norman, A. R., Stainier, D. Y. and Reiter, J. F. (2005). Vertebrate Smoothened functions at the primary cilium. *Nature* **437**, 1018-21.

Cortellino, S., Wang, C., Wang, B., Bassi, M. R., Caretti, E., Champeval, D., Calmont, A., Jarnik, M., Burch, J., Zaret, K. S. et al. (2009). Defective ciliogenesis, embryonic lethality and severe impairment of the Sonic Hedgehog pathway caused by inactivation of the mouse complex A intraflagellar transport gene Ift122/Wdr10, partially overlapping with the DNA repair gene Med1/Mbd4. *Dev Biol* **325**, 225-37.

Cremers, F. P., Armstrong, S. A., Seabra, M. C., Brown, M. S. and Goldstein, J. L. (1994). REP-2, a Rab escort protein encoded by the choroideremia-like gene. *J. Biol. Chem.* **269**, 2111-7.

Cremers, F. P., Brunsmann, F., Berger, W., van Kerkhoff, E. P., van de Pol, T. J., Wieringa, B., Pawlowitzki, I. H. and Ropers, H. H. (1990a). Cloning of the breakpoints of a deletion associated with choroidermia. *Hum. Genet.* **86**, 61-4.

Cremers, F. P., Sankila, E. M., Brunsmann, F., Jay, M., Jay, B., Wright, A., Pinckers, A. J., Schwartz, M., van de Pol, D. J., Wieringa, B. et al. (1990b). Deletions in patients with classical choroideremia vary in size from 45 kb to several megabases. *Am. J. Hum. Genet.* **47**, 622-8.

De Robertis, E. (1956). Morphogenesis of the retinal rods; an electron microscope study. *J Biophys Biochem Cytol* **2**, 209-18.

De Robertis, E. (1960). Some observations on the ultrastructure and morphogenesis of photoreceptors. *J. Gen. Physiol.* **43(6)Suppl**, 1-13.

Deretic, D., Huber, L. A., Ransom, N., Mancini, M., Simons, K. and Papermaster, D. S. (1995). rab8 in retinal photoreceptors may participate in rhodopsin transport and in rod outer segment disk morphogenesis. *J. Cell Sci.* **108**, 215-24.

Deretic, D. and Papermaster, D. S. (1993). Rab6 is associated with a compartment that transports rhodopsin from the trans-Golgi to the site of rod outer segment disk formation in frog retinal photoreceptors. *J. Cell Sci.* **106**, 803-13.

Deretic, D., Traverso, V., Parkins, N., Jackson, F., Rodriguez de Turco, E. B. and Ransom, N. (2004). Phosphoinositides, ezrin/moesin, and rac1 regulate fusion of rhodopsin transport carriers in retinal photoreceptors. *Mol Biol Cell* **15**, 359-70.

Deretic, D., Williams, A. H., Ransom, N., Morel, V., Hargrave, P. A. and Arendt, A. (2005). Rhodopsin C terminus, the site of mutations causing retinal disease, regulates trafficking by binding to ADP-ribosylation factor 4 (ARF4). *Proc Natl Acad Sci U S A* **102**, 3301-6.

Doerre, G. and Malicki, J. (2002). Genetic analysis of photoreceptor cell development in the zebrafish retina. *Mech Dev* **110**, 125-38.

Dowling, J. E. (2001). *Neurons and networks : an introduction to behavioral neuroscience*. Cambridge, Mass. ;: Belknap Press of Harvard University Press.

Dowling, J. E. and Sidman, R. L. (1962). Inherited retinal dystrophy in the rat. *J. Cell Biol.* **14**, 73-109.

Emran, F., Rihel, J., Adolph, A. R., Wong, K. Y., Kraves, S. and Dowling, J. E. (2007). OFF ganglion cells cannot drive the optokinetic reflex in zebrafish. *Proc Natl Acad Sci U S A* **104**, 19126-31.

Fadool, J. M., Fadool, D. A., Moore, J. C., and Linser, P. J. (1999). Characterization of monoclonal antibodies against zebrafish retina. *Invest. Opth. Vis. Sci. Suppl.* **40**, 1251.

Flannery, J. G., Bird, A. C., Farber, D. B., Weleber, R. G. and Bok, D. (1990). A histopathologic study of a choroideremia carrier. *Invest Ophthalmol Vis Sci* **31**, 229-36.

Follit, J. A., San Agustin, J. T., Xu, F., Jonassen, J. A., Samtani, R., Lo, C. W. and Pazour, G. J. (2008). The Golgin GMAP210/TRIP11 anchors IFT20 to the Golgi complex. *PLoS Genet* **4**, e1000315.

Follit, J. A., Tuft, R. A., Fogarty, K. E. and Pazour, G. J. (2006a). The intraflagellar transport protein IFT20 is associated with the Golgi complex and is required for cilia assembly. *Mol Biol Cell* **17**, 3781-92.

Follit, J. A., Tuft, R. A., Fogarty, K. E. and Pazour, G. J. (2006b). The intraflagellar transport protein IFT20 is associated with the Golgi complex and is required for cilia assembly. *Mol. Biol. Cell* **17**, 3781-92.

Furuta, Y., Lagutin, O., Hogan, B. L. and Oliver, G. C. (2000). Retina- and ventral forebrain-specific Cre recombinase activity in transgenic mice. *Genesis* **26**, 130-2.

Garriga, P. and Manyosa, J. (2002). The eye photoreceptor protein rhodopsin. Structural implications for retinal disease. *FEBS Lett* **528**, 17-22.

Gibbs, D., Azarian, S. M., Lillo, C., Kitamoto, J., Klomp, A. E., Steel, K. P., Libby, R. T. and Williams, D. S. (2004). Role of myosin VIIa and Rab27a in the motility and localization of RPE melanosomes. *J. Cell. Sci.* **117**, 6473-83.

Gibbs, D., Kitamoto, J. and Williams, D. S. (2003). Abnormal phagocytosis by retinal pigmented epithelium that lacks myosin VIIa, the Usher syndrome 1B protein. *Proc. Natl. Acad. Sci. U. S. A.* **100**, 6481-6.

Green, E. S., Menz, M. D., LaVail, M. M. and Flannery, J. G. (2000). Characterization of rhodopsin mis-sorting and constitutive activation in a transgenic rat model of retinitis pigmentosa. *Invest. Ophthalmol. Vis. Sci.* **41**, 1546-53.

Grimm, C., Wenzel, A., Hafezi, F., Yu, S., Redmond, T. M. and Reme, C. E. (2000). Protection of Rpe65-deficient mice identifies rhodopsin as a mediator of light-induced retinal degeneration. *Nat Genet* **25**, 63-6.

Gross, J. M., Perkins, B. D., Amsterdam, A., Egana, A., Darland, T., Matsui, J. I., Sciascia, S., Hopkins, N. and Dowling, J. E. (2005). Identification of zebrafish insertional mutants with defects in visual system development and function. *Genetics* **170**, 245-61.

Han, Y. G., Kwok, B. H. and Kernan, M. J. (2003). Intraflagellar transport is required in *Drosophila* to differentiate sensory cilia but not sperm. *Curr Biol* **13**, 1679-86.

Hargrave, P. A. and McDowell, J. H. (1992). Rhodopsin and phototransduction: a model system for G protein-linked receptors. *Faseb J* **6**, 2323-2331.

Haycraft, C. J., Banizs, B., Aydin-Son, Y., Zhang, Q., Michaud, E. J. and Yoder, B. K. (2005). Gli2 and Gli3 localize to cilia and require the intraflagellar transport protein polaris for processing and function. *PLoS Genet* **1**, e53.

Haycraft, C. J., Schafer, J. C., Zhang, Q., Taulman, P. D. and Yoder, B. K. (2003). Identification of CHE-13, a novel intraflagellar transport protein required for cilia formation. *Exp. Cell Res.* **284**, 251-63.

Haycraft, C. J., Swoboda, P., Taulman, P. D., Thomas, J. H. and Yoder, B. K. (2001). The *C. elegans* homolog of the murine cystic kidney disease gene Tg737 functions in a ciliogenic pathway and is disrupted in osm-5 mutant worms. *Development* **128**, 1493-505.

Haycraft, C. J., Zhang, Q., Song, B., Jackson, W. S., Detloff, P. J., Serra, R. and Yoder, B. K. (2007). Intraflagellar transport is essential for endochondral bone formation. *Development* **134**, 307-16.

He, W., Cowan, C. W. and Wensel, T. G. (1998). RGS9, a GTPase accelerator for phototransduction. *Neuron* **20**, 95-102.

Heckenlively, J. R. (1988). *Retinitis pigmentosa*. Philadelphia: J. B. Lippincott.

Ho, R. K. and Kane, D. A. (1990). Cell-autonomous action of zebrafish spt-1 mutation in specific mesodermal precursors. *Nature* **348**, 728-30.

Hou, Y., Pazour, G. J. and Witman, G. B. (2004). A dynein light intermediate chain, D1bLIC, is required for retrograde intraflagellar transport. *Mol Biol Cell* **15**, 4382-94.

Hou, Y., Qin, H., Follit, J. A., Pazour, G. J., Rosenbaum, J. L. and Witman, G. B. (2007). Functional analysis of an individual IFT protein: IFT46 is required for transport of outer dynein arms into flagella. *J Cell Biol* **176**, 653-65.

Houde, C., Dickinson, R. J., Houtzager, V. M., Cullum, R., Montpetit, R., Metzler, M., Simpson, E. M., Roy, S., Hayden, M. R., Hoodless, P. A. et al. (2006). Hippi is essential for node cilia assembly and Sonic hedgehog signaling. *Dev Biol* **300**, 523-33.

Huangfu, D. and Anderson, K. V. (2005). Cilia and Hedgehog responsiveness in the mouse. *Proc. Natl. Acad. Sci. U. S. A* **102**, 11325-30.

Huangfu, D., Liu, A., Rakeman, A. S., Murcia, N. S., Niswander, L. and Anderson, K. V. (2003). Hedgehog signalling in the mouse requires intraflagellar transport proteins. *Nature* **426**, 83-7.

Hughes, A., Saszik, S., Bilotta, J., Demarco, P. J., Jr. and Patterson, W. F., 2nd. (1998). Cone contributions to the photopic spectral sensitivity of the zebrafish ERG. *Vis. Neurosci.* **15**, 1029-37.

Humphries, M. M., Rancourt, D., Farrar, G. J., Kenna, P., Hazel, M., Bush, R. A., Sieving, P. A., Sheils, D. M., McNally, N., Creighton, P. et al. (1997). Retinopathy induced in mice by targeted disruption of the rhodopsin gene. *Nature Genetics* **15**, 216-219.

Insinna, C. and Besharse, J. C. (2008). Intraflagellar transport and the sensory outer segment of vertebrate photoreceptors. *Dev Dyn* **237**, 1982-92.

Iomini, C., Babaev-Khaimov, V., Sassaroli, M. and Piperno, G. (2001). Protein particles in Chlamydomonas flagella undergo a transport cycle consisting of four phases. *J Cell Biol* **153**, 13-24.

Jacobson, S. G., Cideciyan, A. V., Sumaroka, A., Aleman, T. S., Schwartz, S. B., Windsor, E. A., Roman, A. J., Stone, E. M. and MacDonald, I. M. (2006). Remodeling of the human retina in choroideremia: rab escort protein 1 (REP-1) mutations. *Invest Ophthalmol Vis Sci* **47**, 4113-20.

Jekely, G. and Arendt, D. (2006). Evolution of intraflagellar transport from coated vesicles and autogenous origin of the eukaryotic cilium. *Bioessays* **28**, 191-8.

Jowett, T. and Lettice, L. (1994). Whole-mount in situ hybridizations on zebrafish embryos using a mixture of digoxigenin- and fluorescein-labelled probes. *Trends Genet* **10**, 73-4.

Kajiwara, K., Berson, E. L. and Dryja, T. P. (1994). Digenic retinitis pigmentosa due to mutations at the unlinked peripherin/RDS and ROM1 loci. *Science* **264**, 1604-1608.

Kennedy, M. J., Dunn, F. A. and Hurley, J. B. (2004). Visual pigment phosphorylation but not transducin translocation can contribute to light adaptation in zebrafish cones. *Neuron* **41**, 915-28.

Khanna, H., Hurd, T. W., Lillo, C., Shu, X., Parapuram, S. K., He, S., Akimoto, M., Wright, A. F., Margolis, B., Williams, D. S. et al. (2005). RPGR-

ORF15, which is mutated in retinitis pigmentosa, associates with SMC1, SMC3, and microtubule transport proteins. *J Biol Chem* **280**, 33580-7.

Kimmel, C. B., Ballard, W. W., Kimmel, S. R., Ullmann, B. and Schilling, T. F. (1995). Stages of embryonic development of the zebrafish. *Dev. Dyn.* **203**, 253-310.

Kolb, H. and Gouras, P. (1974). Electron microscopic observations of human retinitis pigmentosa, dominantly inherited. *Invest. Ophthalmol.* **13**, 487-98.

Kozminski, K. G., Beech, P. L. and Rosenbaum, J. L. (1995). The *Chlamydomonas* kinesin-like protein FLA10 is involved in motility associated with the flagellar membrane. *J. Cell Biol.* **131**, 1517-27.

Kozminski, K. G., Johnson, K. A., Forscher, P. and Rosenbaum, J. L. (1993). A motility in the eukaryotic flagellum unrelated to flagellar beating. *Proc. Natl. Acad. Sci. U S A* **90**, 5519-23.

Kramer-Zucker, A. G., Olale, F., Haycraft, C. J., Yoder, B. K., Schier, A. F. and Drummond, I. A. (2005). Cilia-driven fluid flow in the zebrafish pronephros, brain and Kupffer's vesicle is required for normal organogenesis. *Development* **132**, 1907-21.

Krock, B. L. and Perkins, B. D. (2008). The intraflagellar transport protein IFT57 is required for cilia maintenance and regulates IFT-particle-kinesin-II dissociation in vertebrate photoreceptors. *J Cell Sci* **121**, 1907-15.

Kunitomo, H. and Iino, Y. (2008). Caenorhabditis elegans DYF-11, an orthologue of mammalian Traf3ip1/MIP-T3, is required for sensory cilia formation. *Genes Cells* **13**, 13-25.

Kwok-Keung Fung, B. and Stryer, L. (1980). Photolyzed rhodopsin catalyzes the exchange of GTP for bound GDP in retinal rod outer segments. *Proc Natl Acad Sci U S A* **77**, 2500-2504.

Larison, K. D. and Bremiller, R. (1990). Early onset of phenotype and cell patterning in the embryonic zebrafish retina. *Development* **109**, 567-76.

Lee, E., Sivan-Loukianova, E., Eberl, D. F. and Kernan, M. J. (2008). An IFT-A protein is required to delimit functionally distinct zones in mechanosensory cilia. *Curr Biol* **18**, 1899-906.

Lehman, J. M., Michaud, E. J., Schoeb, T. R., Aydin-Son, Y., Miller, M. and Yoder, B. K. (2008). The Oak Ridge Polycystic Kidney mouse: modeling ciliopathies of mice and men. *Dev Dyn* **237**, 1960-71.

Lem, J., Krasnoperova, N. V., Calvert, P. D., Kosaras, B., Cameron, D. A., Nicolo, M., Makino, C. L. and Sidman, R. L. (1999). Morphological, physiological, and biochemical changes in rhodopsin knockout mice. *Proc. Natl. Acad. Sci. U S A* **96**, 736-741.

Lerea, C. L., Somers, D. E., Hurley, J. B., Klock, I. B. and Bunt-Milam, A. H. (1986). Identification of specific transducin alpha subunits in retinal rod and cone photoreceptors. *Science* **234**, 77-80.

Li, C., Inglis, P. N., Leitch, C. C., Efimenko, E., Zaghloul, N. A., Mok, C. A., Davis, E. E., Bialas, N. J., Healey, M. P., Heon, E. et al. (2008). An essential role for DYF-11/MIP-T3 in assembling functional intraflagellar transport complexes. *PLoS Genet* **4**, e1000044.

Li, T., Snyder, W. K., Olsson, J. E. and Dryja, T. P. (1996). Transgenic mice carrying the dominant rhodopsin mutation P347S: evidence for defective vectorial transport of rhodopsin to the outer segments. *Proc. Natl. Acad. Sci. U. S. A* **93**, 14176-14181.

Liu, A., Wang, B. and Niswander, L. A. (2005). Mouse intraflagellar transport proteins regulate both the activator and repressor functions of Gli transcription factors. *Development* **132**, 3103-11.

Liu, Q., Tan, G., Levenkova, N., Li, T., Pugh, E. N., Jr., Rux, J. J., Speicher, D. W. and Pierce, E. A. (2007). The proteome of the mouse photoreceptor sensory cilium complex. *Mol Cell Proteomics* **6**, 1299-317.

Luby-Phelps, K., Fogerty, J., Baker, S. A., Pazour, G. J. and Besharse, J. C. (2008). Spatial distribution of intraflagellar transport proteins in vertebrate photoreceptors. *Vision Res* **48**, 413-23.

Lucker, B. F., Behal, R. H., Qin, H., Siron, L. C., Taggart, W. D., Rosenbaum, J. L. and Cole, D. G. (2005). Characterization of the intraflagellar transport complex B core: direct interaction of the IFT81 and IFT74/72 subunits. *J. Biol. Chem.* **280**, 27688-96.

Marszalek, J. R., Liu, X., Roberts, E. A., Chui, D., Marth, J. D., Williams, D. S. and Goldstein, L. S. (2000). Genetic evidence for selective transport of opsin and arrestin by kinesin-II in mammalian photoreceptors. *Cell* **102**, 175-87.

May, S. R., Ashique, A. M., Karlen, M., Wang, B., Shen, Y., Zarbalis, K., Reiter, J., Ericson, J. and Peterson, A. S. (2005). Loss of the retrograde motor for IFT

disrupts localization of Smo to cilia and prevents the expression of both activator and repressor functions of Gli. *Dev Biol* **287**, 378-89.

Mazelova, J., Astuto-Gribble, L., Inoue, H., Tam, B. M., Schonteich, E., Prekeris, R., Moritz, O. L., Randazzo, P. A. and Deretic, D. (2009). Ciliary targeting motif VxPx directs assembly of a trafficking module through Arf4. *Embo J* **28**, 183-92.

McGinnis, J. F., Matsumoto, B., Whelan, J. P. and Cao, W. (2002). Cytoskeleton participation in subcellular trafficking of signal transduction proteins in rod photoreceptor cells. *J Neurosci Res* **67**, 290-7.

McGinnis, J. F., Whelan, J. P. and Donoso, L. A. (1992). Transient, cyclic changes in mouse visual cell gene products during the light-dark cycle. *J Neurosci Res* **31**, 584-90.

Mikami, A., Tynan, S. H., Hama, T., Luby-Phelps, K., Saito, T., Crandall, J. E., Besharse, J. C. and Vallee, R. B. (2002). Molecular structure of cytoplasmic dynein 2 and its distribution in neuronal and ciliated cells. *J Cell Sci* **115**, 4801-8.

Moritz, O. L., Tam, B. M., Hurd, L. L., Peranen, J., Deretic, D. and Papermaster, D. S. (2001). Mutant rab8 impairs docking and fusion of rhodopsin-bearing post-golgi membranes and causes cell death of transgenic *xenopus* rods. *Molecular Biology of the Cell* **12**, 2341-51.

Morris, A. C. and Fadool, J. M. (2005). Studying rod photoreceptor development in zebrafish. *Physiol. Behav.* **86**, 306-13.

Moyer, J. H., M.J. Lee-Tischler, H.-Y. Kwon, J.J. Schrick, E.D. Avner, W.E. Sweeney, V.L. Godfrey, N.L. Cacheiro, J.E. Wilkinson, and R.P. Woychik. (1994).

Candidate gene associated with a mutation causing recessive polycystic kidney disease in mice. *Science* **264**, 1329-1333.

Mullen, R. J. and LaVail, M. M. (1976). Inherited retinal dystrophy: primary defect in pigment epithelium determined with experimental rat chimeras. *Science* **192**, 799-801.

Murcia, N. S., Richards, W. G., Yoder, B. K., Mucenski, M. L., Dunlap, J. R. and Woychik, R. P. (2000). The Oak Ridge Polycystic Kidney (orpk) disease gene is required for left-right axis determination. *Development* **127**, 2347-55.

Mykytyn, K., Mullins, R. F., Andrews, M., Chiang, A. P., Swiderski, R. E., Yang, B., Braun, T., Casavant, T., Stone, E. M. and Sheffield, V. C. (2004). Bardet-Biedl syndrome type 4 (BBS4)-null mice implicate Bbs4 in flagella formation but not global cilia assembly. *Proc Natl Acad Sci U S A* **101**, 8664-9.

Nachury, M. V., Loktev, A. V., Zhang, Q., Westlake, C. J., Peranen, J., Merdes, A., Slusarski, D. C., Scheller, R. H., Bazan, J. F., Sheffield, V. C. et al. (2007). A core complex of BBS proteins cooperates with the GTPase Rab8 to promote ciliary membrane biogenesis. *Cell* **129**, 1201-13.

Nair, K. S., Hanson, S. M., Mendez, A., Gurevich, E. V., Kennedy, M. J., Shestopalov, V. I., Vishnivetskiy, S. A., Chen, J., Hurley, J. B., Gurevich, V. V. et al. (2005). Light-dependent redistribution of arrestin in vertebrate rods is an energy-independent process governed by protein-protein interactions. *Neuron* **46**, 555-67.

Nasevicius, A. and Ekker, S. C. (2000). Effective targeted gene 'knockdown' in zebrafish. *Nat. Genet.* **26**, 216-20.

Nathans, J. (1992). Rhodopsin: structure, function, and genetics. *Biochemistry* **31**, 4923-4931.

Nir, I. and Papermaster, D. S. (1989). Immunocytochemical localization of opsin in degenerating photoreceptors of RCS rats and rd and rds mice. *Prog. Clin. Biol. Res.* **314**, 251-64.

Nishimura, D. Y., Fath, M., Mullins, R. F., Searby, C., Andrews, M., Davis, R., Andorf, J. L., Mykytyn, K., Swiderski, R. E., Yang, B. et al. (2004). Bbs2-null mice have neurosensory deficits, a defect in social dominance, and retinopathy associated with mislocalization of rhodopsin. *Proc Natl Acad Sci U S A* **101**, 16588-93.

Oliver, G., Mailhos, A., Wehr, R., Copeland, N. G., Jenkins, N. A. and Gruss, P. (1995). Six3, a murine homologue of the sine oculis gene, demarcates the most anterior border of the developing neural plate and is expressed during eye development. *Development* **121**, 4045-55.

Omori, Y., Zhao, C., Saras, A., Mukhopadhyay, S., Kim, W., Furukawa, T., Sengupta, P., Veraksa, A. and Malicki, J. (2008). Elipsa is an early determinant of ciliogenesis that links the IFT particle to membrane-associated small GTPase Rab8. *Nat Cell Biol* **10**, 437-44.

Orozco, J. T., Wedaman, K. P., Signor, D., Brown, H., Rose, L. and Scholey, J. M. (1999). Movement of motor and cargo along cilia. *Nature* **398**, 674.

Ostrowski, L. E., Blackburn, K., Radde, K. M., Moyer, M. B., Schlatzer, D. M., Moseley, A. and Boucher, R. C. (2002). A proteomic analysis of human cilia: identification of novel components. *Mol Cell Proteomics* **1**, 451-65.

Ou, G., Blacque, O. E., Snow, J. J., Leroux, M. R. and Scholey, J. M. (2005). Functional coordination of intraflagellar transport motors. *Nature* **436**, 583-7.

Palczewski, K., Buczylko, J., Kaplan, M. W., Polans, A. S. and Crabb, J. W. (1991). Mechanism of rhodopsin kinase activation. *Journal of Biological Chemistry* **266**, 12949-12955.

Pazour, G. J., Agrin, N., Leszyk, J. and Witman, G. B. (2005). Proteomic analysis of a eukaryotic cilium. *J Cell Biol* **170**, 103-13.

Pazour, G. J., Baker, S. A., Deane, J. A., Cole, D. G., Dickert, B. L., Rosenbaum, J. L., Witman, G. B. and Besharse, J. C. (2002a). The intraflagellar transport protein, IFT88, is essential for vertebrate photoreceptor assembly and maintenance. *J. Cell Biol.* **157**, 103-13.

Pazour, G. J., Dickert, B. L., Vucica, Y., Seeley, E. S., Rosenbaum, J. L., Witman, G. B. and Cole, D. G. (2000). *Chlamydomonas* IFT88 and its mouse homologue, polycystic kidney disease gene tg737, are required for assembly of cilia and flagella. *J. Cell Biol.* **151**, 709-18.

Pazour, G. J., Dickert, B. L. and Witman, G. B. (1999). The DHC1b (DHC2) isoform of cytoplasmic dynein is required for flagellar assembly. *J. Cell Biol.* **144**, 473-81.

Pazour, G. J. and Rosenbaum, J. L. (2002). Intraflagellar transport and cilia-dependent diseases. *Trends Cell Biol.* **12**, 551-5.

Pazour, G. J., San Agustin, J. T., Follit, J. A., Rosenbaum, J. L. and Witman, G. B. (2002b). Polycystin-2 localizes to kidney cilia and the ciliary level is elevated in orpk mice with polycystic kidney disease. *Curr. Biol.* **12**, R378-80.

Pazour, G. J., Wilkerson, C. G. and Witman, G. B. (1998). A dynein light chain is essential for the retrograde particle movement of intraflagellar transport (IFT). *J. Cell Biol.* **141**, 979-92.

Pedersen, L. B., Miller, M. S., Geimer, S., Leitch, J. M., Rosenbaum, J. L. and Cole, D. G. (2005). *Chlamydomonas* IFT172 is encoded by FLA11, interacts with CrEB1, and regulates IFT at the flagellar tip. *Curr Biol* **15**, 262-6.

Pedersen, L. B. and Rosenbaum, J. L. (2008). Chapter Two Intraflagellar Transport (IFT) Role in Ciliary Assembly, Resorption and Signalling. *Curr Top Dev Biol* **85**, 23-61.

Perkins, B. D., Kainz, P. M., O'Malley, D. M. and Dowling, J. E. (2002). Transgenic expression of a GFP-rhodopsin COOH-terminal fusion protein in zebrafish rod photoreceptors. *Vis. Neurosci.* **19**, 257-264.

Perkins, B. D., Nicholas, C. S., Baye, L. M., Link, B. A. and Dowling, J. E. (2005). dazed gene is necessary for late cell type development and retinal cell maintenance in the zebrafish retina. *Dev. Dyn.* **233**, 680-94.

Perrone, C. A., Tritschler, D., Taulman, P., Bower, R., Yoder, B. K. and Porter, M. E. (2003). A novel dynein light intermediate chain colocalizes with the retrograde motor for intraflagellar transport at sites of axoneme assembly in chlamydomonas and Mammalian cells. *Mol. Biol. Cell* **14**, 2041-56.

Peterson, J. J., Tam, B. M., Moritz, O. L., Shelamer, C. L., Dugger, D. R., McDowell, J. H., Hargrave, P. A., Papermaster, D. S. and Smith, W. C. (2003). Arrestin migrates in photoreceptors in response to light: a study of arrestin localization using an arrestin-GFP fusion protein in transgenic frogs. *Exp Eye Res* **76**, 553-63.

Philp, N. J., Chang, W. and Long, K. (1987). Light-stimulated protein movement in rod photoreceptor cells of the rat retina. *FEBS Lett* **225**, 127-32.

Piperno, G. and Mead, K. (1997). Transport of a novel complex in the cytoplasmic matrix of *Chlamydomonas* flagella. *Proc Natl Acad Sci U S A* **94**, 4457-62.

Porter, M. E., Bower, R., Knott, J. A., Byrd, P. and Dentler, W. (1999). Cytoplasmic dynein heavy chain 1b is required for flagellar assembly in *Chlamydomonas*. *Mol Biol Cell* **10**, 693-712.

Portera-Cailliau, C., Sung, C. H., Nathans, J. and Adler, R. (1994). Apoptotic photoreceptor cell death in mouse models of retinitis pigmentosa. *Proc Natl Acad Sci U S A* **91**, 974-978.

Postlethwait, J. H., Woods, I. G., Ngo-Hazelett, P., Yan, Y. L., Kelly, P. D., Chu, F., Huang, H., Hill-Force, A. and Talbot, W. S. (2000). Zebrafish comparative genomics and the origins of vertebrate chromosomes. *Genome Res* **10**, 1890-902.

Preising, M. and Ayuso, C. (2004). Rab escort protein 1 (REP1) in intracellular traffic: a functional and pathophysiological overview. *Ophthalmic Genet.* **25**, 101-10.

Purves, D. and Williams, S. M. (2001). *Neuroscience.* Sunderland, Mass.: Sinauer Associates.

Qin, H., Burnette, D. T., Bae, Y. K., Forscher, P., Barr, M. M. and Rosenbaum, J. L. (2005). Intraflagellar transport is required for the vectorial movement of TRPV channels in the ciliary membrane. *Curr Biol* **15**, 1695-9.

Qin, H., Diener, D. R., Geimer, S., Cole, D. G. and Rosenbaum, J. L. (2004). Intraflagellar transport (IFT) cargo: IFT transports flagellar precursors to the tip and turnover products to the cell body. *J. Cell Biol.* **164**, 255-66.

Qin, H., Rosenbaum, J. L. and Barr, M. M. (2001). An autosomal recessive polycystic kidney disease gene homolog is involved in intraflagellar transport in *C. elegans* ciliated sensory neurons. *Curr. Biol.* **11**, 457-61.

Qin, H., Wang, Z., Diener, D. and Rosenbaum, J. (2007). Intraflagellar transport protein 27 is a small G protein involved in cell-cycle control. *Curr Biol* **17**, 193-202.

Rana, A. A., Barbera, J. P., Rodriguez, T. A., Lynch, D., Hirst, E., Smith, J. C. and Beddington, R. S. (2004). Targeted deletion of the novel cytoplasmic dynein mD2LIC disrupts the embryonic organiser, formation of the body axes and specification of ventral cell fates. *Development* **131**, 4999-5007.

Riley, B. B., Chiang, M., Farmer, L. and Heck, R. (1999). The deltaA gene of zebrafish mediates lateral inhibition of hair cells in the inner ear and is regulated by pax2.1. *Development* **126**, 5669-78.

Rompolas, P., Pedersen, L. B., Patel-King, R. S. and King, S. M. (2007). *Chlamydomonas* FAP133 is a dynein intermediate chain associated with the retrograde intraflagellar transport motor. *J Cell Sci* **120**, 3653-65.

Rosenbaum, J. L., Cole, D. G. and Diener, D. R. (1999). Intraflagellar transport: the eyes have it. *J. Cell Biol.* **144**, 385-8.

Rosenbaum, J. L. and Witman, G. B. (2002). Intraflagellar transport. *Nat. Rev. Mol. Cell. Biol.* **3**, 813-25.

Saszik, S. and Bilotta, J. (1999). The effects of temperature on the dark-adapted spectral sensitivity function of the adult zebrafish. *Vision Res.* **39**, 1051-8.

Schmitt, E. A. and Dowling, J. E. (1999). Early retinal development in the zebrafish, Danio rerio: light and electron microscopic analyses. *J. Comp. Neurol.* **404**, 515-36.

Scholey, J. M. (2003). Intraflagellar transport. *Annu Rev Cell Dev Biol* **19**, 423-43.

Seabra, M. C. (1996). New insights into the pathogenesis of choroideremia: a tale of two REPs. *Ophthalmic Genet.* **17**, 43-6.

Seabra, M. C., Brown, M. S., Slaughter, C. A., Sudhof, T. C. and Goldstein, J. L. (1992). Purification of component A of Rab geranylgeranyl transferase: possible identity with the choroideremia gene product. *Cell* **70**, 1049-57.

Seabra, M. C., Ho, Y. K. and Anant, J. S. (1995). Deficient geranylgeranylation of Ram/Rab27 in choroideremia. *J. Biol. Chem.* **270**, 24420-7.

Serra, R. (2008). Role of intraflagellar transport and primary cilia in skeletal development. *Anat Rec (Hoboken)* **291**, 1049-61.

Shastry, B. S. (1994). Retinitis pigmentosa and related disorders: phenotypes of rhodopsin and peripherin/RDS mutations. *American Journal of Medical Genetics* **52**, 467-474.

Signor, D., Wedaman, K. P., Orozco, J. T., Dwyer, N. D., Bargmann, C. I., Rose, L. S. and Scholey, J. M. (1999). Role of a class DHC1b dynein in retrograde transport of IFT motors and IFT raft particles along cilia, but not dendrites, in chemosensory neurons of living *Caenorhabditis elegans. J Cell Biol* **147**, 519-30.

Sloboda, R. D. and Rosenbaum, J. L. (2007). Making sense of cilia and flagella. *J Cell Biol* **179**, 575-82.

Smith, J. C., Northey, J. G., Garg, J., Pearlman, R. E. and Siu, K. W. (2005). Robust method for proteome analysis by MS/MS using an entire translated genome: demonstration on the ciliome of *Tetrahymena thermophila*. *J Proteome Res* **4**, 909-19.

Snell, W. J., Pan, J. and Wang, Q. (2004). Cilia and flagella revealed: from flagellar assembly in Chlamydomonas to human obesity disorders. *Cell* **117**, 693-7.

Snow, J. J., Ou, G., Gunnarson, A. L., Walker, M. R., Zhou, H. M., Brust-Mascher, I. and Scholey, J. M. (2004). Two anterograde intraflagellar transport motors cooperate to build sensory cilia on *C. elegans* neurons. *Nat Cell Biol* **6**, 1109-13.

Sorsby, A., Franceschetti, A., Joseph, R. and Davey, J. B. (1952). Choroideremia; clinical and genetic aspects. *Br. J. Ophthalmol.* **36**, 547-81.

Starr, C. J., Kappler, J. A., Chan, D. K., Kollmar, R. and Hudspeth, A. J. (2004). Mutation of the zebrafish choroideremia gene encoding Rab escort protein 1 devastates hair cells. *Proc. Natl. Acad. Sci. U S A* **101**, 2572-7.

Sukumaran, S. and Perkins, B. D. (2009b). Early defects in photoreceptor outer segment morphogenesis in zebrafish ift57, ift88 and ift172 Intraflagellar Transport mutants. *Vision Res* **49**, 479-89.

Sun, Z., Amsterdam, A., Pazour, G. J., Cole, D. G., Miller, M. S. and Hopkins, N. (2004). A genetic screen in zebrafish identifies cilia genes as a principal cause of cystic kidney. *Development* **131**, 4085-93.

Sung, C. H., Davenport, C. M. and Nathans, J. (1993). Rhodopsin mutations responsible for autosomal dominant retinitis pigmentosa. Clustering of functional classes along the polypeptide chain. *J. Biol. Chem.* **268**, 26645-26649.

Sung, C. H., Makino, C., Baylor, D. and Nathans, J. (1994). A rhodopsin gene mutation responsible for autosomal dominant retinitis pigmentosa results in a protein that is defective in localization to the photoreceptor outer segment. *J. Neurosci.* **14**, 5818-5833.

Syed, N., Smith, J. E., John, S. K., Seabra, M. C., Aguirre, G. D. and Milam, A. H. (2001). Evaluation of retinal photoreceptors and pigment epithelium in a female carrier of choroideremia. *Ophthalmology* **108**, 711-20.

Tai, A. W., Chuang, J. Z., Bode, C., Wolfrum, U. and Sung, C. H. (1999). Rhodopsin's carboxy-terminal cytoplasmic tail acts as a membrane receptor for cytoplasmic dynein by binding to the dynein light chain Tctex-1. *Cell* **97**, 877-87.

Tam, B. M., Moritz, O. L., Hurd, L. B. and Papermaster, D. S. (2000). Identification of an outer segment targeting signal in the COOH terminus of rhodopsin using transgenic *Xenopus laevis*. *J. Cell. Biol.* **151**, 1369-80.

Tobin, J. L. and Beales, P. L. (2007). Bardet-Biedl syndrome: beyond the cilium. *Pediatr Nephrol* **22**, 926-36.

Tolmachova, T., Anders, R., Abrink, M., Bugeon, L., Dallman, M. J., Futter, C. E., Ramalho, J. S., Tonagel, F., Tanimoto, N., Seeliger, M. W. et al. (2006). Independent degeneration of photoreceptors and retinal pigment epithelium in conditional knockout mouse models of choroideremia. *J. Clin. Invest.* **116**, 386-94.

Tomita, T. (1970). Electrical activity of vertebrate photoreceptors. *Q Rev Biophys* **3**, 179-222.

Tsao, C. C. and Gorovsky, M. A. (2008). Different effects of *Tetrahymena* IFT172 domains on anterograde and retrograde intraflagellar transport. *Mol Biol Cell* **19**, 1450-61.

Tsujikawa, M. and Malicki, J. (2004). Intraflagellar transport genes are essential for differentiation and survival of vertebrate sensory neurons. *Neuron* **42**, 703-16.

Vandenbranden, C. A., Yazulla, S., Studholme, K. M., Kamphuis, W. and Kamermans, M. (2000). Immunocytochemical localization of the glutamate transporter GLT-1 in goldfish (*Carassius auratus*) retina. *J. Comp. Neurol.* **423**, 440-51.

Vaughan, D. K., Fisher, S. K., Bernstein, S. A., Hale, I. L., Linberg, K. A. and Matsumoto, B. (1989). Evidence that microtubules do not mediate opsin vesicle transport in photoreceptors. *J Cell Biol* **109**, 3053-62.

Vihtelic, T. S., Doro, C. J. and Hyde, D. R. (1999). Cloning and characterization of six zebrafish photoreceptor opsin cDNAs and immunolocalization of their corresponding proteins. *Vis. Neurosci.* **16**, 571-85.

Vollrath, D., Feng, W., Duncan, J. L., Yasumura, D., D'Cruz, P. M., Chappelow, A., Matthes, M. T., Kay, M. A. and LaVail, M. M. (2001). Correction of the retinal dystrophy phenotype of the RCS rat by viral gene transfer of Mertk. *Proc. Natl. Acad. Sci. U S A* **98**, 12584-9.

Weng, J., Mata, N. L., Azarian, S. M., Tzekov, R. T., Birch, D. G. and Travis, G. H. (1999). Insights into the function of Rim protein in photoreceptors and etiology of Stargardt's disease from the phenotype in abcr knockout mice. *Cell* **98**, 13-23.

Westerfield, M. (1995). *The zebrafish book*. Eugene: University of Oregon Press.

Whelan, J. P. and McGinnis, J. F. (1988). Light-dependent subcellular movement of photoreceptor proteins. *J Neurosci Res* **20**, 263-70.

Wolfrum, U. and Schmitt, A. (2000). Rhodopsin transport in the membrane of the connecting cilium of mammalian photoreceptor cells. *Cell Motil Cytoskeleton* **46**, 95-107.

Wong, K. Y., Gray, J., Hayward, C. J., Adolph, A. R. and Dowling, J. E. (2004). Glutamatergic mechanisms in the outer retina of larval zebrafish: analysis of electroretinogram b- and d-waves using a novel preparation. *Zebrafish* **1**, 121-31.

Yau, K. W. and Nakatani, K. (1985). Light-suppressible, cyclic GMP-sensitive conductance in the plasma membrane of a truncated rod outer segment. *Nature* **317**, 252-255.

Yazulla, S. and Studholme, K. M. (2001). Neurochemical anatomy of the zebrafish retina as determined by immunocytochemistry. *J Neurocytol* **30**, 551-92.

Yeh, T. Y., Peretti, D., Chuang, J. Z., Rodriguez-Boulan, E. and Sung, C. H. (2006). Regulatory dissociation of Tctex-1 light chain from dynein complex is essential for the apical delivery of rhodopsin. *Traffic* **7**, 1495-502.

Yoder, B. K., Richards, W. G., Sweeney, W. E., Wilkinson, J. E., Avener, E. D. and Woychik, R. P. (1995). Insertional mutagenesis and molecular analysis of a new gene associated with polycystic kidney disease. *Proc Assoc Am Physicians* **107**, 314-23.

Young, R. W. (1967). The renewal of photoreceptor cell outer segments. *J. Cell Biol.* **33**, 61-72.

Young, R. W. (1969). A difference between rods and cones in the renewal of outer segment protein. *Invest. Ophthalmol.* **8**, 222-31.

Zhang, Q., Davenport, J. R., Croyle, M. J., Haycraft, C. J. and Yoder, B. K. (2005). Disruption of IFT results in both exocrine and endocrine abnormalities in the pancreas of Tg737(orpk) mutant mice. *Lab Invest* **85**, 45-64.

Zhang, Z., Tanaka, Y., Nonaka, S., Aizawa, H., Kawasaki, H., Nakata, T. and Hirokawa, N. (1993). The primary structure of rat brain (cytoplasmic) dynein heavy chain, a cytoplasmic motor enzyme. *Proc Natl Acad Sci U S A* **90**, 7928-32.

VITA

Name:	Bryan L. Krock
Address:	Texas A&M University Department of Biology. 3258 TAMU College Station, TX 77843
Email Address:	k_rock1@hotmail.com
Education:	B.S., Biology, The Pennsylvania State University, 2003